"Dimerization of the transcription factor STAT3 analyzed by single-molecule fluorescence spectroscopy and advanced microscopy."

Von der Fakultät für Mathematik, Informatik und Naturwissenschaften der RWTH Aachen University zur Erlangung des akademischen Grades eines Doktors der Naturwissenschaften genehmigte Dissertation

vorgelegt von

M.Sc.-Biologe

Tamás Domoszlai

aus Miskolc, Ungarn

Berichter: Professor Dr. rer. nat. Gerhard Müller-Newen

Universitätsprofessor Dr. rer. nat. Walter Richtering

Tag der mündlichen Prüfung: 17.04.2013

Diese Dissertation ist auf den Internetseiten der Hochschulbibliothek online verfügbar.

"Discovery consists of seeing what everybody has seen, and thinking what nobody has thought."

Albert Szent-Györgyi

"Two paradoxes are better than one; they may even suggest a solution."

Ede Teller

"The more original a discovery, the more obvious it seems afterwards."

Artur Kösztler

Publications and coauthorships

Domoszlai T., Schmitz-Van de Leur H. , Küster A., Martincuks A., Müller-Newen G.
Dimerization of the transcription factor STAT3: from preformed to activated dimers.
(In preparation)

Mohr A.*, Domoszlai T.*, Küster A., Poli V., Müller-Newen G.
STAT3 dynamics in neuron-like cells differentiated from STAT3-YFP knock-in embryonic stem cells.
(In preparation.)
* These authors contributed equally in this work.

Vogt M., Domoszlai T., Kleshchanok D., Lehmann S., Schmitt A., Poli V., Richtering W., Müller-Newen G.
The role of the N-terminal domain in dimerization and nucleocytoplasmic shuttling of latent STAT3.
J Cell Sci. 2011.124 900-9.

Mohr A., Chatain N., Domoszlai T., Rinis N., Sommerauer M., Vogt M., Müller-Newen G.
Dynamics and non-canonical aspects of JAK/STAT signalling.
Eur J Cell Biol. 2012. 91 524-32.

Acknowledgements

I am forever grateful to my supervisor, Prof. Dr. Gerhard Müller-Newen, for his mentoring and outstanding guidance during my work in his laboratory. His dedication to research and to always stay open minded represented to me a profound source of inspiration.

I would like to thank Prof. Dr. Walter Richtering for his kind support and for the excellent collaboration at the frontier of biology, chemistry and physics.

I am grateful for the European Union (EU), for the European Commission Marie Curie program (ReceptEUR network) providing excellent financial support and giving me the chance to get in contact and change experiences with the leading research laboratories in Europe from the JAK/STAT field.

I owe many thanks to our "practical brains" in the laboratory: Hildegard Schmitz-Van de Leur and Andrea Küster for their continous help and neverending kindness.

I am grateful to all my collegues in Labor 13 (10), that we met, and spent a nice time with each other: Anne Mohr, Anne Worsch, Corina Zimmermann, Liv Brolund, Natalie Rinis, Sara Zafarnia, as well as Anton Martincuks, Dieter Görtz, Dirk Fahrenkamp, Michael Vogt, Nicolas Chatain and Tobias Recker.

I would like to acknowledge all co-workers and laboratory members from Flur 42 for their help and kindness, generating an excellent working atmosphere.

In the end I would like to say special thanks to my family and friends for their constant support and patience.

Abstract

STAT3 (signal transducer and activator of transcription-3) is activated by numerous cytokines and growth factors. As a transcription factor, STAT3 plays important roles in many processes including embryonic development, immunity and different types of cancer progressions.

In response to cytokine stimulation, STAT3 is activated through phosphorylation of a single tyrosine residue. The phosphorylated STAT3 molecules dimerize via a reciprocal interaction between the phosphorylated tyrosine of one and the SH2 (Src homology 2)-domain of the other monomer, accumulate in the nucleus and bind to specific DNA sequences, which is followed by the target gene expression.

In addition, STAT3 is able to dimerize in the absence of cytokine treatment. However the structural background and the function of these preformed dimers are not known.

We analyzed the structural organizations and requirements of the nonphosphorylated and phosphorylated STAT3 dimer associations using fluorescence based microscopy techniques as dual-focus fluorescence correlation spectroscopy (2f-FCS) and Förster resonance energy transfer (FRET).

Results presented in this thesis reveal the similar parallel associations of the non-activated and activated STAT3 dimer forms, however the dimers are stabilized by diverse interdomain interactions.

We demonstrate the importance of the N-terminal domain in dimerization of latent STAT3, moreover we showed that this dimer is mostly stabilized by homotypic interactions between the N-terminal fragments, similar to other STAT family members.

In addition, we identified a single residue (L78) in the N-terminal domain of STAT3 promoting this dimerization, but also the tetramerization of the molecules on specific DNA sequences.

We showed that inhibition of latent STAT3 dimers positively affects the phosphorylation of STAT3, demonstrating the importance of preassociation in the negative regulation of STAT3 activation.

These structural findings reveal the unique structural characteristics of STAT3 in the STAT family and partially explains the different biochemical features, functions and the constitutive activation in various diseases of this very important transcription factor.

Table of contents

Publications and coauthorships ..... **III**

Acknowledgements ..... **IV**

Abstract ..... **V**

Table of contents ..... **VI**

Abbreviations ..... **IX**

1 Introduction **1**

1.1. Cytokines 1

1.2. Interleukin-6 (IL-6)-type cytokines 2

1.3. The JAK/STAT pathway 3

1.3.1. The canonical view of JAK/STAT signalling 4

1.3.2. The non-canonical view of JAK/STAT signalling 5

1.4. Signal transducers and activators of transcription (STATs) 6

1.5. Signal transducer and activator of transcription 3 (STAT3) 7

1.5.1. Structure and function 7

1.5.2. Activation and inactivation 8

1.5.3. STAT3 and diseases 10

1.6. Dimers and higher molecular complexes in the STAT family 11

1.6.1. Preformed and activated dimers 12

1.6.2. Tetramers and higher molecular complexes 13

1.7. Single-molecule spectroscopy and advanced microscopy techniques 15

1.7.1. Fluorescence correlation spectroscopy (FCS) 15

1.7.2. Förster resonance energy transfer (FRET) 18

1.8. Hypothesis and aims 20

2. Materials and methods **22**

2.1. Materials 22

2.1.1. Chemicals and reagents 22

2.1.2. Cytokines and receptors 22

2.1.3. Antibodies 22

2.1.4. Plasmids 22

2.2. Cell lines and culture techniques 24
2.2.1. Prokaryotic cells and cultivation 24
2.2.2. Transformation of competent bacteria 24
2.2.3. Eukaryotic cells and cultivation 25
2.2.4. Transfection of eukaryotic cells 25
2.3. Molecular biology techniques 26
2.3.1. Polymerase chain reaction (PCR) 26
2.3.2. Isolation of plasmid DNA 27
2.3.3. Determination of the plasmid DNA concentration 27
2.3.4. Digestion of DNA using restriction endonucleases 27
2.3.5. Agarose gel electrophoresis 28
2.3.6. Isolation of DNA fragments 28
2.3.7. Ligation of DNA fragments 28
2.3.8. DNA sequencing 29
2.3.9. Site directed mutagenesis 29
2.3.10. Reporter gene assay 29
2.4. Protein analysis and immunological methods 30
2.4.1. Protein extraction 30
2.4.2. Determination of protein concentration 30
2.4.3. SDS polyacrylamide gel electrophoresis (SDS-PAGE) 31
2.4.4. Western blot and immunodetection 32
2.4.5. Blue native PAGE 33
2.5. Fluorescence techniques 34
2.5.1. Confocal laser scanning microscopy (CLSM) 34
2.5.2. Potein labelling with genetically encoded fluorophores 35
2.5.3. Chemical labelling of proteins 36
2.5.4. SNAP-tag labelling procedure 37
2.5.5. Imaging of fixed probes 37
2.5.6. Imaging of living cells 38
2.5.7. Dual focus fluorescence correlation spectroscopy (2f-FCS) 38
2.5.8. Förster resonance energy transfer (FRET) 41

3. Results 44
3.1. Characterization of STAT3 fusion protein constructs 44
3.2. Control experiments for acceptor photobleaching FRET (APB FRET) 46
3.3. STAT3 dimerization prior to and after activation 48
3.3.1. FRET between N-terminal domains 48
3.3.2. FRET between N- and C-terminal domains 50
3.3.3. FRET between C-terminal domains 52
3.3.4. Live cell FRET 53
3.4. Role of the N-terminal domain in dimerization of latent STAT3 55
3.4.1. Complex formation of latent STAT3 analyzed by dual-focus fluorescence correlation spectroscopy (2f-FCS) 55
3.4.2. Function of the N-terminal domain in dimerization of latent STAT3 analyzed by FRET 57
3.5. Characterization of N-terminal domain mediated interactions 58
3.5.1. Homotypic N-terminal domain interactions 58
3.5.2. Importance of L78 residue in dimerization of N-terminal domains 61
3.5.3. Importance of L78 residue in tetramerization 62
3.6. Importance of L78R residue in dimerization of latent STAT3 64
3.6.1. Characterization of N-terminally mutated STAT3(L78R) constructs 64
3.6.2. L78R mutation prevents the dimerization of latent STAT3 *in vitro* and *in vivo* 66
3.7. Function of preformed dimers in STAT3 activation 68
3.8. Intramolecular FRET measurements on STAT3 72
4. Summary and discussion 75
4.1. STAT3 dimers prior to activation 75
4.2. Activated STAT3 dimers and tetramers 80
4.3. STAT3 dimer formations in the JAK/STAT3 pathway 83
5. Conclusions and perspectives 84
References 86
Supporting materials 96
List of figures and tables 98

Abbreviations

A	
AA	amino acid
ACF	autocorrelation function
APB	acceptor photobleaching
APD	avalanche photodiode
APRF	acut phase response factor
APS	ammonium persulfate
B	
β-Gal	β-galactosidase
BRET	bioluminescence resonance energy transfer
C	
CCD	coiled-coil domain
CCF	cross correlation function
CD45	cluster of differentiation 45, membrane-bound tyrosine phosphatase
CDK5	cyclin dependent kinase 5
CFP	cyan fluorescent protein
CLL	chronic lymphocytic leukaemia
CLSM	confocal laser scanning microscopy
CNTF	ciliary neurotrophic factor
CT	cardiotrophin
C-terminal	carboxy-terminal
D	
DBD	DNA-binding domain
ddH_2O	double destilled water
DdSTAT	*Dyctiostelium discoideum* STAT
DMSO	dimethyl sulfoxide
DNA	deoxyribonucleic acid
dNTP	deoxyribonucleotide triphosphate
E	
EDTA	ethylenediaminetetraacetic acid
EGF	epidermal growth factor
eGFP	enhanced green fluorescent protein
EPO	erythropoietin
EtBr	ethidium bromide
F	
FCS	fluorescence correlation spectrocopy
FCCS	fluorescence cross correlation spectroscopy
FLIP	fluorescence loss in photobleaching

F

FP	fluorescent protein
FRAP	fluorescence recovery after photobleaching
FRET	Förster resonance energy transfer

G

GAPDH	glyceraldehyde 3-phosphate dehydrogenase
GH	growth hormone
GFP	green fluorescent protein
Gp130	glycoprotein 130

H

HIES	hyperimmunoglobulin E syndrome

I

IFN	interferon
IHCA	inflammatory hepatocellular adenoma
IL	interleukin
IL-6-Rα	interleukin-6 receptor α

J

JAK	Janus kinase

L

LD	linker domain
LIF	leukaemia inhibitory factor
LGL leukaemia	large granular lymphocytic leukaemia

M

min	minutes
mRNA	messenger RNA
MS	multiple sclerosis

N

nm	nanometer
NTD	N-terminal domain
N-terminal	amino-terminal

O

OD	optical density
OSM	oncostatin M

P

PAGE	polyacrylamide gel electrophoresis
PCR	polymerase chain reaction
PBS	phosphate buffered saline
PDGF	platelet-derived growth factor
PIAS	protein inhibitor of activated STAT
PKC	protein kinase C

P

PMT	photomultiplier tube
PPTase	phosphopantetheinyl transferase
PMSF	phenylmethylsulfonyl fluoride
PTEN	phosphatase and tensin homolog
PTP	protein tyrosin phosphatase
pTyr	phosphotyrosine
PVDF	polyvinilydene-difluoride

R

RA	rheumatoid arthritis
RNA	ribonucleic acid
ROI	region of interest

S

s	seconds
sFCS	scanning FCS
SHP	hematopoietic cell phosphatase
SH2	Src homology 2 domain
sR	soluble IL-6-R α
SOCS	suppressor of cytokine signaling
Src	sarcoma/proto-oncogenic tyrosine kinase
STAT	signal transducer and activator of transcription
SUMO	small ubiquitin-related modifier

T

TEMED	tetramethylethylenediamine
Th17	T helper 17 cell
TK	tyrosine kinase
TMR	tetramethylrhodamine
TPO	thrombopoietin

U

UV light	ultraviolet light

W

WB	western blot

Y

YFP	yellow fluorescent protein

Numerical

2f-FCS	dual-focus fluorescence correlation spectroscopy

1. Introduction

1.1. Cytokines

An essential condition for normal functioning of multicellular organisms is the existence of a well organized cell-cell communication system. Its breakdown can lead to malfunctions and diseases like cancer, chronic inflammation, autoimmune disorders or multiple sclerosis (MS). In MS, a focal lymphocytic infiltration leads to the damage of myelin in the brain and spinal cord [1], driving the neurons unable to effectively conduct electrical signals and communicate with each other.

Two different forms of cell-cell information transfer can be distinguished: direct and indirect. Direct communication can be achieved with cytoplasm-connection of neighboring cells through gap-junctions. The indirect way is performed by messenger molecules like hormones, mediators or neurotransmitters, which are released by cells and recognized by other cells expressing the cognate receptors. Well known members of the mediator-system are the cytokines.

The term „cytokine" was firstly introduced by Stanley Cohen in 1974 for mediator substances, which play a role in various aspects of host defense [2]. The synonym form interleukin (IL) refers to the capability of acting as a communicator between leukocytes. Chemically, cytokines are small (15-40 kDa), water-soluble glycoproteins, generally acting at low concentrations (nano/pico molar range).

Cytokines are secreted by a high variety of cell types like white blood cells, fibroblasts or endothelial cells, and act via binding to specific cell surface receptors [3]. Receptor binding leads to the activation of signalling cascades, which results in changes in the transcriptional activity of the host cell.

As chemical communicators, cytokines play major roles in mediating and regulating immunity, inflammation, hematopoiesis and embryogenesis [3]. Dysregulation in the cytokine-driven signalling network can result in several diseases and correlates with pathophysological states, as acute and chronic inflammatory diseases, neoplastic disorders, cancer and autoimmune diseases [4, 5].

After secretion, cytokines mainly act in two different ways: autocrine (effect on the cytokine producing cell) or paracrine (impact on the nearby cell). Some members of the cytokine family also have the capability to act in an endocrine manner (cytokine effect on distant cell) [6].

Special features of cytokine-action are the following: a single cytokine is able to act on different types of cells (pleiotropy), similar functions can be achieved by different cytokines (redundancy), the effect of two different cytokines is stronger than their additive effects (synergy) and they can inhibit the effect of other cytokines (antagonism).
The classification can be based on different aspects. Based on functionality, cytokines can be grouped as pro- or anti-inflammatory cytokines [7]. On a functional basis and the used receptor system, four major group can be formed: interferons, interleukins, growth factors and chemokines [8].

1.2. Interleukin-6 (IL-6)-type cytokines

One important subfamily of cytokines is the IL-6-type cytokine family. The group is formed by cytokines having similar three-dimensional topology, a so called four-helix bundle structure (Figure 1). This motif seems to be a common feature in the structure of mediator substances like interleukins, interferons and some growth factors, indicating the functional and evolutional relationship [9].

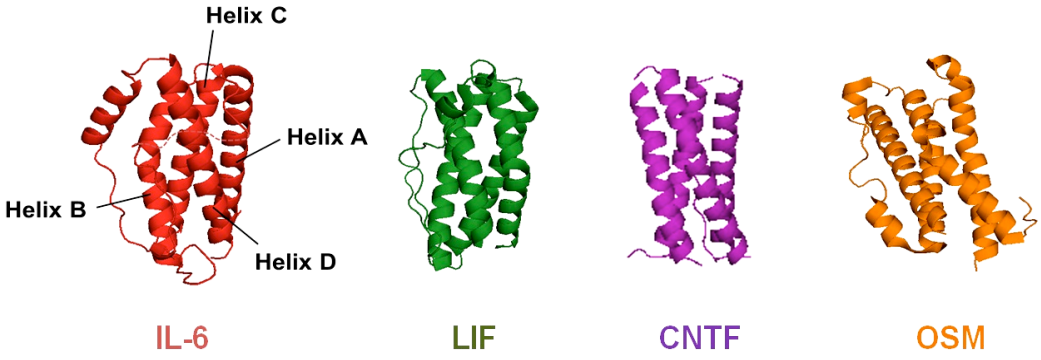


Figure 1: Representative crystal structures of IL-6-type cytokine family members. (RCSB Protein Data Bank accession numbers for IL-6, LIF, CNTF and OSM are 1ALU, 1EMR, 1CNT and 1EVS respectively).

Members of the IL-6 family are: IL-6 (interleukin-6), IL-11 (interleukin-11), IL-27 (interleukin-27), IL-31 (interleukin-31), LIF (leukaemia inhibitory factor), OSM (oncostatin M), CNTF (ciliary neutrophic factor), CT-1 (cardiotrophin-1) and CLC (cardiotrophin-like cytokine). These cytokines play crucial role in the regulation process of immune and acute phase responses, but are also critical in mediating haematopoiesis, neuronal regeneration or embryonal development [8].

The signalling procedure follows a combined route with the use of two different receptor systems: the short-chain α-receptors and the long-chain β-receptors, consisting of 3 or 5-8 immunoglobulin (Ig)/fibronectin-like domains, respectively. All family members use the 130 kDa glycoprotein (gp130) as signal transducing β-receptor forming homo- or heterodimeric complexes. A special case is the IL-31 signalling route, where the cytokine binds to a heterodimeric complex, consisting of oncostatin M receptor (OSM-R) and a gp130-like protein (GPL) [10].

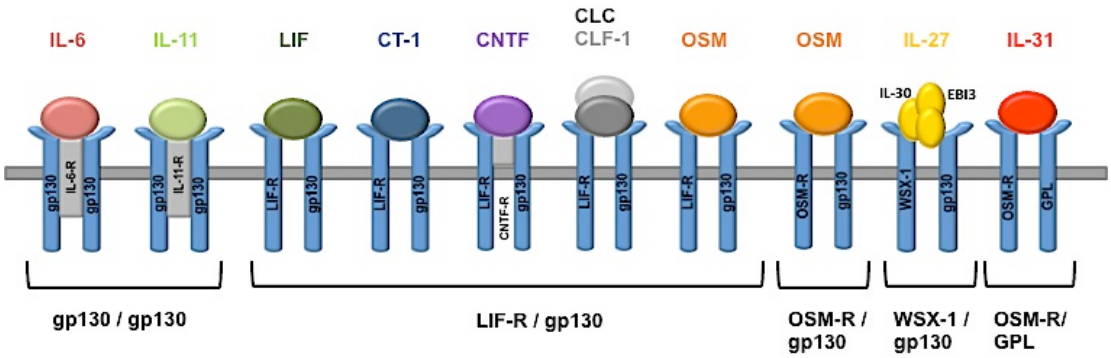


Figure 2: Receptor complexes of the IL-6-type cytokine family. Interleukin-6-type cytokines signal through different combination of the receptor subunits (modified from Ref. [8]).

Some members of the IL-6 family signal without α-receptor (OSM, LIF, CT-1, IL-31). Other cytokines need to have an additional α-receptor subunit for the formation of the receptor complex. The α-receptors exist as membrane bound forms, as IL-6 receptor (IL-6-R) for IL-6, IL-11 receptor (IL-11-R) for IL-11 and ciliary neutrophic factor receptor (CNTF-R) for CNTF signalling. In other scenarios, the short-chain receptors are soluble, as in the case of IL-27, where the Epstein-Barr virus induced gene (EBI3) form together with IL-30 (p28) the composite cytokine IL-27 [10, 11].
The binding of the cytokine leads to receptor-oligomerization or structural changes in the receptor complex, forming a functionally active conformation, which is able to initiate the intracellular signalling cascade.

1.3. The JAK/STAT pathway

The classical, canonical model describes the JAK/STAT pathway in a simple and basic form but exhibit some critical points. This hiatus should be refined with the non-canonical aspects of JAK/STAT signalling.

1.3.1. The canonical view of JAK/STAT signalling

In the canonical view, the cytokines are recognized by specific cell surface receptors and ligand binding leads to the dimerization of the receptor subunits (Figure 3). The cytoplasmic part of the receptors is associated with members of the Janus kinase (JAK) family. The receptor dimerization brings the JAKs into close proximity, allowing to transphosphorylate each other resulting in their activation [12, 13]. The activated JAKs subsequently phosphorylate tyrosine residues on the receptor, which act as docking sites for proteins containing Src homology 2 (SH2) domains, as various adaptor proteins (Shc, Grb2) [14], or most importantly, transcription factors from the signal transducer and activator of transcription (STAT) family. STATs are recruited to the receptor and become phosphorylated on a tyrosine residue by JAKs. The phosphorylated STATs form dimers (homo- or heterodimers) through a reciprocal interaction between the phosphotyrosine motif of one and the SH2 domain of the other monomer [15]. The dimerized STAT molecules translocate to the nucleus, bind to specific DNA sequences and activate the cytokine-driven target gene expression [16].

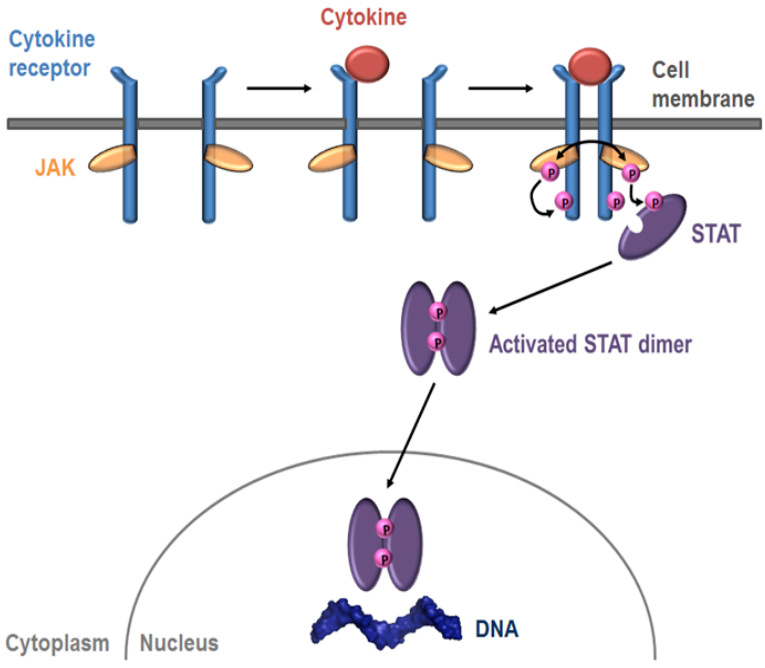


Figure 3: Canonical JAK/STAT signalling. Ligand binding leads to the dimerization of the receptors and the activation of JAKs. Phosphorylated STAT monomers dimerize, and the activated dimers translocate to the nucleus to induce target gene expression (modified from Ref. [17]).

1.3.2. The non-canonical view of JAK/STAT signalling

In the non-canonical model the cytokine receptors exist as dimers prior to activation (Figure 4), and ligand binding leads to a conformational change from an inactive to an active receptor dimer [17].
In addition, an increasing number of studies demonstrate the existence of STAT dimers in unstimulated state, and the capability of STATs to exert biological functions independently of phosphorylation [18].
These non-canonical functions of STATs were demonstrated in various biological processes, as controlling heterochromatin [19] and microtubule stability [20], or regulating metabolic functions in mitochondria [21].

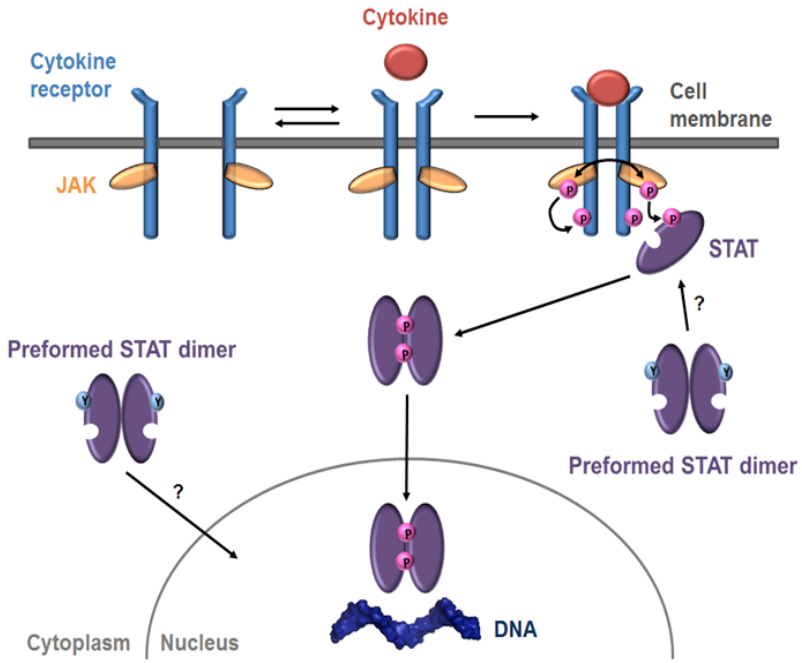


Figure 4: Non-canonical JAK/STAT signalling. Cytokine receptors and STATs are also dimerized prior to activation. Preformed STAT dimers are possibly involved in biological processes as gene expression regulation. The activation (phosphorylation) possibly leads to a stuctural conversion of the STAT dimer from "inactive" to "active" dimer conformation (more details of the non-canonical function of STATs see in Ref. [17]).

The inactivation of STAT signalling is achieved by different regulator proteins at different stages in the activation cycle such as suppressor of cytokine signalling (SOCS) proteins, protein inhibitor of activated STATs (PIAS) or tyrosine phosphatases (SHP1, PTP-1B, TC45) [13].

1.4. Signal transducers and activators of transcription (STATs)

The name Signal Transducers and Activators of Transcription (STATs) refers to dual function proteins which are able to receive the activating signal from the cell surface and carry it toward the nucleus to activate gene transcription [22]. The first members of the STAT family were identified using biochemical separation and purification of factors involved in interferon (IFN) induced transcriptional activation [23].
The STAT protein family consist of seven members: STAT1, STAT2, STAT3, STAT4, STAT5a, STAT5b and STAT6, encoded by different genes, localized on three chromosomes [24]. Numerous ligands are able to activate STAT transcription factors, including interferons, interleukins, growth factors and hormons (Table 1). Primary roles of the protein family were defined by gene-targeted removal in mice of each of the seven genes [13] (Table 1).

STAT family member	Activating ligands	Phenotype of null mice
STAT1	IFN-α, IFN-β, EGF	viable, impaired responses to interferons
STAT2	IFN-α, IFN-β	viable, impaired responses to interferons
STAT3	IL-6, IL-11, LIF, CT-1, CNTF, OSM, EGF, G-CSF, leptin	embryonic lethal
STAT4	IL-12	loss of IL-12 responsiveness
STAT5a	IL-2, IL-3, IL-5, IL-7, IL-9, IL-15, Prolactin, EPO, TPO, GH, G-CSF	impaired mammary gland development
STAT5b		defective NK cell development
STAT6	IL-4, IL-13	loss of IL-4 responsiveness

Table 1: Functions of the STAT family members.
The listed ligands induce the activation of the corresponding STAT family member. The phenotype describes the effect of the specific STAT gene deletion (adopted and modified from Ref. [13]. and Ref. [25]).

In overall, STATs are playing crucial roles in many processes like hematopoiesis, immunity and embryonic developement [17]. The dysregulated activation of STAT signalling is involved in chronic inflammation [26] and in various malignant progressions of human tumors, including blood malignancies (leukaemias/lymphomas) or solid tumors (head and neck squamosus cell carcinoma, breast cancer) [27].
There are STAT homologues in other species, like in the fruitfly *Drosophila melanogaster* (*D*-Stat/stat92e or marelle) [28], or in the social amoeba *Dyctiostelium discoideum*, where *Dyctiostelium* STATs (*Dd*STATs) play critical roles in the early developement and cellular differentiation [29].

1.5. Signal transducer and activator of transcription 3 (STAT3)

The third member of the STAT family (in order of description) was discovered by Wegenka et al. [30] in our institute in 1993 as a nuclear factor and termed acute-phase response factor (APRF), which is rapidly activated by IL-6. In 1994 Zhong et al. [31] identified STAT3 by cDNA library screen as a 92 kDa DNA binding protein which is activated by EGF and IL-6, but not by IFN-γ. In the same year, Akira et al. [32] purified and cloned APRF/STAT3, that binds to IL-6 responsive elements in promoters of acute phase genes.

1.5.1. Structure and function

The STATs consist of 750-850 amino acids and share a common structural organization representing six distinct and functionally conserved domains: N-terminal domain (NTD), coiled-coil domain (CCD), DNA-binding domain (DBD), linker domain (LD), Src homology 2 (SH2) domain, and the C-terminally located transactivation (TAD) domain (Figure 5).
The N-terminal domain was shown to be involved in protein-protein interaction [33], dimerization of the non-activated STATs [34], but also in tetramerization on specific gene promoters [34, 35].
The CCD domain adopts an elongated structure, formed by a 4-helix bundle, connected with short loops [15], has a functional role in the interaction with other proteins like c-JUN [36], but is also implicated in STAT3 receptor recruitment and binding [37].
The DNA-binding domain is localized in the central region of the molecule and contains the amino acid residues that interact with specific enhancer sequences in the promoter region of target genes.

The linker domain has a small helical structure which connects the DNA-binding domain to the SH2 domain.
The SH2 domain contains the binding site for phosphotyrosine (pTyr) motifs and is therefore essential for binding to the activated receptor [38], and required for the activated dimer formation through reciprocal intermolecular interaction between the pTyr and SH2 domain of two monomers [39].
The transactivation domain (TAD) is a structurally disordered, highly flexible, natively unfolded domain [28]. TAD participates in protein-protein interactions [40] but is also involved in an intramolecular interaction with CCD and SH2 domains, which might be crucial for receptor binding [41].

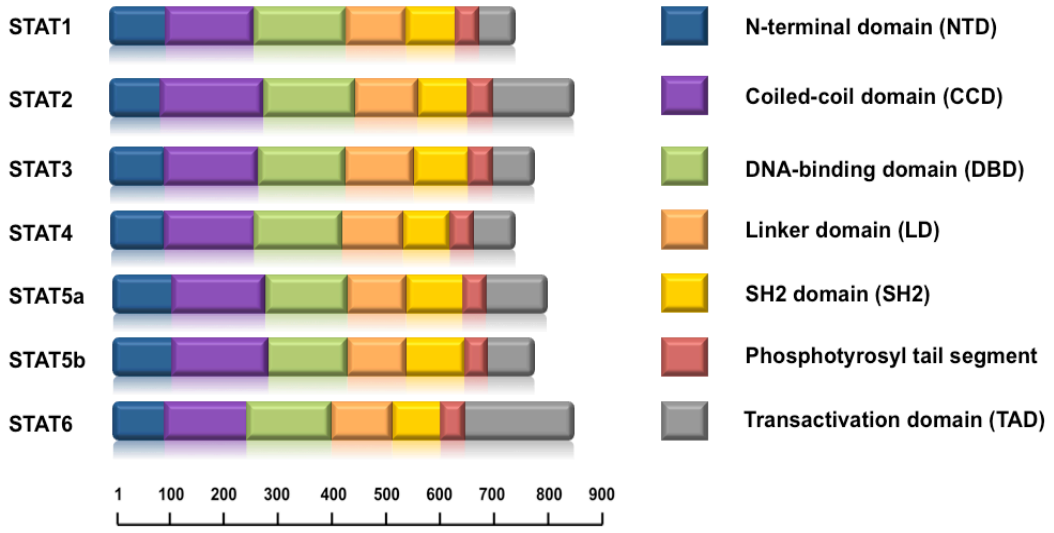


Figure 5: STAT family members and their functional domains. The STATs share a common structure, consisting of six distinct functional domains. The phosphotyrosyl tail segment [28] contains the conserved tyrosine residue involved in phosphorylation and dimerization.

Shorter isoforms, distinct from the full length STAT (α-isoform) are generated by alternative mRNA splicing or post-translational proteolytic processing (β, γ, δ isoforms) [42].

1.5.2. Activation and inactivation

STAT3 is activated by numerous cytokines and growth factors (Table 1), as well by oncogenic proteins such as Src [43]. During activation, a single tyrosine residue located at the C-terminal end of the molecule (amino acid position 705) gets phosphorylated by receptor-associated tyrosine kinases

(TK) like JAKs, members of the Src family, or by activated growth factor receptors with intrinsic TK activity like EGF or PDGF receptor [27].
Additionally, serine kinases including protein kinase C (PKC), mitogen-activated protein kinases (MAPKs) or CDK5 [43], are able to phosphorylate a serine residue (amino acid 727) of STAT3. Function of serine phosphorylation seems to be controversial, where studies revealed the necessity for maximal transcriptional activation of STAT3 [44] but also the possible involvement in negative regulation [45]. Constitutive and exclusive phosphorylation of STAT3 on serine 727 showed to be a "hallmark" of chronic lymphocytic leukaemia (CLL), suggesting STAT3 as therapeutic target in this type of hematologic malignancy [46].
Besides tyrosine/serine phosphorylation, some other modifications also target STATs, such as acetylation, methylation, ubiquitination or sumoylation. STAT3 was found to be reversibly acetylated by histone acetyltransferase p300 at a single lysine residue (amino acid 685) which was shown to be critical for stable dimer formation [47].
The negative regulation of STAT3 activation is performed in several ways including inhibitory proteins, as the suppressor of cytokine signalling (SOCS), protein inhibitor of activated STAT (PIAS) and protein phosphatases, or through proteosomal degradation.
The supressor of cytokine signalling (SOCS) protein family consist of eight members: SOCS-1, SOCS-2, SOCS-3, SOCS-4, SOCS-5, SOCS-6, SOCS-7 and the cytokine-inducible SH2-domain containing protein CIS. The SOCS proteins with a central SH2-domain are able to bind to phosphotyrosine residues in cytokine receptors or in JAKs, supressing cytokine signalling at different steps by inhibiting JAKs activities (by direct binding), competing with STATs for receptor binding or targeting the signalling proteins for proteosomal degradation [48].
The members of the PIAS family (PIAS1, PIAS2, PIAS3, PIAS4, PIASx and PIASy) are constitutively expressed nuclear proteins with SUMO-E3 ligase activity [49]. PIAS3 is able to interact directly with the activated STAT3 molecules and specifically inhibit DNA binding and STAT3-mediated gene expression [50].
Negative regulation of STAT3 signalling can also be performed by dephosphorylation (remove of phosphate group) by protein phosphatases as TC-PTP (TC45) or SHP1 and SHP2 [51].
The ubiquitin dependent proteosomal pathway includes series of enzymatic reactions leading to the degradion of the target proteins such as regulatory molecules or transcription factors, including STAT3 [52] representing a regulation mode of protein stability [53].

1.5.3. STAT3 and diseases

In the past years an increasing number of publications revealed STAT3 as a key player in chronic inflammation, autoimmune diseases or in different types of cancer progressions. The impaired function of STAT3 signalling is caused by genetic aberrations (mutations) or (in most cases) by the constitutive activation of the transcription factor.
In hyperimmunoglobulin-E syndrome (HIES, Job's disease), heterozygous mutations (missense or in-frame microdeletions) in the DNA-binding [54] and SH2-domains of STAT3 [55] result in the expression a full length but dysfunctional STAT3 molecules. These forms act as dominant negative resulting in ~75% inhibition of the active STAT3 homodimers. This inhibition effects Th17-cells function, resulting in immunodeficiency and susceptibility to infections [56].
In large granular lymphocytic leukaemia (LGL leukaemia), the SH2 and transactivation domain of STAT3 are frequently mutated (Figure 6) resulting in a hyperactivation of STAT3. This aberrant signalling underlies the pathogenesis of this disease [57].
Somatic mutations were also found in benign liver tumors (Figure 6 and 7) leading to so called inflammatory hepatocellular adenomas (IHCAs). The aminoacid changes affect the N-terminal, coiled-coil, linker and the SH2 domain of the molecule, resulting in a mutant STAT3, which is constitutively active in a ligand independent manner [58].

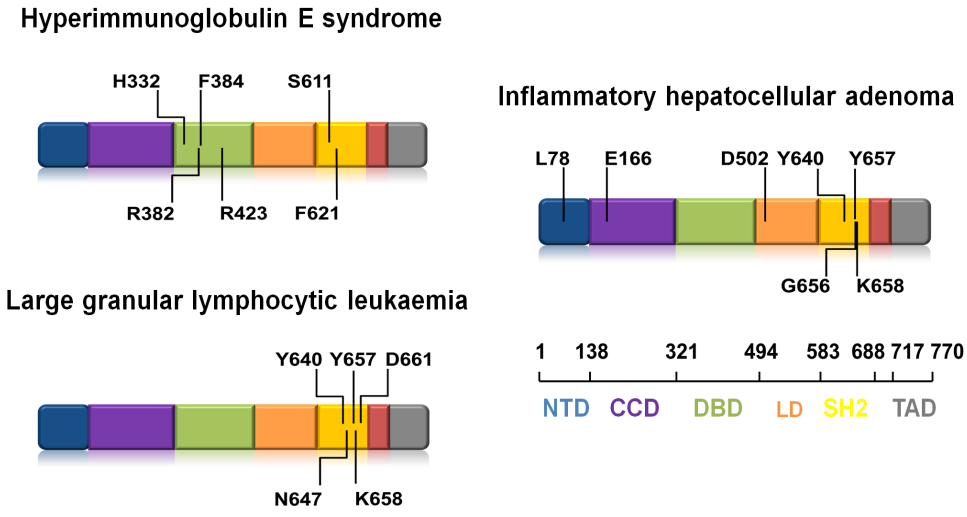


Figure 6: The identified mutations found in different diseases, targeting structural domains of STAT3. Most of the mutations were found in the SH2-domain, but were also identified in N-terminal, coiled-coil, DNA binding or linker domains.

STAT3's role in cancer is a major topic in the biomedical research field. In contrast to the normal (transient) activation, STAT3 is frequently overactivated (persistent activation) in a variety of human solid tumors and blood malignancies including breast, head and neck, lung, pancreatic and prostate cancers, as well as melanomas, multiple myelomas, leukaemias and lymphomas [59].
This dysregulated activation brings STAT3 to the field as a central player in cancer cell growth, proliferation, survival, angiogenesis, metastasis and invasion. Thus, STAT3 is emerging as a promising drug target for cancer treatment [60].
STAT3 also contributes in progression or remission in other diseases including rheumatoid arthritis (RA) [61], psoriasis [62], inflammatory bowel disease [63] or atherosclerosis [64].

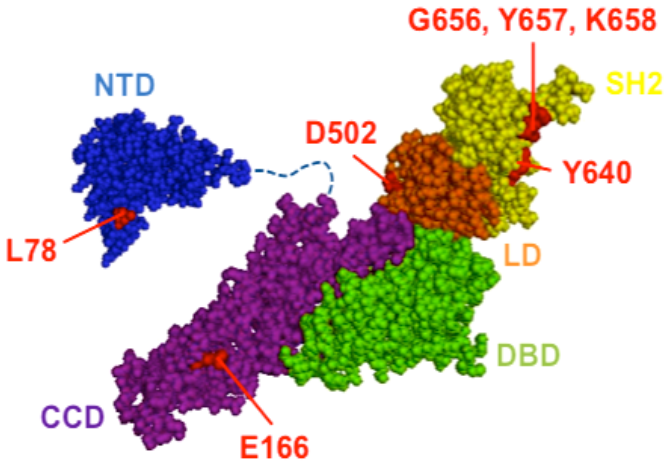


Figure 7. Distribution of STAT3 somatic mutations identified in inflammatory hepatocellular adenomas (IHCAs) highlighted in the crystal structure of STAT3. (NTD: N-terminal domain, CCD: coiled-coil domain, DBD: DNA binding domain, LD: linker domain, SH2: SH2 domain. RCSB Protein Data Bank accession number is 1BG1, and 1BGF for STAT3 and N-terminal domain of STAT4 respectively, mutation sites and residues are highlighted in red).

1.6. Dimers and higher molecular complexes in the STAT family

In the early studies STATs were proposed in unstimulated state as latent monomeric proteins present in the cytosol of the cell, and dimerization occurs only upon phosphorylation after cytokine stimulation [39, 65].

In recent years several publications reported the existence of preformed (unstimulated) STAT dimers, tetramers (on DNA) but also associations of STATs in high molecular mass complexes, as statosomes, nuclear bodies or signalling endosomes.

1.6.1. Preformed and activated dimers

It is a well established phenomenon, and demonstrated by various techniques that STATs are able to form stable dimers prior to stimulation [66-70], and have the capability of shuttling constitutively between cytoplasmic and nuclear compartments [71, 72].
Structurally the N-terminal domain seems to have the central role in the formation of unphosphorylated STAT dimers [73]. In context of STAT1 a model was proposed where the different STAT1 dimer conformations, performing antiparallel to parallel conversion, are involved in the activation-inactivation cycle [74, 75] (Figure 8 and Figure 9).

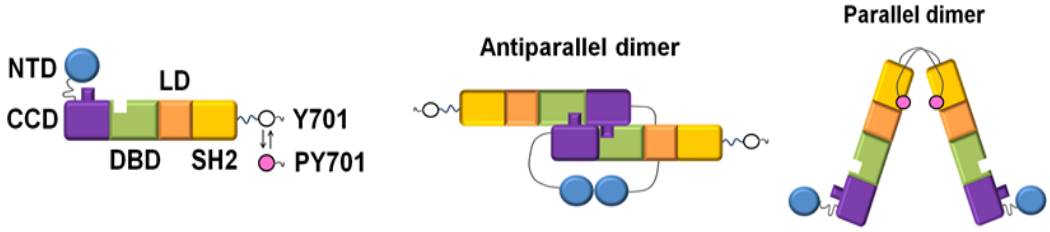


Figure 8: Antiparallel and parallel dimer formations of STAT1. Antiparallel dimer formation is driven by N-terminal domain (NTD) homotypic interactions, and stabilized by interdomain interactions between coiled-coil (CCD) and DNA binding domains (DBD). Parallel dimers are stabilized by reciprocal interactions between phosphotyrosine motif and SH2 domain (adopted and modified from Ref. [75]).

In this scenario the intermolecular interactions between the N-terminal domains are critical for the non activated dimer formation, and additional interactions between CCD and DNA-binding domain stabilize this antiparallel conformation, where the two C-terminal regions are localized in the opposite ends of the dimer. Following activation, the antiparallel dimer recruit the receptor, and after activation by tyrosine phosphorylation the dimer adopts a parallel conformation, stabilized through the „conventional“ reciprocal interaction between the phophotyrosine-motif and the SH2 domain. This connection orientates the dimer in a parallel formation and structurally allows the activated STAT1 dimers to bind to specific DNA sequences.

After the release from the DNA, the newly established interaction between the N-terminal domains dissociates the phosphotyrosine-SH2 interaction and stabilizes the dimer in an antiparallel conformation, facilitating the dephosphorylation procedure by exposing the phospho-tyrosine residues to phosphatases [75].

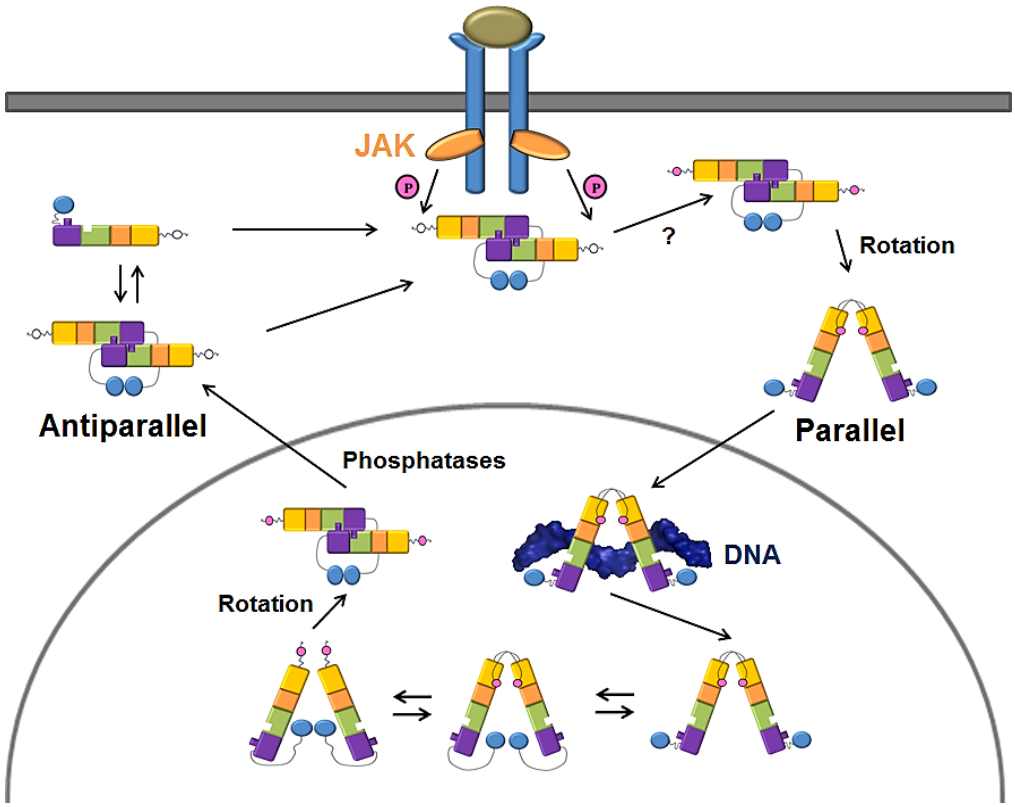


Figure 9: STAT1 dephosphorylation model. Prior to stimulation STAT1 dimerize in an antiparallel orientation. Activation (through tyrosine phosphorylation) leads to the disruption of the antiparallel dimers and the molecules adopt a parallel orientation. The parallel dimers translocate to the nucleus and bind to specific DNA sequences. After the release from DNA the N-terminal domain driven reorientation and rotation of the dimer molecule leads to the re-formation of the antiparallel dimer, which exposes the tyrosine residues to phosphatases and facilitates the dephosphorylation procedure (adopted and modified from Ref. [75]).

1.6.2. Tetramers and higher molecular complexes

The activated STAT dimers recognize consensus palindrom sequences on DNA: TTCN$_{3\text{-}4}$GAA [76].

They can also bind cooperatively on promoters containing two or more binding sites, leading to tetramer formation, which is stabilized by interactions between N-terminal domains of the individual dimers [34].
Stable tetramer formation on specific gene promoters is essential for maximal transcriptional activation [35], for cytokine responses and normal immune functions [77].
The first evidence that STAT proteins are also able to form high molecular weight complexes was found by gel filtration chromatography analysis in the cytosol fraction of liver cells. The protein assemblies were termed as statosome I (200-400 kDa) and statosome II (1-2 MDa) [78]. Similar large STAT oligomers were detected in living cells as slow diffusing components using fluorescence correlation spectroscopy (FCS) [79]. Statosomes possibly contain multiple STAT molecules associated with other proteins including scaffolding (caveolin-1) or heat shock proteins [80].
Special enrichment of STAT3 was found in the nuclear region in response to IL-6 stimulation, termed as nuclear bodies (Figure 10), possibly involved in active gene transcription or serving as reservoirs of the activated molecules [81].

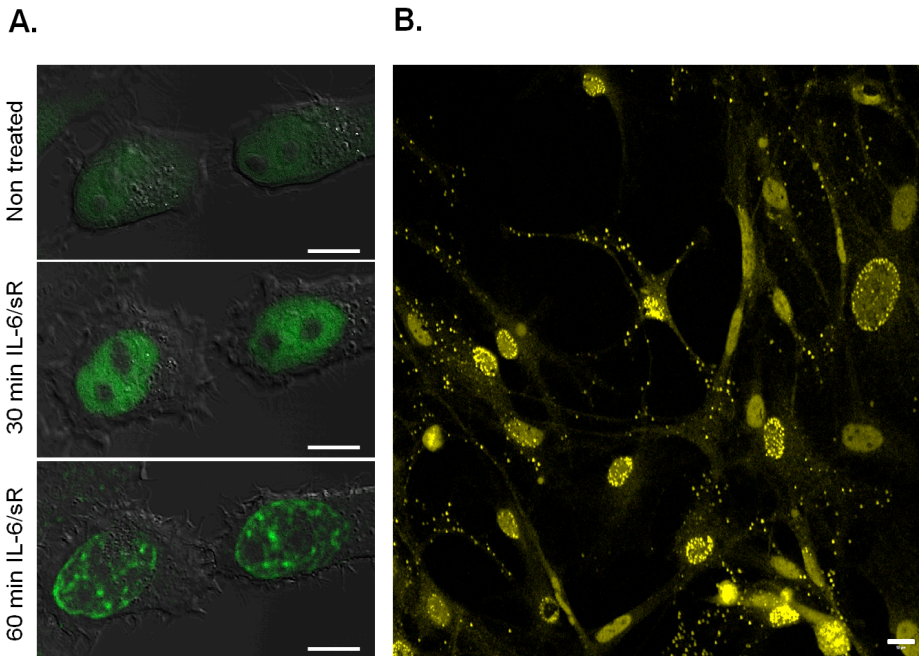


Figure 10: (A) STAT3 nuclear body formation in response to stimulation in HeLa cells. HeLa cells stably expressing STAT3-eGFP induced with doxycycline (10 ng/ml, 24 hours) and stimulated with IL-6 and soluble receptor (adopted from [82]). **(B) STAT3 accumulation in nuclear and axonal region in embryonic stem (ES) cell differentiated neuron-like cells after cytokine addition.** STAT3-YFP knock in ES cells (generous gift of Valeria Poli) derived neurons were stimulated with 100 ng/ml CNTF and analyzed with confocal microscopy. Bars, 10 µm.

Similar to nuclear bodies, accumulated STAT1 and STAT3 in nuclear particles were identified as paracrystals serving as dynamic reservoirs protecting STATs from dephosporylation [83].
The signalling endosome hypothesis describes a specialized way of signal transmission and is well established in long distance axonal communication [84]. After ligand binding the receptor complex is internalized by endocytosis. This complex recruits signalling molecules and associates with the microtubuli transport system forming a "signalling endosome" which is capable to initiate signalling. In the cell body, signalling endosomes may either initiate local signalling or move to the nucleus and start the transcriptional response [85]. The importance of signalling endosomes in JAK/STAT signal transduction still needs to be validated whether it is a common way of signal transmission or unique in specific cell types like neurons or dendritic cells.

1.7. Single-molecule spectroscopy and advanced microscopy techniques

Single-molecule spectroscopy methods such as fluorescence correlation spectroscopy (FCS) allows the real-time analysis of biologically relevant molecules in solution or in living cells, giving access to molecular parameters like diffusion coefficients, hydrodynamic radii or concentrations [86].
Advanced fluorescence microscopy techniques including Förster resonance energy transfer (FRET) or various bleaching based methods (FRAP, FLIP) represent powerful tools to visualize and analyze complex dynamic events and interactions in cells, organelles or sub-organelle components in biological specimens [87].

1.7.1. Fluorescence correlation spectroscopy (FCS)

Fluorescence correlation spectroscopy (FCS) technique was developed in the early 1970s as a „miniaturized“ version of dynamic light scattering. In the first application, FCS was used to study the reversible binding reaction of ethidium bromide (EtBr) to DNA [88].
In general, FCS analyzes the fluctuations of fluorescently labelled molecules, which arise from the diffusion through a subfemtoliter detection volume illuminated by a focused laser beam (Figure 11).

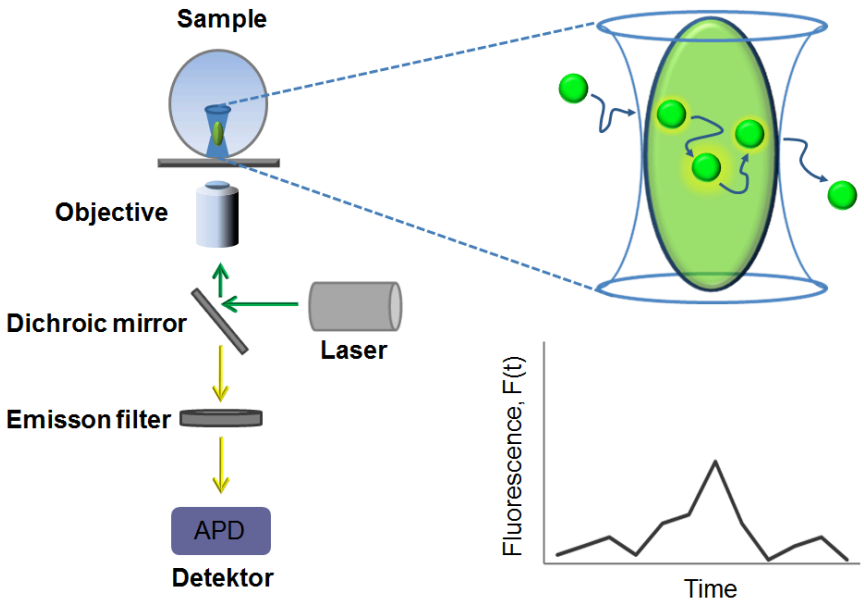


Figure 11: Basic features of fluorescence correlation spectroscopy (FCS). The exciting laser beam is directed to the objective with the use of a dichroic mirror and focused on the sample generating a very small detection volume. The diffusion of the fluorescently labelled particles in and out from the excitation volume is detected in time as fluctuations in the fluorescence signal. The fluorescence light collected by the objective, passes through the dichroic mirror, emission filter and is focused on a detector with single photon sentitivity (APD: avalanche photodiode).

The fluctuation traces are recorded in time and quantified by autocorrelation analysis (Figure 12). The autocorrelation function (ACF) describes the variance of fluorescence fluctuations and provides a measure for the self-similarity of the signal as a function of time.
The mathematical analysis of the ACF provide quantitative information about the mobility (diffusion coefficient, D) or the concentration (C) of the investigated molecule [89].
During the past years new variations of FCS were established: scanning FCS (sFCS), the two color fluorescence cross correlation spectroscopy (FCCS) [90] or two focus FCS (2f-FCS) [91].
sFCS is a modified fluorescence spectroscopy technique, where the detection volume is moved across the sample in a defined way and circumvents some detection problems (slower dynamics, photobleaching) of the standard FCS and makes the technique more applicable in biological systems [92].

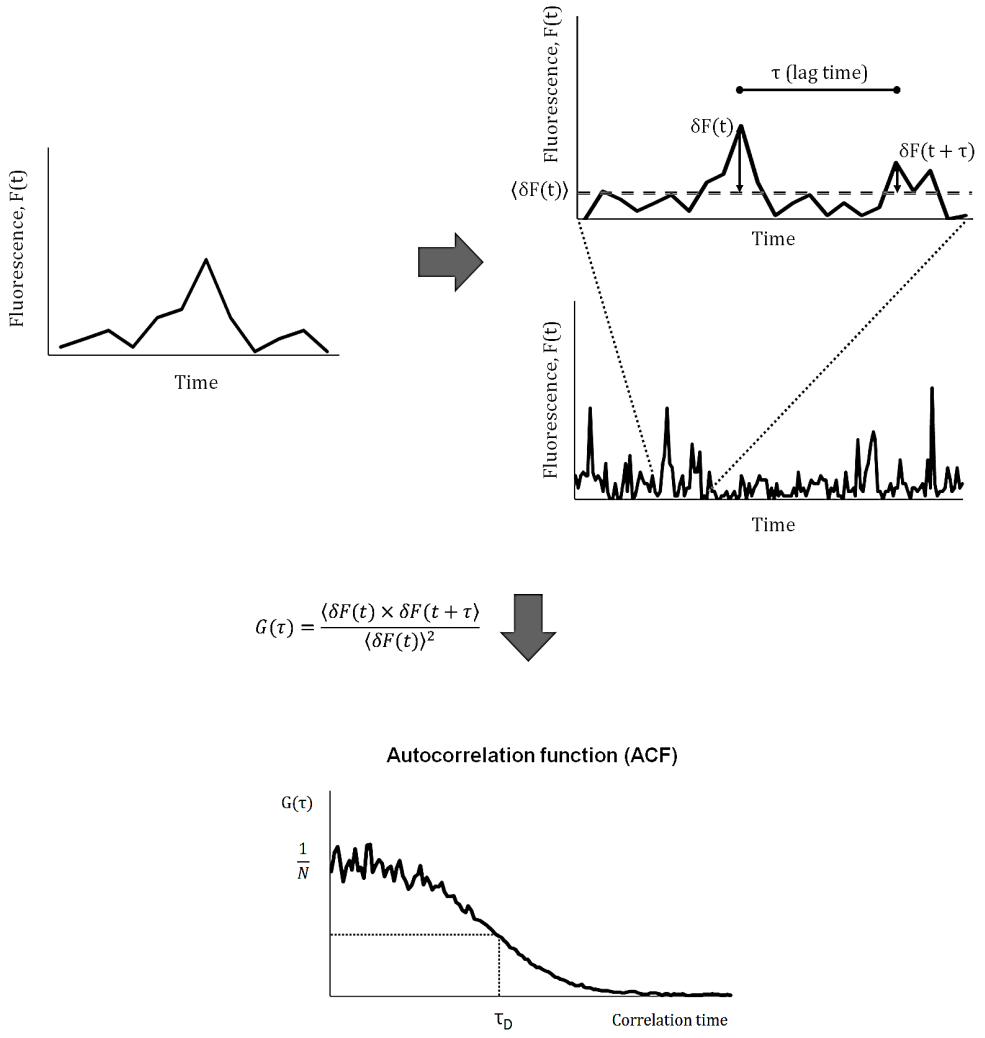


Figure 12. Fluorescence correlation spectroscopy analyzes the fluctuations of the fluorescence signal. The fluorescencently labelled particles move in and out from the detection volume (due to the Brownian motion) which causes the fluctuations in the fluorescence intensity. The intensity changes are followed and analyzed over time (F: fluorescence intensity, τ: lag time, t: time). The fluctuations are quantified by autocorrelating the recorded signals (observe the self similarity of the fluorescence signal in a time intervals). The experimental autocorrelation function (ACF) is fitted with a mathematical model to extract information such as molecular mobility or concentation (N: number of particles, τ_D: diffusion time).

The two color version of FCS, the fluorescence cross correlation spectroscopy (FCCS) in therory has been suggested in 1994 [93] and experimentally verified in 1997 [94]. The FCCS analyzes the movement of two differently (with spectrally distinct fluorophores) labelled particles to gain information about their mobilities or interactions. The technique is well suited to study direct protein-protein interactions, enzyme kinetics or dynamic colocalizations in biological samples [95].

The dual-focus or two-focus fluorescence correlation spectroscopy (2f-FCS) is an improved FCS-setup, which introduces an external ruler (two laterally shifted but overlaping laser foci with a fixed and well known distance) in the system and measures the absolute values of diffusion coefficients with high precision and accuracy, without the need of further referencing [91].
In recent years the FCS became a widely used technique to follow and study dynamic processes in biological systems. In our study we applied the 2f-FCS to analyze the diffusion properties and complex formation of the transcription factor STAT3.

1.7.2. Förster resonance energy transfer (FRET)

The resonance energy transfer initially was investigated by Jean Perrin at the beginning of the 20th century, and the correct theoretical basis was described by Theodor Förster in 1948, as a process in which energy is transferred in a nonradiative manner via long-range dipol-dipol coupling from a donor fluorophore (in electronic excited state) to an acceptor chromophore [96] (Figure 13).

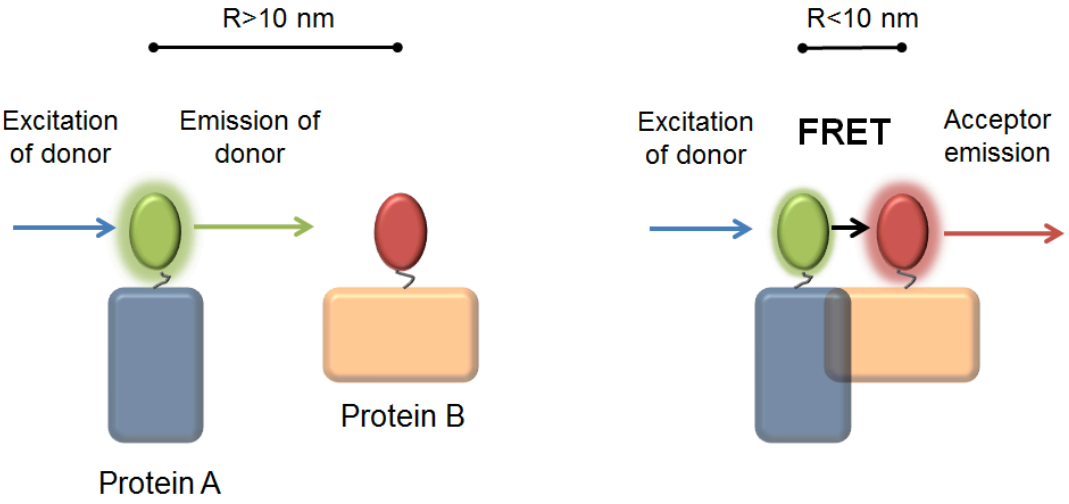


Figure 13: Basic principles of Förster resonance energy transfer (FRET). When the donor (green) and acceptor (red) fluoorophore are distant from each other, as a consequence of donor excitation, donor fluorescence will detectable. If the two fluorophores are located in close proximity, energy can transfer non-radiatively from the donor to the acceptor fluorophore (FRET) and can be detected as incrased acceptor fluorescence emission. Donor emission is reduced as a consequence of the energy transfer.

FRET is an acronym from Förster resonance energy transfer or from the oftenly used fluorescence resonance energy transfer, where fluorescence refers to the use of fluorescent donor and acceptor chromophores (energy is not transferred through fluorescence).
Energy transfer occurs between small distances (1-10 nm) and allows the detection of direct molecular interactions beyond the limit of conventional light microscopes (improved spatial resolution). The transfer rate is dependent on the sixth power of distance, thus FRET can be used as „spectroscopic ruler“ to reveal proximity relationships in biological macromolecules [97].
FRET can be performed inter- (donor and acceptor localized at different molecules) or intramolecularly (donor and acceptor are at the same molecule) and is a widely used technique in molecular biology to study direct interactions or conformational changes.
The energy transfer can be visualized in several ways and using different approaches, but in general three oftenly used strategies can be distinguished: acceptor photobleaching (APB), sensitized emission (SE) and fluorescence lifetime imaging (FLIM).
Sensitized emission (SE), is a quantitative imaging approach [98], in which only the donor fluorophore is excited, and as a consequence of FRET the acceptor fluorophore becomes excited instead, which can be detected as increased acceptor emission.
In fluorescence lifetime imaging (FLIM), the donor fluorescence quenching is detected, and can be determined as decrease of fluorescence decay time of the donor fluorophore in the presence of FRET [99].
In acceptor photobleaching (APB) technique, the acceptor fluorophore is selectively bleached and the donor fluorescence intensity is analyzed over time. If FRET occurs the disruption of the energy transfer (bleaching) leads to an increased donor emission as the consequence of losing the quenching effect
In our work we used the APB to follow the dimerization and structural changes of STAT3 prior and upon activation.

1.8. Hypothesis and aims

The transcription factor STAT3 plays crucial roles in many biological processes and the constitutively activation occurs in various human tumors. This aberrant activation validates STAT3 as a promising cancer drug target and intensive research focuses on the generation of specific inhibitors against the protein.

The design of inhibitor molecules undermining the malignant phenotype could be performed in different ways and directly effect different interfaces or domains of the STAT3 molecule, as SH2 domain (dimerization inhibitors), DNA-binding domain, or inhibitors against the N-terminal domain. Indirect targeting could be achieved by inhibition of upstream components of the pathway (tyrosine phosphorylation inhibitors) [100].

The dimerization of STAT3 is not restricted to „activation modus", but also occurs in latent state, in absence of tyrosine phosphorylation, as it is confirmed by various techniques like FRET [70] or BRET[69]. However the structural requirement of preformed dimers and the possible functions in context of STAT3 signalling is not known.

In our research we focused on the dimerization and complex formation of STAT3 prior and after stimulation. For the correct visualization we used fluorescence based microscopy techniques as two-focus fluorescence correlation spectroscopy (2f-FCS) or Förster resonance energy transfer (FRET) method.

For this purpose we focused on the following points:

- Generate fluorescently labelled STAT3 constructs for 2f-FCS and donor/acceptor pairs for FRET mesurements.
- Establish the sample preparation and micrsocopy setup for detecting molecular dynamics of STAT3 with two-focus fluorescence correlation spectroscopy.
- Optimize the imaging setup and analysis for the correct interpretation and visualization of the FRET signal between fluorescently labelled STAT3 molecules.

Given the previous findings in context of STAT3 dimerization, our gain was to analyze the structural requirement of the unphosphorylated STAT3 dimers, more specifically:

- Examine which interdomain interaction stabilize the preformed dimer (homotypic or heterotypic interdomain interaction)
- Identify which domain(s), and which amino acid residue(s) are critical in the dimerization of the non-activated STAT3 molecules.

While investigating the structural background of dimerization, our goals were:

- Visualize the conversion of STAT3 homodimers from preformed „non activated“ state to „activated“ form.
- Functionally analyze and identify the possible roles of preformed dimers in the STAT3 activation cycle.

Focusing on the N-terminal domain of STAT3 we were interested in:

- Interdomain interactions of N-terminal fragment with other structural domains of STAT3.

- N-terminal homotypic interactions in the stabilization of STAT3 tetramers on specific gene promoter regions.

- Structural requirements of STAT3 tetramerization.

2. Materials and methods

2.1. Materials

2.1.1. Chemicals and reagents

All chemicals and reagents were prepared according to pro analysi quality standards. All water solutions were prepared in double destilled water.

2.1.2. Cytokines and receptors

Recombinant human IL-6 (1400 U/μl) and soluble IL-6 receptor (sR) were prepared as described in [101] and [102].

2.1.3. Antibodies

Antibody	Recognized site	Source	Derived from	Company
Anti-STAT3 (C20)	STAT3 C-teminal region	polyclonal	Rabbit	Santa Cruz, USA
Anti-STAT3 (H190)	STAT3 N-terminal region	polyclonal	Rabbit	Santa Cruz, USA
Anti-pSTAT3 (pY705)	STAT3 phosphotyrosine 705 motive	polyclonal	Rabbit	Cell Signaling, USA
Anti-GAPDH (6C5)	GAPDH	monoclonal	Mouse	Santa Cruz, USA

2.1.4. Plasmids

All plasmid constructs were generated with the use of pcDNA5/FRT/TO expression vector (Invitrogen, USA).
The vector contains a hybrid human cytomegalovirus CMV/TetO2 promoter for high-level and tetracycline-regulated expression, a multiple cloning site (MCS), ampicillin resistance gene, FLP Recombination Target (FRT) site for Flp recombinase-mediated integration of the vector and hygromycin resistance for the selection of stable cell lines.

Name	Vector	Comments
eGFP	Clontech, USA	eGFP encoding plasmid
pSNAP-Cox8A	SNAP-tag control plasmid (New England Biolabs, USA)	cytochrome C oxidase subunit 8-2 fused to the N-terminal end of SNAP-tag
SNAP-eGFP	pcDNA5/FRT/TO	SNAP tag fused to eGFP with a TGDDDDKA linker (positive FRET control)
eGFP-STAT3	pcDNA5/FRT/TO	eGFP fused to the N-terminal end of STAT3α
STAT3-eGFP	pcDNA5/FRT/TO	eGFP fused to the C-terminal end of STAT3α
SNAP-STAT3	pcDNA5/FRT/TO	SNAP-tag fused to the N-terminal end of STAT3α
STAT3-SNAP	pcDNA5/FRT/TO	SNAP-tag fused to the C-terminal end of STAT3α
ΔNTD-STAT3-eGFP	pcDNA5/FRT/TO	N-terminal (aa 1-125) deleted STAT3α, eGFP fused to the C-terminal end of STAT3
ΔTAD-STAT3-SNAP	pcDNA5/FRT/TO	C-terminal (aa 710-770) truncated STAT3α, SNAP-tag fused to the C-terminal of STAT3
SNAP-NTD	pcDNA5/FRT/TO	SNAP-tag fused to the N-terminal domain (aa 1-125) of STAT3α
SNAP-NTD(L78R)	pcDNA5/FRT/TO	SNAP-tag fused to the N-terminal domain (aa 1-125) of STAT3α, where L78 residue is mutated
SNAP-STAT3(L78R)	pcDNA5/FRT/TO	N-terminal residue L78 mutated, SNAP-tag fused to the N-terminal end of STAT3α
STAT3(L78R)-SNAP	pcDNA5/FRT/TO	N-terminal residue L78 mutated, SNAP-tag fused to the C-terminal end of STAT3α
eGFP-STAT3-SNAP	pcDNA5/FRT/TO	eGFP fused to the N-terminal, SNAP-tag to the C-terminal of STAT3α
eGFP-STAT3(R609Q)-SNAP	pcDNA5/FRT/TO	eGFP fused to the N-terminal, SNAP-tag to the C-terminal of STAT3α, where R609 residue is mutated

Table 2. Summary of plasmid constructs used in this thesis.

2.2. Cell lines and culture techniques

2.2.1. Prokaryotic cells and cultivation

For molecular cloning the following *E.coli* bacterium strains were used:

JM83: F^- ara Δ(lac-proAB) rpsL (Str^r) [ϕ80 d lacΔ (lacZ)M15] thi

DH5alpha: F^- endA1 glnV44 thi-1 recA1 relA1 gyrA96 deoR nupG Φ80d*lacZ*ΔM15 Δ(*lacZYA-argF*)U169, hsdR17(r_K^- m_K^+), λ–

XL-10: endA1 glnV44 recA1 thi-1 gyrA96 relA1 lac Hte Δ(mcrA)183 Δ(mcrCB-hsdSMR-mrr)173 tet^R F'[proAB $lacI^qZ$ΔM15 Tn10(Tet^R Amy Cm^R)]

XL1-blue: endA1 gyrA96(nal^R) thi-1 recA1 relA1 lac glnV44 F'[::Tn10 $proAB^+$ $lacI^q$ Δ(lacZ)M15] hsdR17(r_K^- m_K^+)

Recombinant *E. coli* cells were cultivated in LB-medium with ampicillin (100mg/l). For long-term storage, the bacterial cells were stored at -80°C with 20% glycerin.

LB-(Luria-Bertani) medium:	5 g/L	NaCl
	5 g/L	yeast extract (Difco, USA)
	10 g/L	Trypton (Difco, USA)

2.2.2. Transformation of competent bacteria

Plasmid DNA (1-5 ng) or 10-20 µl from the ligation solution was mixed with 100 µl competent bacteria and incubated for 30 minutes on ice. Incubation was followed by a heat shock at 42°C for 90 seconds and with another incubation step on ice for 120 seconds. The mixture was plated on a selective (ampicillin, 100 mg/l) LB-agar plate, and incubated overnight at 37°C. Clones were screened and selected for further analysis.

2.2.3. Eukaryotic cells and cultivation

The eukaryotic cell lines (Cos-7, HeLa and HepG2) were cultivated in the indicated cell culture media, supplemented with fetal calf serum (FCS) and penicillin/streptomycin. Cells were grown at 37°C in a humidified atmosphere containing 5% CO_2 and passed by trypsinization. First, cells were washed with phosphate buffered saline (PBS), followed by the addition of trypsin/EDTA and an incubation step for 5 minutes at 37°C. Cells were detached with the addition of growth medium followed by gentle pipette action and seeded in new culture flask with a delution from 1:5 to 1:10. Long term storage was carried out in liquid nitrogen at -150°C with the addition of 10% dimethyl sulfoxide (DMSO).

Cos-7: african green monkey kidney fibroblast-like cell line (A.T.C.C., USA), cultivated in phenol red free DMEM-medium (Gibco, Germany), supplemented with 10% FCS and 1% penicillin/streptomycin.

HeLa : human cervix adenocarcinoma cell line (A.T.C.C., USA), cultivated in phenol red free DMEM-medium (Gibco, Germany), supplemented with 10% FCS and 1% penicillin/streptomycin.

HepG2: human liver hepatocellular carcinoma cell line (A.T.C.C., USA), cultivated in DMEM/F12-Medium (Gibco, Germany), supplemented with 10% FCS and 1% penicillin/streptomycin.

PBS (phosphate buffered saline):	200 mM	NaCl
	2,5 mM	KCl
	8 mM	Na_2HPO_4
	1,5 mM	KH_2PO_4
		pH 7.4

2.2.4. Transfection of eukaryotic cells

Transfection was performed transiently, when cells reached a density of 60-80% confluence, by using transfection reagent TransIT-LT1 (Mirus Bio LLC, USA), and OPTIMEM (Gibco, Germany) as serum free medium. Conditions and protocols used according to the manufacturer´s instructions.

2.3. Molecular biology techniques

2.3.1. Polymerase chain reaction (PCR)

Polymerase chain reaction is a widely used technique in molecular biology to specifically amplify single DNA sequences. The name of the method is derived from the DNA polymerase, which is the key component of the DNA replication procedure.
Components required for a PCR reaction are: DNA template (DNA sequence to be copied), primers (single stranded oligonucleotides, sense and antisense), heat stable DNA polymerase (Phusion HF, New England Biolabs, USA), dNTPs (deoxyribonucleotide triphosphates, building blocks for DNA) and buffer solution (generating the optimal conditions for the reaction).
The three basic steps of a PCR reaction are: denaturation, annealing and extension step, which are repeated 25-35 times, taking place at different temperatures. In the end of the reaction millions of copies generated from the target DNA sequence.

PCR reaction mixture:	5 ng	Template DNA
	500 pmol	Sense primer
	500 pmol	Antisense primer
	1 mM	dNTP mix
	1U	DNA polymerase
	10 µl	Reaction buffer

add H_2O to 50 µl

PCR reaction cycles:

	Initial denaturation	98°C	(30s)
25-35 cycles {	Denaturation	94°C	(5-10s)
	Annealing	48°C	(10-30s)
	Extension	72°C	(15-30s)
	Final extension	72°C	(5-10min)

2.3.2. Isolation of plasmid DNA

Plasmid MiniPrep:

A single bacterial colony was picked from the plate, and inoculated in 3 ml ampicillin (100 mg/l) containing LB-medium. Incubated overnight at 37°C, using vigorous shaking. In the next step, the bacterial cells were harvested by centrifugation (6000 rpm, 10 minutes, at room temperature), the pellet was resuspended and plasmid DNA extraction and purification performed using QIAprep-Miniprep-Kit (Qiagen, Germany) according to the manufacturer´s protocol.

Plasmid MaxiPrep:

250 ml ampicillin (100 mg/l) containing LB-medium was inoculated with 100 µl bacterial suspension, and incubated overnight at 37°C with vigorous shaking. Next, bacterial cells were harvested by centrifugation (6000 rpm, 15 minutes, at 4°C), the pellet was resuspended and plasmid DNA extraction and purification was performed using QIAprep-Maxiprep-Kit or with HiSpeed Maxy Kit (Qiagen, Germany) according to the manufacturer´s protocol.

2.3.3. Determination of the plasmid DNA concentration

Plasmid DNA concentration was calculated based on the value of OD_{260nm} (optical density at 260 nm) using UV-spectrophotometer (NanoDrop, ThermoScientific, USA). The ratio of OD 260 and OD 280 nm indicates the purity of the DNA (for pure DNA: OD_{260nm} / OD_{280nm}: 1.8-2.0).

2.3.4. Digestion of DNA using restriction endonucleases

DNA digestion with restriction endonucleases was performed according to the manufacturer´s protocol. In analytical digestion 0.5-1 µg, for preparative 2-5 µg DNA was used. In case of digestion with two endonucleases, the selected buffer ensured at least 75% efficiency for both enzymes. After digestion, DNA-fragments were analyzed with agarose gel electrophoresis.

2.3.5. Agarose gel electrophoresis

Gel electrophoresis is used in molecular biology to separate a mixed population of DNA molecules from 50 bp to several kilobases. The method is based on the applicaton of an electric field to move the negatively charged molecules through an agarose matrix. Larger DNA fragments migrate more slowly and move smaller distances than the shorter ones, therefore DNA fragments of different size can be seperated from each other.
DNA samples were mixed with 1/10 volume of 10 × loading buffer, loaded on a 1% agarose gel (Seakem-LE-Agarose, Biozym, Germany in TAE-Puffer) and separated by using an electric field of 5V/cm^2.
DNA was visualized with UV-light and the size of the DNA-fragments was estimated using 1 Kb DNA ladder (Invitrogen, Germany).

10 × DNA loading buffer:	25%	Ficoll
	0.4%	Xylencyanol blue
	0.4%	Bromophenol blue

1 × TAE:	40 mM	Tris base
	20 mM	Acetic acid
	1 mM	EDTA

2.3.6. Isolation of DNA fragments

After agarose gel electrophoresis, the appropriate DNA bands were excised from the agarose gel. Elution and purification was performed using QIAquick-Gel-Extraction-Kit (Quiagen, Germany) according to the to the manufacturer´s protocol.

2.3.7. Ligation of DNA fragments

Purified, double-stranded DNA fragments were ligated to the linearized plasmid (molar ratio 3:1) with T4 DNA ligase (in 10 × ligation buffer) and incubated at room temperature for 2-4 hours. Following the incubation step, ligated DNA samples were transformed into competent *E. coli* cells.

2.3.8. DNA sequencing

DNA sequencing analysis was performed by MWG Biotech AG (Martinsried, Germany) using the appropriate sequencing primers.

2.3.9. Site directed mutagenesis

Site directed mutagenesis was performed by using QuickChange mutagenesis kit (Agilent Technologies, USA) to introduce mutations into STAT3.
A pair of primers was used to generate L78R mutation into the wild type STAT3. They are: 5-'CAAGAGTCCAATGTCCGCTATCAGCACAACCTTC-3' and 5'-GAAGGTTGTGCTGATAGCGGACATTGGACTCTTG-3'.

2.3.10. Reporter gene assay

A reporter gene assay was used to study the induction of the α2-macroglobulin promoter by STAT3.
HepG2 cells were grown in six-well plates and transfection was performed with 1 µg β-galactosidase expression vector (pCR3lacZ, Pharmacia, Sweden), 300 ng of luciferase reporter construct (α2-macroglobulin) and the indicated plasmid constructs using TransIT-LT1 transfection reagent (Mirus Bio LLC, USA) according to the manufacturer´s instructions.
After 24 hours cells were stimulated for 4 hours, lysed and incubated on ice for 30 minutes. Following incubation the samples were centrifugated (14,000 rpm, 10 minutes, at 4°C), supernatants were collected and used for the further experiments. β-Gal measurements were performed with 100 µl cell extracts and 100 µl ortho-Nitrophenyl-β-galactoside (ONPG) in 500 µl β-Gal buffer. Samples were incubated at 37°C, and the reaction was stopped with the addition of 500 µl Na_2CO_3. Absorbance was measured at 420 nm. Luciferase assays were performed using a luciferase assay kit (Promega, Germany) and values were normalized to transfection efficiencies derived from β-Gal expression.

β-galactosidase buffer:		
	60 mM	Na_2HPO_4
	40 mM	NaH_2HPO_4
	1 mM	KCl
	1 mM	$MgCl_2$
	3.86 ml/l	β-Mercaptoethanol

2.4. Protein analysis and immunological methods

2.4.1. Protein extraction

All steps of protein extraction were performed at 4°C with pre-cooled buffers. Cells were washed with PBS, collected and incubated with 150 µl RIPA lysis buffer for 30 minutes on ice. After vortexing, the sample was centrifuged (14,000 rpm, 10 minutes, at 4°C), supernatants were collected and stored for further analysis at -20°C.

RIPA-Lysisbuffer:		
	50 mM	Tris/HCl, pH 7.4
	150 mM	NaCl
	1 mM	EDTA
	0.5 %	Nonidet P-40
	1 mM	NaF
	15 %	Glycerol
	20 mM	β-Glycerolphosphate

Protease inhibitors were added to the lysis buffer prior to use.

Protease inhibitor:		
	1 mM	Na-Vanadate
	0,5 mM	EDTA
	0,25 mM	PMSF
	5µg/ml	Aprotinin
	1µg/ml	Leupeptin

2.4.2. Determination of protein concentration

Protein concentrations were determined using Bradford assay. The method is based on the detection of the absorbance shift (465 nm to 595 nm) from the Coomassie Brilliant Blue G-250 dye upon protein binding.

The OD_{595nm} is directly proportional to the concentration of the proteins. For measuring the protein concentrations after extraction, 5 µl protein lysate was used with 200 µl Bradford reagent (BioRad, Germany) and ddH_2O in a total volume of 1000 µl. The protein samples were incubated for 5 minutes at room temperature and absorbance was measured at 595 nm.

2.4.3. SDS polyacrylamide gel electrophoresis (SDS-PAGE)

SDS-PAGE (sodium dodecyl sulfate polyacrylamide gel electrophoresis) is a common method for protein separation based on their electrophoretic mobility in denaturated conditions. Protein extracts (containing same amount of proteins: 20 µg) were denaturated by heating at 95°C for 5 minutes in Laemmli-buffer (4×) and centrifugated at 4°C (13,200 rpm, 30 seconds). After centrifugation, the samples were loaded on SDS gel and electrophoresis was performed with 35 mA at room temperature.

SDS-running puffer:	1,5	%	Tris-Base, pH 8.3
	7,2	%	Glycine
	0,5	%	SDS
4 × Laemmli-buffer:	40	%	Glycerol
	8	%	SDS
	250	mM	Tris/HCl, pH 6.8
	0,4	%	Bromphenolblue
	20	%	β-Mercaptoethanol
Separation gel:	10	%	Acrylamide
	375	mM	Tris/HCl, pH 8.8
	0,1	%	SDS
	0,02	%	TEMED
	0,1	%	APS

Stacking gel:	5	%	Acrylamide
	125	mM	Tris/HCl, pH 6.8
	0,1	%	SDS
	0,02	%	TEMED
	0,1	%	APS

2.4.4. Western blot and immunodetection

To detect protein of interest, the separated protein samples were electrically transferred to a polyvinilydene (PVDF) membrane (PALL, Germany) using the Western blot technique.

Anode buffer I:	300	mM	Tris-Base, pH 10.4
Anode buffer II:	25	mM	Tris-Base, pH 10.4
Cathode buffer:	400	mM	6-Aminohexanoic acid

After blotting, the PVDF membrane was blocked for 45 minutes with 10% bovine serum albumin (BSA) to prevent the non specific binding of primary/secondary antibodies. After blocking, the membrane was washed in TBS-N buffer for 5 minutes at room temperature. Following washing step, the primary antibody was deluted in TBS-N (1:1000) and the membrane incubated over night at 4°C.
Next day, primary antibody was removed and the membrane was washed three times for 10 minutes with TBS-N, followed by the addition of secondary antibody (1:2000 delution in TBS-N) and incubation for 1-1.5 hours. After incubation, the membrane was washed with TBS-N (three times, 10 minutes) and proteins were detected using ECL-detection system (Millipore, USA) with a chemiluminescence detektor LAS-4000 (FujiFilm, Japan).
For protein counterstaining, the PVDF membrane was incubated with stripping buffer, containing freshly added β-mercaptoethanol and incubated at 70°C for 25 minutes. Stripping was followed by blocking with 10% BSA, washing steps with TBS-N and addition of the primary antibody of interest and the previously described process was repeated.

TBS-N buffer:	20 mM	Tris/HCl, pH 7.4
	137 mM	NaCl
	0.1 %	Nonidet P-40
Stripping-buffer:	100 ml	20% SDS
	62.5 mM	Tris/HCl, pH 6.7

2.4.5. Blue native PAGE

Proteins can be separated from each other in non-denaturating conditions using the blue native page technique [103].
Electrophoresis was performed with 30 µg protein, over night at 4°C with 40V. Fluorescence detection of STAT3-YFP was performed by using a fluorescence scanner (Typhoon, GE Healthcare, UK). The probe was excited with 488 nm laser line and the emission detected using 515-555 nm band filter setting.

5 × Probe buffer:	100 mM ε-Aminocapronic acid
	50 % Glycerol
	1 % Coomassie Brilliant-Blue G250
Cathode buffer:	50 mM Tricine
	15 mM BisTris, pH 7
	0.002 % CoomassieBrilliant-BlueG 250
Anode buffer:	50 mM BisTris/HCl, pH 7

2.5. Fluorescence techniques

2.5.1. Confocal laser scanning microscopy (CLSM)

The conventional light microscopes are well established devices to observe cell structures and compartments illuminated by visible light source. The confocal laser scanning microscopy (CLSM) uses a laser beam for illumination and combines the high-resolution optical imaging with improved depth selectivity [104]. The original technique was invented by Marvin Minsky in 1957 [105].
The key feature of CLSM is the acquisition of well focused images from various depth in the sample (optical sectioning) with a pinhole in front of the detector, which shields the emitted out of focus light [87] (Figure 14).

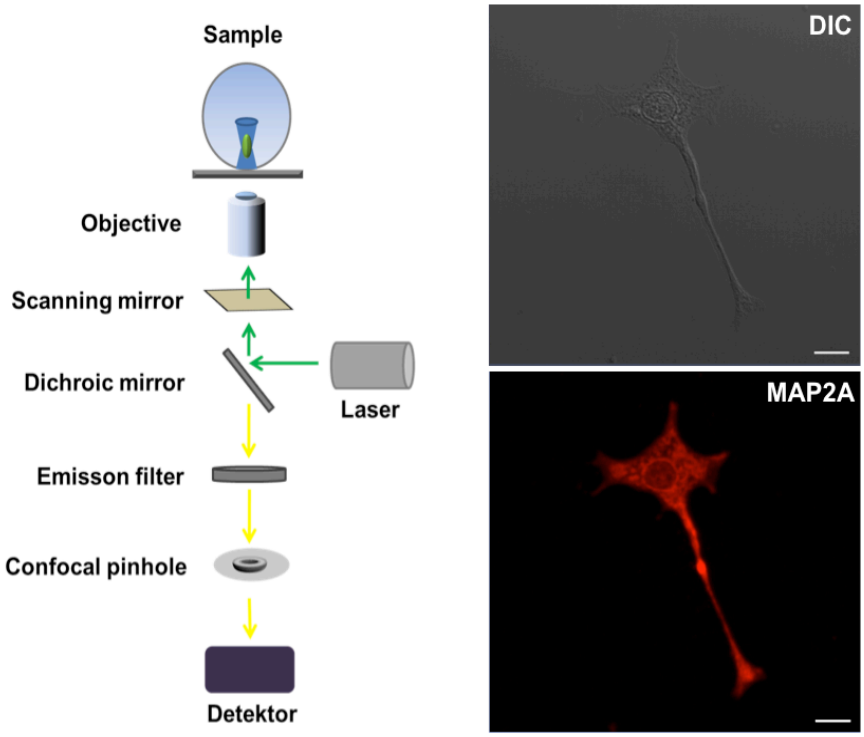


Figure 14: Schematic illustration of the confocal ligth path with respresentative image. The laser beam is focused on the sample and the fluorescence light is re-collected by the objective lens. The collected light passes through the dichroic mirror, emission filter and confocal pinhole to the detector (PMT or APD). The represenative images are ES cell differentiated neuron-like cells labelled with antibody against an early neuronal marker (MAP2A) and visualized by confocal imaging (DIC: differential interference contrast image). Bars, 10 µm.

2.5.2. Potein labelling with genetically encoded fluorophores

The term „fluorescence" was first coined by George G. Stokes in 1852 to describe the phenomenon when a mineral fluorite emits photons in the visible spectrum upon irradiation with ultraviolet light [106].
The main step for applying fluorescence in biological systems was the developement of genetically encoded fluorescent proteins (FPs). Specific labelling of biological molecules with fluorescent tags gives a very powerful tool to specifically follow subcellular localization or dynamics in living cells.

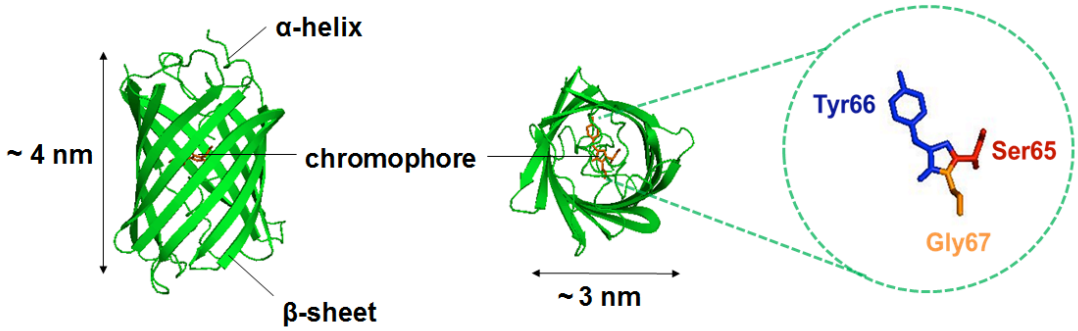


Figure 15: Structural background of green fluorescent protein (GFP). GFP adopts a 11-stranded β-barrell structure associated with an α-helix. The chromophore is located in the deep centre of the molecule and composed of a conjugated ring structure derived from amino acids Ser65, Tyr66 and Gly67 (RCSB Protein Data Bank accession numbers for GFP is 1GFL).

A widely used member of the FP-family is the green fluorescence protein (GFP). The original protein was firstly isolated by Osamu Shimomura from the jellyfish *Aequorea victoria* in 1960s [107]. 30 years later, Martin Chalfie presented GFP as a potential marker of gene expression [108]. The improvement of the original fluorophore and also the generation of new variants for biological research by protein engineering was pioneered by Roger Tsien [109].
For the discovery and development of *Aequorea victoria* GFP as a widely applied tool for cell biology Shimomura, Chalfie and Tsien were awarded the Nobel Prize in chemistry in 2008.
The wild type form of GFP which was found in *A. victoria* is a 27 kDa protein, which following translation folds into a 11-stranded β-barrell structure with an α-helix, which runs through the centre of the barrell.

The chromophore (4-p-hydroxy-benzylidene-5-imidazolinone) is formed deep in the hydrophobic core and composed of a conjugated ring structure derived from amino acids Ser65-Tyr66-Gly67 [110, 111] (Figure 15).
In our work we used the enhanced version of GFP (eGFP), carrying the S65T mutation, leading to improved spectral properties (brightness, photostability) of the fluorophore [109] and a F64L substitution, which results in a better folding efficiency at 37°C [112].

2.5.3. Chemical labelling of proteins

Besides the conventional method of protein labeling with genetically encoded fluorophores, there are other possibilities of specifically and covalently "tagging" the protein of interest with a label of choice using chemical modifications. So called, tag-based protein labeling methods can be grouped into three families: self labeling tags (tetracysteine tag, tetraserine tag), self labeling proteins (Halotag, SNAP-tag, CLIP-tag) and enzyme mediated labeling of tags (PPTase and biotin ligase) [113].
In our work we used a self labeling protein tag family member, the SNAP-tag, to generate fluorescently labeled protein samples for our investigations.

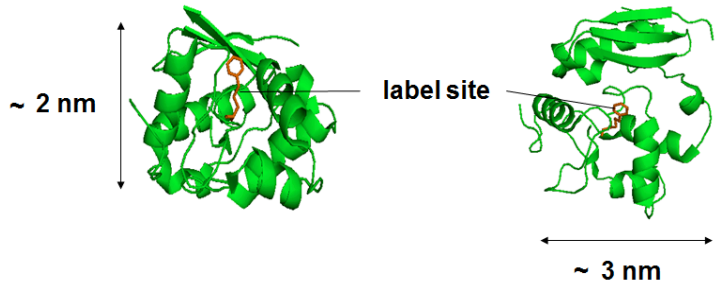


Figure 16: Structural organization of the SNAP-tag. The SNAP-tag is an engineered version of O^6-alkylguanine-DNA-alkyltransferase (AGT). The original form is a repair protein which plays a role in the defense against O^6-alkylation of guanine in DNA by alkylating agents. This repair is catalyzed by AGT, transferring the alkyl group to one of its own cysteine residues [114] (RCSB Protein Data Bank accession numbers for SNAP-tag is 3KZZ).

The SNAP-tag (Figure 16) is a 20 kDa protein, which is an engineered version of the DNA repair protein, O^6-alkylguanine-DNA-alkyltransferase (AGT)[115]. After subcloning and expression of the SNAP fusion protein construct, in the labelling reaction the modified AGT forms a covalent thioether bond specifically reacting with O^6-benzylguanine (BG) derivates carrying the fluorophore, resulting in covalently and specifically labeled

protein [116] (Figure 17). Using cell permeable fluorescent substrates, labeling can be also performed in living cells, making the SNAP-tag technology a very useful method in different fluorescence based microscopy applications as localizable calcium indicators, photoswitchable probes for super resolution microscopy techniques or FRET-based fluorescent sensors [117].

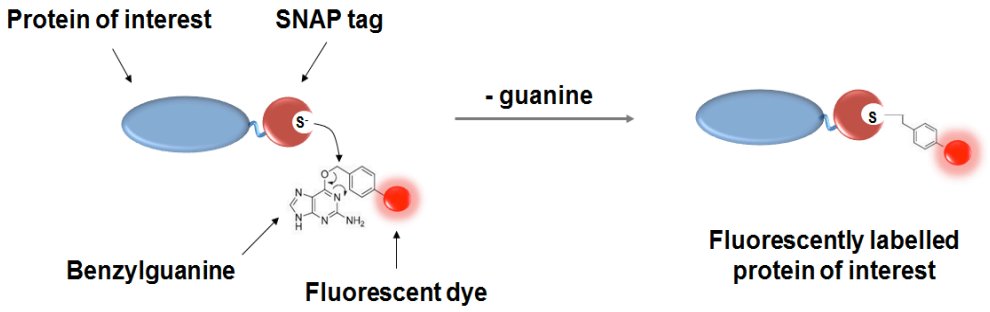


Figure 17: The SNAP-tag labelling mechanism. In the labelling reaction the SNAP-tag forms a covalent thioether bond with O^6-benzylguanine (BG) derivates carrying the fluorophore, resulting in covalently labelled protein of interest (modified from Ref. [117]).

2.5.4. SNAP-tag labelling procedure

The labelling of the SNAP-tag fusion proteins was performed using SNAP-Cell TMRstar substrate (New England Biolabs, USA). Labelling procedure was carried out according to the manufacturer´s protocol.

2.5.5. Imaging of fixed probes

Cells were seeded and grown on Lab Tek four well chamber slides (Nunc, Thermo Fisher Scientific, USA) in phenol red free medium. Transfection was performed as described previously.
After removing the medium, cells were washed two times in PBS^{++}. Fixation was performed by addition of 200 µl methanol to the cells, followed by incubation in the dark, for 20 minutes at room temperature.
After incubation, the cells were washed once with PBS^{++} and quenched with 50mM NH_4Cl (deluted in PBS^{++}) for 5 minutes.

Coverslips were mounted with Immu-Mount (Thermo Fisher Scientific, USA) and the samples kept in the dark until further investigation.

PBS^{++}:	1 mM	$MgCl_2$
	0.1 mM	$CaCl_2$
	in	PBS

2.5.6. Imaging of living cells

For live cell imaging, cells were plated on 35 mm glass bottom dishes (Ibidi, Germany) in phenol red free medium 48 hours before the experiment and transfected as described previously. Cells were imaged at 37°C and 5% CO_2 in the cell incubator a of Zeiss LSM 710 microscope (Carl Zeiss, Germany)
For living cell FRET experiments, cells were plated and seeded on eight well µ-Slides (Ibidi, Germany) and analyzed as described before.

2.5.7. Dual focus fluorescence correlation spectroscopy (2f-FCS)

The basic concept of 2f-FCS is the use of two laterally shifted and overlapping foci (detection volume) with a fixed and well known distance, serving as an external ruler in the experiment.
The analysis of the autocorrelation functions (ACFs) from each foci, and the cross-correlation function (CCF) between both foci allows one to calculate the absolute diffusion coefficents of the fluorescently labelled species without further referencing or calibration [91, 118].
The 2f-FCS experiments were performed on cell lysates from COS-7 cells, transfected with 2 µg plasmids, encoding eGFP, STAT3-eGFP or ΔNTD-STAT3-eGFP. Cells were lysed in BRIJ-96V lysis buffer (lacking glycerol).

BRIJ-96V-lysisbuffer:	0.1 M	Phosphate buffer, pH 8.0
	0.5 %	BRIJ-96V
	1.5 %	Glycerol
	0.5 mM	EDTA

Measurements were carried out using a setup based on a standard confocal epi-fluorescence microscope [119]. eGFP and eGFP-tagged fusion protein constructs were excited with a 470 nm laser beam (LDH-P-C-470B). Fluorescence emission light was split from the excitation light by using a clearup bandpass filter (490-520 nm). The light was focused by confocal optics with a pinhole diameter of 200 µm onto a single photon avalanche diode (SPAD, PDM series, Micro Photon Devices, Bolzano, Italy). The temperature was controlled using a home-made thermostatted device at 25°C [120].

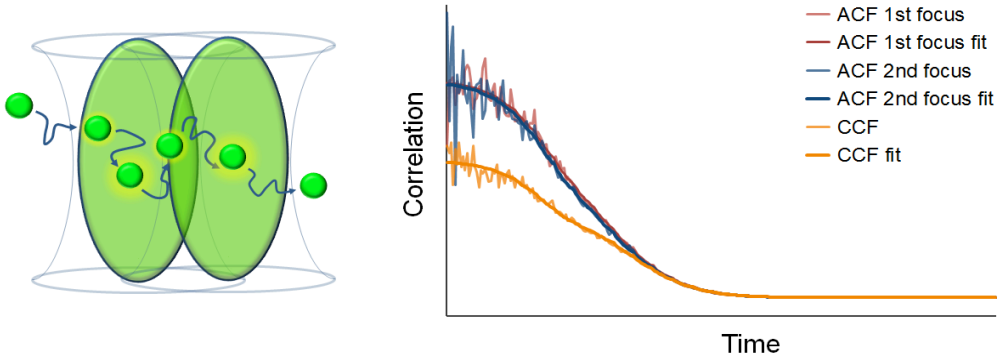


Figure 18: Basic concept of two focus FCS (2f-FCS) and the representative autocorrelation functions (ACFs). The 2f-FCS technique introduced an external ruler in the measurement of diffusion properties by generating two laterally shifted and overlapping laser foci, with a fixed and well known distance. Analyzing the ACFs in both foci and additonally the cross-correlation function (CCF) between both foci, diffusion properties of the measured particles can be identified without the need of further referencing or calibration.

An adequate model [91] for ACF/CCF is given by:

$$g(t,\delta,\mathrm{v}) = \frac{c}{4}\sqrt{\frac{\pi}{Dt}}\int \mathrm{d}z_1 \int \mathrm{d}z_2 \frac{\kappa(z_1)\kappa(z_2)}{8Dt + w^2(z_1) + w^2(z_2)} \times \exp\left[-\frac{(z_2 - z_1 - v_z t)^2}{4Dt} - 2\frac{(\delta - v_x t)^2 + v_y^2 t^2}{8Dt + w^2(z_1) + w^2(z_2)}\right] \quad (1)$$

where δ is the lateral distance between the detection volume centers, t is the lag time of correlation, v is particle velocity, x,y and z are Cartesian coordinates with z along the optical axis, c is the concentration of the fluorescent molecules and D is the diffusion coefficient.

The functions of κ(z) and w(z) are given by the following equations:

$$w(z) = w_0\left[1 + \left(\frac{\lambda_{ex} z}{\pi w_0^2 n}\right)^2\right]^{1/2} \quad (2)$$

and

$$\kappa(z) = 2\int_0^a \frac{d\rho\rho}{R^2(z)} \exp\left(-\frac{2\rho^2}{R^2(z)}\right) = 1 - \exp\left(-\frac{2a^2}{R^2(z)}\right) \quad (3)$$

with

$$R(z) = R_0\left[1 + \left(\frac{\lambda_{em} z}{\pi R_0^2 n}\right)^2\right]^{1/2} \quad (4)$$

where λ_{ex} and λ_{em} are excitation and emission wavelengths, n is the refractive index of the sample, α is the confocal pinhole radius, ω_0 and R_0 are fit parameters [91, 118].

2f-FCS experiments were performed with three independent samples per construct and 120 minutes detection time for each measurement.

The fitting procedure of experimental data is carried out globally for both the ACFs and CCF using a single particle diffusion model including triplet state correction (without necessity to imply a dual particle diffusion model suggesting a second slow-moving component).

The hydrodynamic radius (R_h) of the measured complexes was calculated by the Einstein-Stokes relation:

$$R_h = \frac{KT}{6\pi\eta D} \quad (5)$$

where R_h is the hydrodynamic radius, K is the Boltzmann-constant, T is the temperature, η is the viscosity and D is the diffusion coefficient.

Molecular mass estimation of the measured particles (assuming spherical symmetry) was calculated with the known molecular mass of eGFP (27 kDa) using the following equation:

$$MM_{sample} = \left(\frac{D_{eGFP}}{D_{sample}}\right)^3 \times MM_{eGFP} \quad (6)$$

where MM is the molecular mass, and D is the diffusion coefficient from 2f-FCS experiments.

2.5.8. Förster resonance energy transfer (FRET)

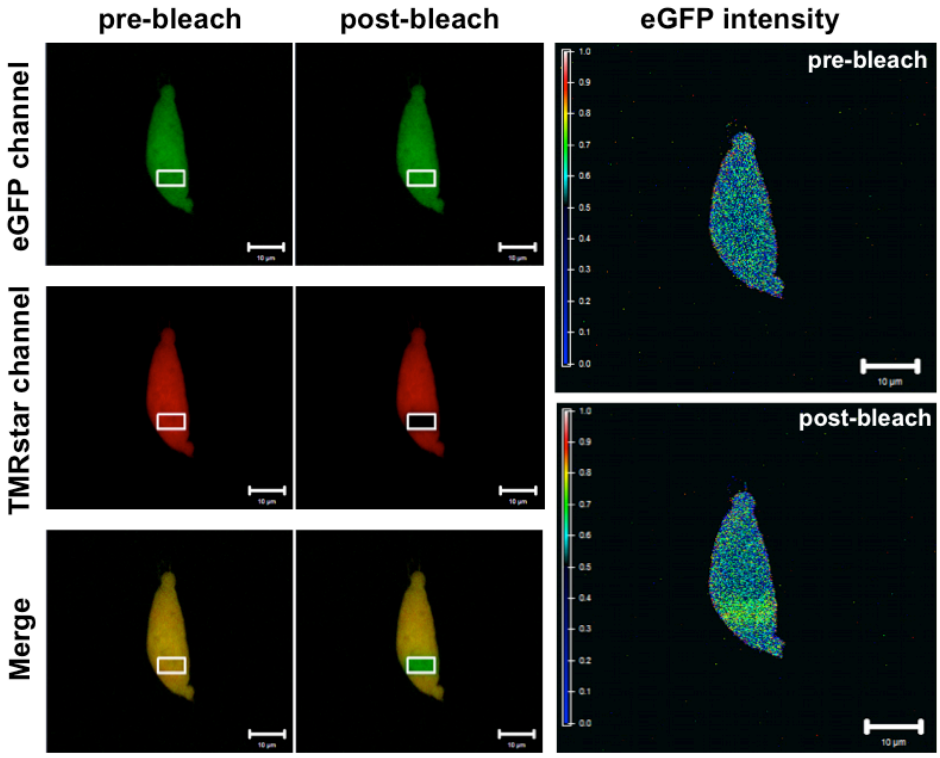
FRET is a widely used technique in cell biology to visualize and detect direct protein-protein, ligand-receptor or receptor-receptor interactions, but also applied in the design of biosensors to monitor ion concentrations [121] or to follow activities of protein kinases or small GTPases [122].
FRET can be detected in several ways and with different approaches, but in general three oftenly used strategies can be distinguished: acceptor photobleaching (APB), sensitized emission (SE) and fluorescence lifetime imaging (FLIM).
In this work we applied the acceptor photobleaching (APB) method (Figure 19). In APB, the acceptor fluorophore is selectively bleached (photochemical destruction leads to the permanent loss of the acceptor fluorophore´s ability to emit fluorescence) with a strong laser pulse in a defined area (region of interest). During the bleaching procedure, the fluorescence intensities of the donor fluorophore are analyzed before (D_{pre}) and after the bleaching procedure (D_{post}).

The difference between these donor intensities enables the calculation of the FRET efficiency ($FRET_{eff}$) [123] using the following equation:

$$FRET_{eff} = \frac{D_{post} - D_{pre}}{D_{post}} \quad (7)$$

where D_{pre} and D_{post} are the donor fluorescence intensities before and after photobleaching respectively.

A.



B.

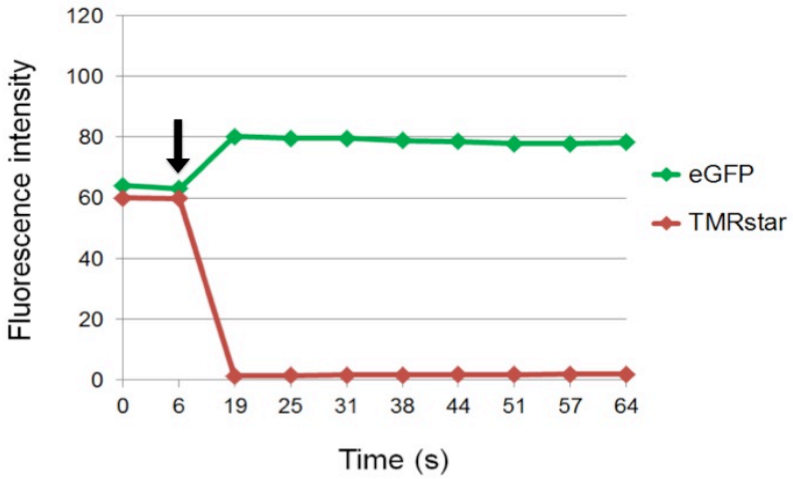


Figure 19 (A) Acceptor photobleaching (APB) FRET. Representative confocal images of fixed HeLa cells expressing SNAP-tag-eGFP fusion construct (positive FRET control, SNAP-tag is labelled with TMRstar substrate). Images were captured simultaneously and bleaching was performed in TMRstar (acceptor) channel. FRET was visualized as an increase in eGFP (donor) fluorescence. **(B) Fluorescence intensity traces from the representative images.** Two eGFP / TMRstar image pairs were collected before photobleaching in TMRstar channel and fluorescence intensity changes are followed over time. Bleach pulse is indicated by arrow.

In the FRET measurements, HeLa cells were examined with a LSM 710 confocal microscope (Carl Zeiss, Germany) using 40×, 1.1 NA water immersion objective with 3× zoom, and 512×512 pixel resolution. Emission filters were 505-550 nm for 488 nm excitation (eGFP detection, donor channel), and 575-616 nm for 561 nm excitation (TMRstar detection, acceptor channel). Images were collected using multi-track mode, with 2% laser intensity. Two eGFP / TMRstar image pairs were collected before the photobleaching (Figure 19B). Bleaching was performed in a rectangular region of interest (ROI) in TMRstar channel using the 561 nm laser line at maximum laser power (100% transmission) for 100 iterations (Figure 19A and B).
Cells displaying comparable levels of eGFP and TMRstar were selected for FRET analysis to avoid the artifacts and interfererences from the different donor-to-acceptor ratios. The measurement setup was established and optimized from the experiments based on the positive control.
FRET efficiencies (%) were calculated using Zen software (Carl Zeiss, Germany), based on the equation described before (in section 2.5.8, equation 7), taken into account the threshold and background noise in each channel.

For live cell FRET imaging, HeLa cells were plated and seeded on eight well μ-Slides (Ibidi, Germany) and 24 hours after transfection were placed in the cell incubator of Zeiss LSM 710 microscope (Carl Zeiss, Germany) at 37°C and 5% CO_2. FRET measurements were performed using the same setup (gain settings, resolution, optical components) as described before.

3. Results

3.1. Characterization of STAT3 fusion protein constructs

To investigate the homodimerization of STAT3 with FRET imaging we applied eGFP (enhanced green fluorescent protein) as donor fluorophore, and SNAP-tag, reacted with TMRstar substrate (cell permeable fluorescent label, based on tetramethylrhodamine) as acceptor molecule.
To get access to all possible FRET pair combinations, the target protein was labelled N- or C-terminally with the donor or with the acceptor fluorophore representing four different fusion protein constructs for the experiments (Figure 20).



Figure 20: Summary of differently labelled STAT3 constructs used in FRET experiments. eGFP-tagged STAT3 proteins serve as donors, SNAP-tag fusion constructs labelled with TMRstar substrate are the acceptor molecules. All four donor/acceptor fusion proteins were used in different combinations as FRET pairs in this study.

To study the expression and functional properties of STAT3 fusion constructs, HeLa cells were transfected with plasmids encoding SNAP-STAT3, STAT3-SNAP, eGFP-STAT3 or STAT3-eGFP. Cells were stimulated with IL-6 and soluble IL-6 receptor (sR) for 30 minutes or left untreated, lysed and analyzed by immunoblotting (Figure 21A).
After cytokine stimulation, all constructs showed specific phosphorylation at the tyrosine residue 705, demonstrating that labelling with eGFP or SNAP-tag (N- or C-terminally) does not interfere with the phosphorylation of the fusion protein. After stripping, the blot was reprobed with antibody against STAT3 (Figure 21A lower panel).
For further characterization, differently tagged STAT3 proteins were expressed in HeLa cells and the nuclear translocation (as a consequence of activation) was followed in real time with confocal microscopy after IL-6/sR addition (Figure 21B).

All four constructs accumulated in the nucleus in response to cytokine treatment, indicating that tagging or labelling does not affect the activation or the transport of the labelled STAT3 molecules.

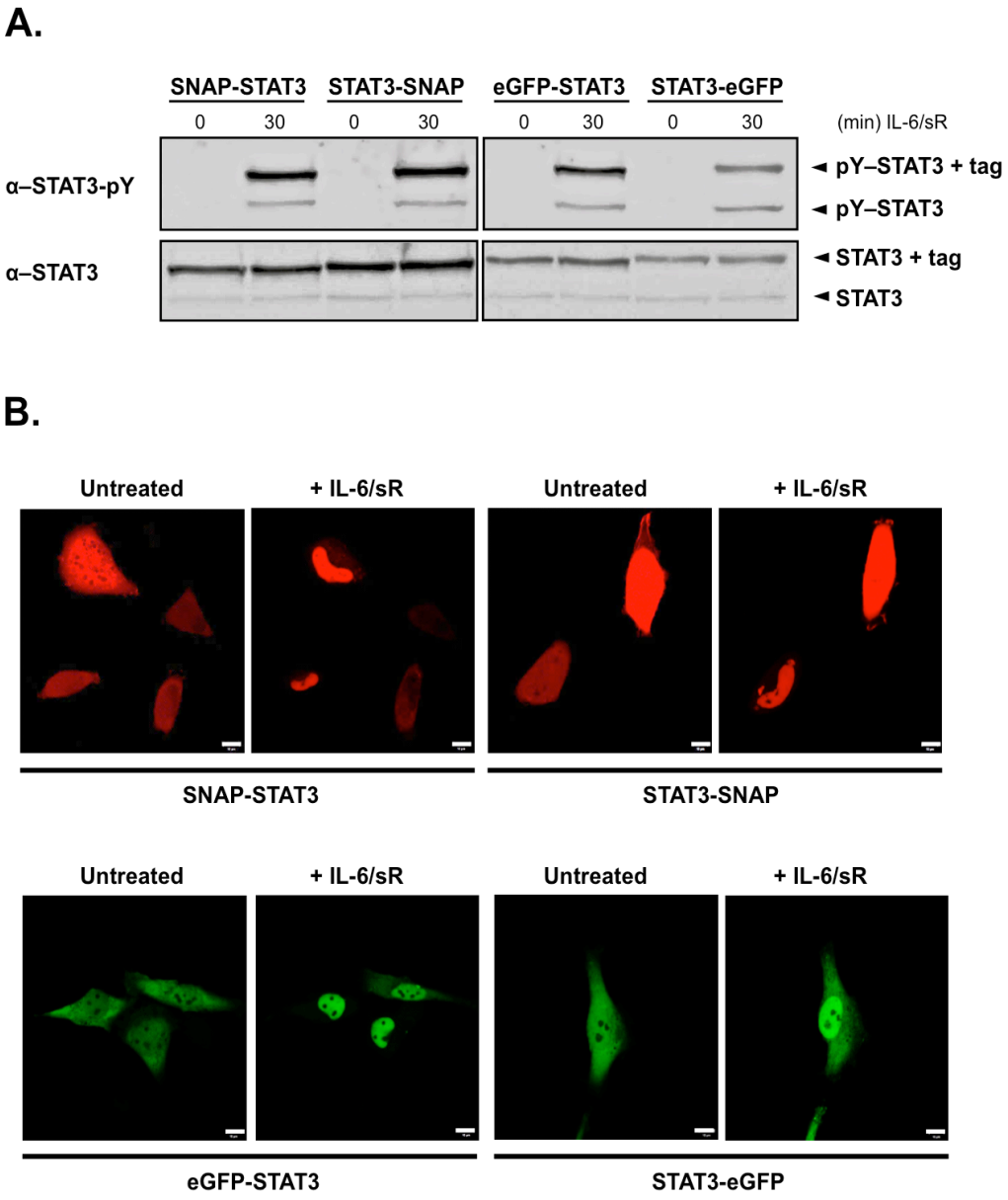


Figure 21: (A) Functional analysis of STAT3-tag constructs. HeLa cells were transfected with the indicated expression vectors encoding SNAP-STAT3, STAT3-SNAP, eGFP-STAT3 or STAT3-eGFP. Cells were stimulated with 20 ng/ml IL-6 and 500 ng/ml soluble IL-6 receptor (sR) for 30 minutes, or left unstimulated. Lysates were analyzed by western blotting using STAT3 phosphotyrosine 705 (STAT3-pY) and STAT3 specific antibodies. **(B) Ligand induced nuclear accumulation of STAT3 fusion proteins.** Localization of the fluorescently labelled STAT3 followed in real time after stimulation with 20 ng/ml IL-6 and 500 ng/ml soluble IL-6 receptor using confocal microscopy in living HeLa cells. Bars, 10 µm.

In summary the results confirmed that fluorescence labelling of STAT3 (N- or C-terminally) does not interfere with the activation or nuclear translocation of the protein, which is in good agreement with previously published data from our laboratory [81] and from others [124]. Thus, the fusion proteins represent functional molecules for further experiments.

3.2. Control experiments for acceptor photobleaching FRET (APB FRET)

To monitor the interactions and conformational changes between two fluorescently labelled STAT3 molecules, we analyzed FRET with acceptor photobleaching technique (Figure 22). In general, when a suitable donor and acceptor fluorophore are in close proximity, non radiative energy transfer (FRET) can occur between the molecules.

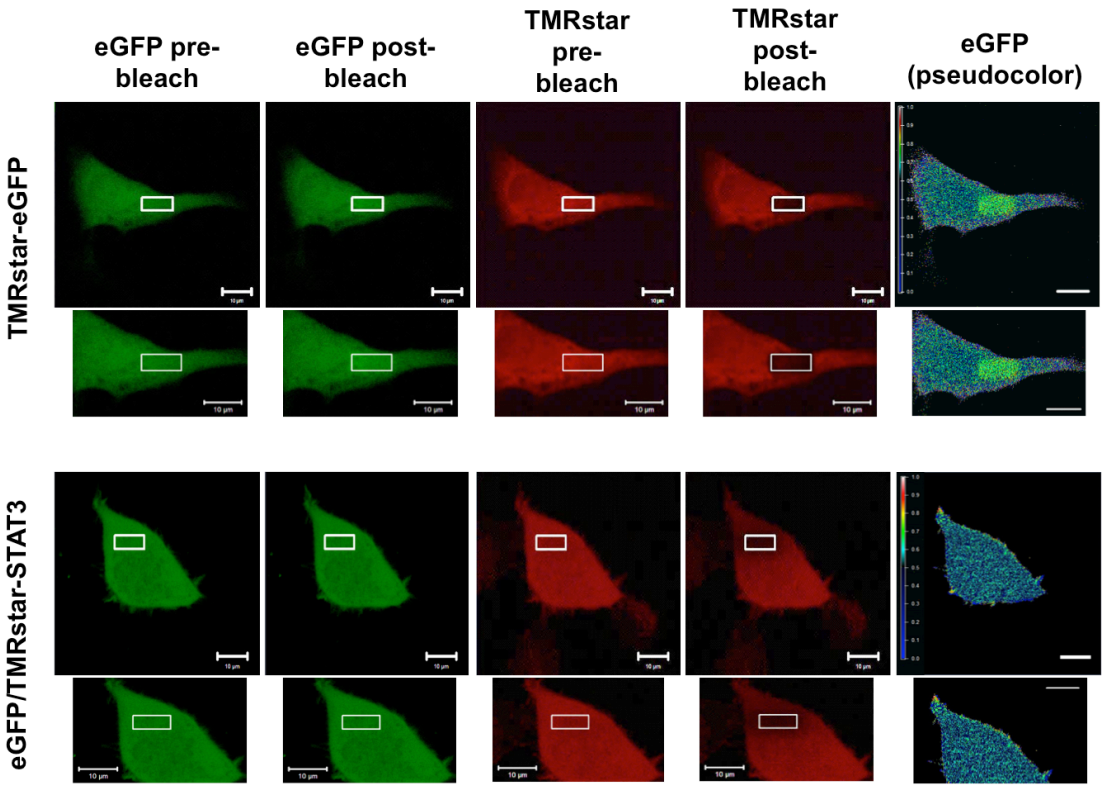


Figure 22: Acceptor photobleaching FRET (APB FRET). As positive FRET control, TMRstar labelled SNAP-tag-eGFP fusion construct (TMRstar-eGFP) showed specific increase of eGFP (donor) fluorescence after acceptor (TMRstar) bleaching in a rectangular region of interest, as it is visualized in a pseudocolor image of eGFP intensity changes. In the negative control, where eGFP was coexpressed with TMRstar-STAT3, no intensity changes in eGFP signal was visible after bleaching of TMRstar. Bars, 10 µm.

Disruption of the energy transfer by selective bleaching of acceptor molecules (TMRstar) leads to an increase in donor (eGFP) fluorescence signal as a response to loss of the quenching effect.
The intensity changes in donor fluorescence were followed over time, prior and after the photobleaching procedure (Figure 22), quantified (Figure 23) and applied to determine and analyze direct interactions or proximity changes in the measured samples.

Although eGFP is a well documented donor fluorophore in various FRET systems [125, 126] and SNAP-tag technology is also well established in time-resolved FRET (TR-FRET) applications [127], combination of the two labelling methods for quantitative fluorescence imaging in biological systems is not typical.
There are publications reporting the use of eGFP-tetramethylrhodamine (TMR) dye pair for FRET detection [128, 129], but (to our knowledge) there is no published data from the combined use of eGFP and TMR-labelled SNAP-tag for FRET applications. To take this into consideration, essential control experiments were performed.
To set up the experimental conditions for FRET detection, background and maximal FRET signal were analyzed on the appropriate negative and positive FRET controls (Figure 23).

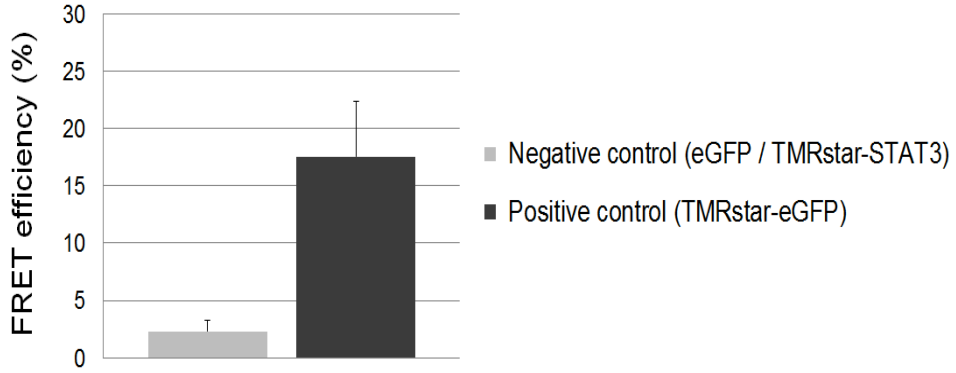


Figure 23. Representative FRET control experiments. eGFP alone, as donor fluorophore coexpressed with TMRstar-STAT3 construct served as negative control in FRET measurements (FRET efficiency: 2.28±1.01%). The positive control consisted of TMRstar-eGFP fusion contruct, where SNAP-tag was labelled with TMRstar substrate as acceptor fluorophore (FRET eff.: 17.55±4.84%). (N: 20 cells)

As negative control, eGFP was coexpressed with TMRstar-STAT3, where only a low FRET signal (2.28±1.01%) was detectable.
Additonal controls (Figure S1 in supporting material) including Cox8A (cytochrome oxidase 8-2 subunit, mitochondrial localization)-TMRstar coexpressed with eGFP (Cox8A-TMRstar/eGFP), or donor (eGFP) and acceptor (TMRstar-STAT3) alone samples also showed low efficiency values as 1.05±0.66%, 0.69±.1.12% and 0.60±0.98% respectively.
Energy transfer efficiencies of the positive control (SNAP-tag fused to eGFP with an eight amino acid long linker) was calculated as 17.55±4.84%, which represented the highest detectable FRET signal in our setup.
The selection of cells for FRET measurements and microscope settings were based on the positive control (relative expression levels of donor and acceptor are invariable), to avoid the influence of different donor-to-acceptor ratios, which beside other parameters (spectral overlap, molecular distance, applied method), were shown to effect and have impact on the measured FRET efficiency values [130].

3.3. STAT3 dimerization prior to and after activation

Dimerization of STAT3 before and after cytokine treatment was followed by the analysis of FRET signals between N-terminally, C-terminally, as well as N- and C-terminally labelled STAT3 monomers. The results from differently combined donor/acceptor pairs are discussed in more details in this section.

3.3.1. FRET between N-terminal domains

To follow the orientation of N-terminal domains during the dimerization procedure, eGFP-STAT3 and TMRstar-STAT3 were coexpressed (carrying donor and acceptor fluorophore at the N-terminus of the host molecule) and examined in nuclear and cytoplasmic region of fixed HeLa cells, before and after cytokine addition (Figure 24).
Prior to activation, a significant FRET signal ($p<0.001$) was detectable compared with negative control in both compartments (nucleus: 5.42±2.05%, cytoplasm: 5.50±1.91%).
The results indicate the existence of latent STAT3 dimers and the close proximity of N-terminal domains in this structure (Figure 25).

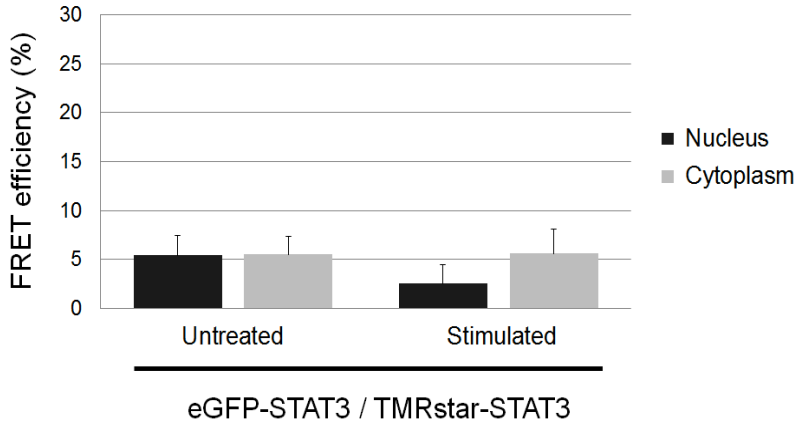


Figure 24. FRET efficiencies (%) between N-terminally labelled STAT3 molecules. Compared to negative control, a significant ($p<0.001$) FRET signal was detectable prior to stimulation in nuclear and cytoplasmic compartment in fixed HeLa cells. Stimulation (20 ng/ml IL-6 and 500 ng/ml soluble IL-6 receptor for 30 minutes, to provide optimal activation) leads to a decreased FRET signal, indistinguishable from negative control in the nuclear compartment ($p=0.517$). The FRET efficiency of the cytoplasmic population remained unchanged ($p=0.829$) compared to the untreated sample. (N: 38-40 cells)

Upon activation STAT3 molecules get phosphorylated, translocate to the nuclear compartment and acting as transcription factors through binding to specific DNA sequences. This activated and nuclearly localized STAT3 fraction has completely lost the FRET signal, indicating the separation of the N-terminal domains in this activated dimer conformation (Figure 25).

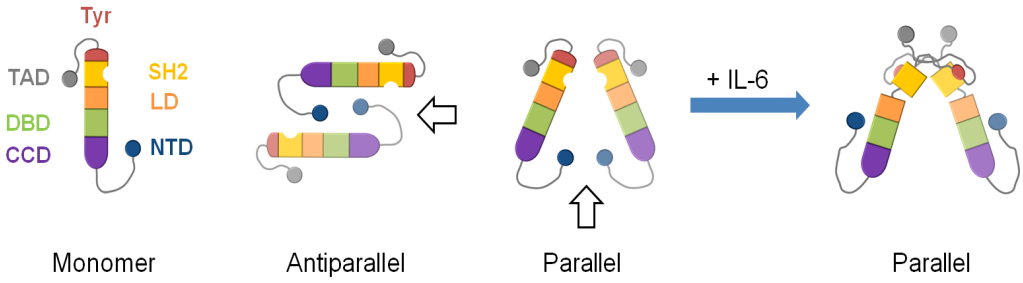


Figure 25. Possible STAT3 dimer formations. STAT3 monomers prior to stimulation dimerize in a parallel or antiparallel manner. In these conformations the N-terminal domains are localized close to each other (indicated by arrows). Following cytokine addition (+ IL-6), STAT3 molecules get phosphorylated and dimerize in a parallel form (stabilized by reciprocal interactions between pTyr residues and SH2 domains) where the N-terminal domains are widely separated from each other (NTD: N-terminal domain, CCD: coiled-coil domain, DBD: DNA binding domain, LD: linker domain, Tyr: tyrosine tail segment, TAD: transactivation domain).

FRET efficiencies in the cytoplasmic fraction, showed no significant difference (p=0.829) compared to untreated cells, assuming the existence of a non-activated/de-activated STAT3 dimer fraction in this compartment after 30 minutes of cytokine stimulation.
These results are in good agreement with data in context of STAT5a [131], where similar to our results, loss of FRET signal was detectable after stimulation between the N-terminal domains of CFP-STAT5a and YFP-STAT5a.
These findings suggest the separation of N-terminal domains upon activation, which leads to a structural rearrangement of the dimers to form the transcriptionally active conformation (Figure 25), where the N-terminal regions of each monomer are distantly located [15].

3.3.2. FRET between N- and C-terminal domains

We next examined the orientation of N- and C-terminal domains in respect to each other using two separate combinations of N- and C-terminally labelled STAT3 donor/acceptor pairs: eGFP-STAT3 / STAT3-TMRstar or TMRstar-STAT3 / STAT3-eGFP.
No differences were detectable between the two donor/acceptor constructs (Figure 26) and both measurements revealed an increased FRET signal ($p<0.001$) after stimulation compared to untreated samples.

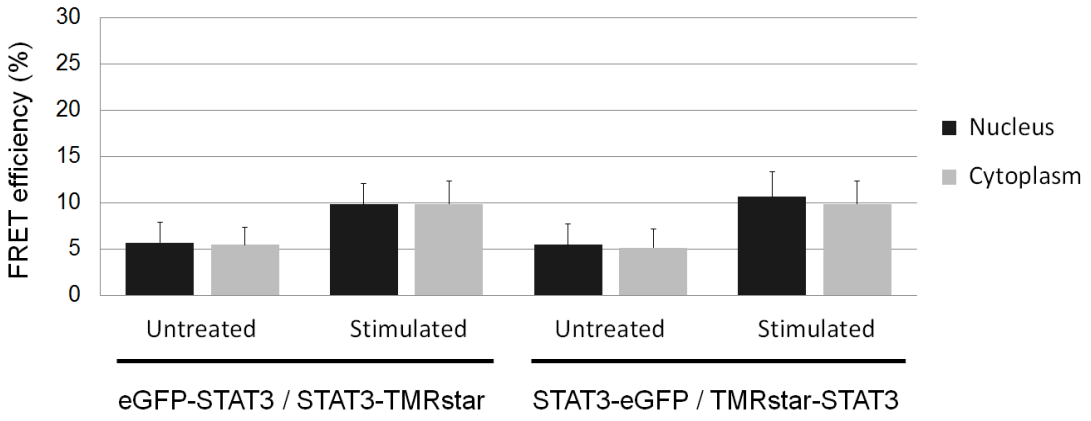


Figure 26. FRET efficiencies (%) from reciprocally tagged STAT3 constructs. Increased FRET signals were detectable after activation, indicating the closer proximity of N-terminus of one and C-terminus of the other monomer in the activated dimer. (N: 40 cells)

This almost doubled energy transfer efficiency indicates the closer orientation of the N-terminal domain of one and C-terminal end of the other monomer in the actived STAT3 dimer.
This close proximity of reciprocal domains could be simply explained as the consequence of reciprocal binding of the pTyr residue of one monomer to the SH2 domain of the other dimer partner, which decreases the distance between the N- and C-termini of the two STAT molecules in an activated dimer.
This hypothesis could also be supported by molecular dynamics simulation studies on STAT3 molecules [132, 133]. Their model showed the reciprocal binding of the C-terminal fragment to the SH2 domain, where the carboxy terminus of one molecule wraps around the SH2 domain of the other monomer. This phenomenon could structurally explain the increased FRET signal after stimulation.

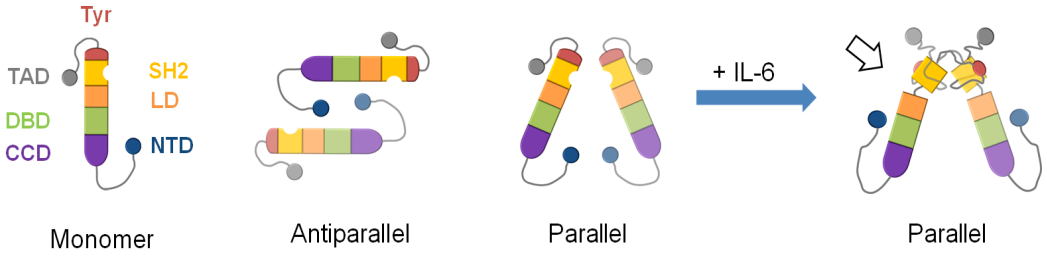


Figure 27. Closely oriented reciprocal domains in the activated STAT3 dimer. C-terminal domains are reciprocally associated with SH2 domains of the other monomers in the activated dimer and oriented into a closer proximity to the N-terminal regions (indicated by arrow).

To support our hypothesis, we analyzed a C-terminally truncated STAT3 form (ΔTAD-STAT3-TMRstar), which lacks the flexible TAD fragment of STAT3. This construct showed no increased FRET efficiency after activation (Figure S2 in supporting material).
Taken together, the previously measured separation of N-terminal domains upon activation, which is followed by pTyr-SH2 interaction and additionally a reciprocal binding between the C-terminal fragment of one and the SH2 domain of the other monomer in the activated dimer, structurally allows the reciprocal N- and C-termini fragments to get in closer proximity (Figure 27), which is detectable as an increased energy transfer efficiency in FRET measurements after cytokine addition.

3.3.3. FRET between C-terminal domains

In this section we followed the FRET signal between C-terminal domains of STAT3 molecules with the coexpression of STAT3-eGFP and STAT3-TMRstar protein constructs.
Prior to activation, a strong FRET signal was detectable between the C-terminal domains of two STAT3 monomers in a preformed dimer structure (nucleus: 10.09±1.79%, cytoplasm: 10.26±2.26%) indicating the close proximity of the C-terminal regions in this non activated dimer form.
FRET analysis revealed an increased energy transfer efficiency only in the nuclear compartment after cytokine treatment (Figure 28), in comparison with untreated cells (p=0.00016), which is in good agreement with the previously published FRET results on STAT3-CFP and STAT3-YFP contructs [70, 134].

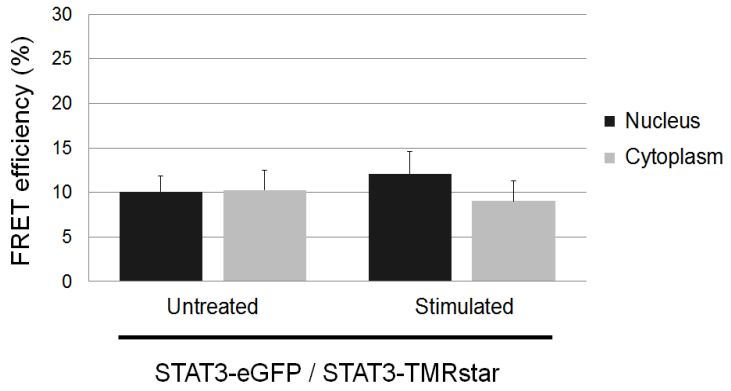


Figure 28. FRET efficiencies (%) from C-terminally tagged STAT3 constructs. An increased FRET signal was detectable in the nucleus after stimulation, whereas the cytoplasmic FRET remained unchanged (p=0.02). This slightly increased efficiency proposes the close orientation of the C-terminal domains prior to activation. (N: 36-40 cells)

The cytoplasmic fraction (similar to FRET experiments between the N-terminal domains of STAT3, Figure 24) showed equivalent proximity of the C-terminal fragments as in untreated cells, indicating the presence of non-activated dimers in the cytoplasm.
FRET-results showed the closer orientation of C-terminal domains after activation, however this difference compared to non-stimulated sample is not that robust to propose the antiparallel orientation, but rather parallel to parallel conversion upon activation (Figure 29).
The antiparallel dimers of STAT1 and STAT5 [131, 135] are stabilized by interactions between core fragments involving coiled-coil and DNA-

binding domains. However this interface was not visible in the unphosphorylated STAT3 structure [136] proposing a different type of dimer organization.
This parallel assembly of unphosphorylated STAT3 molecules seems to be in contrast to the N-terminal domains mediated antiparallel association of non activated STAT1 monomers, where the two SH2 domains are localized on the opposite end of the dimer [135].
In summary, the FRET results on C-terminally labelled STAT3 constructs strongly indicate the parallel-parallel conversion of STAT3 upon activation, from preformed to activated dimers (Figure 29).
In support of this hypothesis, measurements on ΔTAD-STAT3-TMRstar and STAT3-eGFP, showed no detectable changes in FRET efficiency after stimulation (Figure S3 in supporting material).

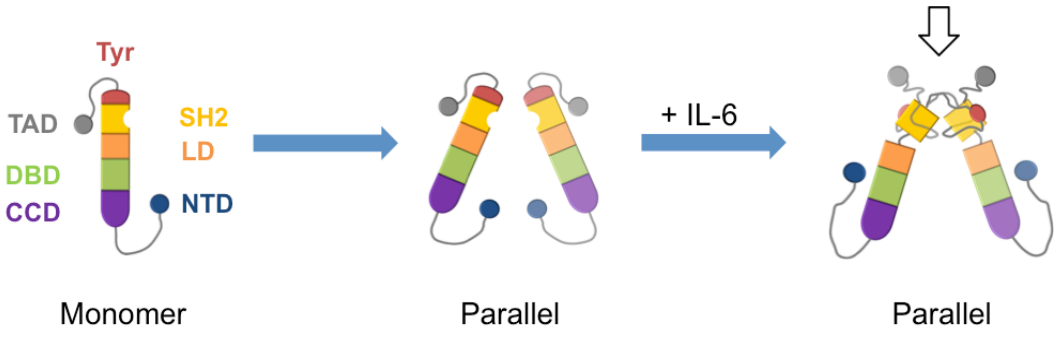


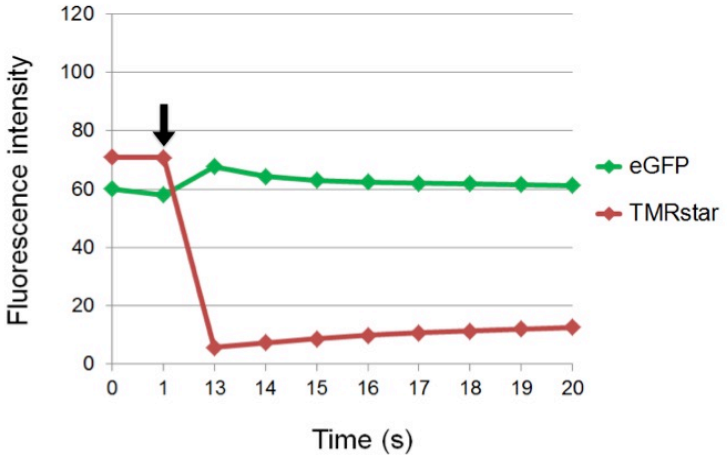
Figure 29. STAT3 monomers are associated prior and after stimulation in parallel arrangements. In both situations, the C-terminal domains are localized at the same end of the dimer, representing the parallel oriented dimer formations.

3.3.4. Live cell FRET

To strengthen our findings, FRET was measured in living HeLa cells using the same FRET method (Figure 30A) and experimental setup as in fixed cells.
Similar to measurements in fixed samples, distantly separated N-domains were detectable in STAT3 dimer structures in the nuclear region after stimulation (FRET efficiency: 2.53 ±1.87%), whereas the cytoplasmic population showed the same FRET signal as untreated cells (5.61±2.53%). Comparable to our *in vitro* findings, closer proximity of the reciprocal fragments (increased FRET signal betweeen eGFP-STAT3/STAT3-TMRstar pair) was also detectable, as well as the more closely oriented C-terminal domains in the nuclear compartment after cytokine addition

(11.45±2.13%), while the cytoplasmic fraction showed a less efficient energy transfer (8.85±2.45%).
In summary, the results from living cell FRET experiments confirmed the above presented data from measurements on fixed cells.

A.



B.

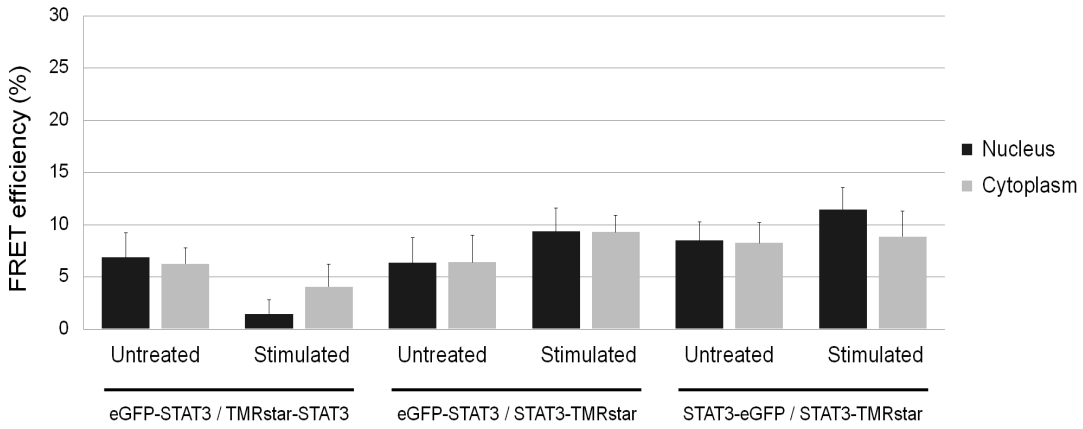


Figure 30 (A) Representative fluorescence intensity traces from live cell FRET measurement. Acceptor (TMRstar) was bleached similar to *in vitro* measurement, and donor (eGFP) emission followed over time. FRET is dectectable only in shorter time periods as a consequence of the recovery (by diffusion) of fluorescently labelled particles into the bleached area (bleach pulse is indicated by arrow). **(B) Summary of live cell FRET measurements.** Living HeLa cells measured and analyzed at 37°C and 5% CO_2 using the same experimental setup as for fixed samples. (N:14-20 cells)

3.4. Role of the N-terminal domain in dimerization of latent STAT3

To follow up the homodimer formation of latent STAT3, we were interested in the structural requirements for dimerization.
Structural studies on STAT1 demonstrated the importance of N-domain interactions in the formation of unphosphorylated dimers [135]. NTD-mediated preformed dimers play also a crucial role in the activation of STAT4 [137].
In context of STAT3, the nonphosphorylated core fragment (AA 137-688) was shown to exist only as a monomer form [136], indicating similarly to other members of the STAT-family the possible involvement of the N-terminal domains in latent dimerization.
To test this hypothesis, a deletion mutant of STAT3-eGFP, lacking the N-terminal domain (STAT3-ΔNTD-eGFP) was generated and investigated by fluorescence correlation spectroscopy (FCS) and FRET analysis.

3.4.1. Complex formation of latent STAT3 analyzed by dual-focus fluorescence correlation spectroscopy (2f-FCS)

Complex formation and diffusion properties of STAT3 and STAT3-ΔNTD were analyzed by dual-focus fluorescence spectroscopy (2f-FCS).
Cos-7 cells were transfected with STAT3-eGFP, STAT3-ΔNTD-eGFP or eGFP as a control. Cell lysates were prepared and analyzed with 2f-FCS. Fluctuations of the fluorescence signal (which arise from the movement of fluorescently labelled particles) were followed over time, and the generated autocorrelation functions (ACFs) (Figure 31) evaluated by using a one component fitting routine including triplet state correction.
Mathematical analysis of ACFs provided quantitative information about the fluorescently labelled molecules as diffusion coefficient or hydrodynamic radius (Table 3).
The calculated diffusion coefficient of eGFP ($1.03\pm0.04\times10^{-6}$ cm²/s), derived from our measurements, is in good agreement with the previously published data of eGFP mobility (0.9×10^{-6} cm²/s) in aqueous solution [138].
Full length STAT3 showed slower diffusion ($0.54\pm0.08\times10^{-6}$ cm²/s) than the N-terminally deleted mutant ($0.70\pm0.03\times10^{-6}$ cm²/s), indicating that the N-terminally truncated form is deficient in complex formation in unstimulated state.

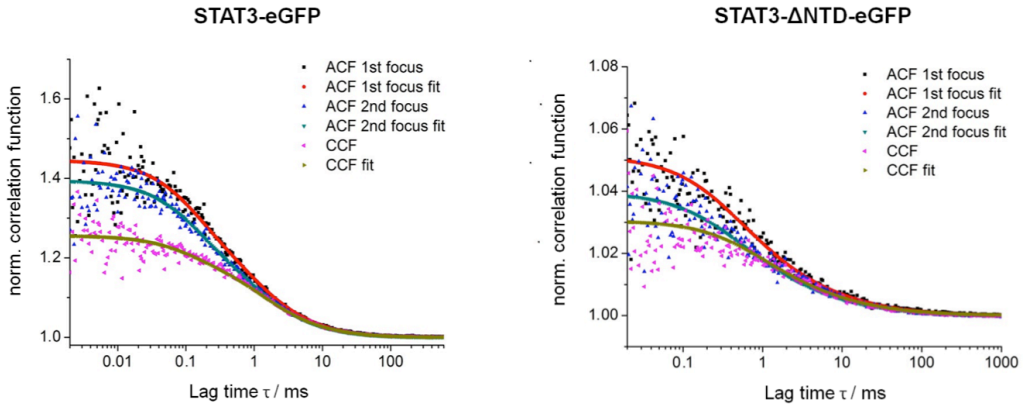


Figure 31. Representative autocorrelation functions (ACFs) from the analyzed samples using 2f-FCS experiments. Experiments were performed with three independent samples per construct and 120 minutes detection time for each measurement. Fitting procedure of the experimental data was carried out globally for both the ACFs and CCF using a single particle diffusion model including triplet state correction (ACF: autocorrelation function, CCF: cross correlation function).

To extract informations about the size of the detected complexes, hydrodynamic radii (according to Einstein-Stokes relation, Equation 5 in section 2.5.7.) and molecular masses (based on the measured diffusion coefficient and known molecular mass of eGFP, Equation 6 in section 2.5.6.) were calculated (Table 3). The resulting molecular mass of STAT3-ΔNTD-eGFP (88±11 kDa) is in good agreement with the predicted molecular mass of monomer STAT3-ΔNTD-eGFP (99 kDa). The apparent molecular mass of the full length form, STAT3-eGFP (216±99 kDa) fits well with the predicted molecular mass of a STAT3-eGFP dimer complex (236 kDa).

Protein	Number of measurements	Diffusion coefficient ($\times 10^{-6}$) (cm^2/second)	Hydrodynamic radius (nm)	Average molecular mass (kDa)	Predicted molecular mass (kDa)
eGFP	3	1.03 ± 0.04	2.4 ± 0.1	-	27
STAT3-eGFP	12	0.54 ± 0.08	4.6 ± 0.8	216 ± 99	236 (dimer)
STAT3-ΔNTD-eGFP	10	0.70 ± 0.03	3.5 ± 0.2	88 ± 11	99 (monomer)

Table 3. Diffusion coefficients and molecular masses derived from 2f-FCS experiments. Total number of measurements from three independent samples are given. The predicted molecular masses were calculated from the known amino acid sequences of the proteins.

Taken together, the results from 2f-FCS measurements show the ability of full-length STAT3 to form dimer complexes in unstimulated state. In contrast, the N-terminally deleted STAT3 exists only as a monomer in resting cells.

3.4.2. Function of the N-terminal domain in dimerization of latent STAT3 analyzed by FRET

Additionally, FRET was measured between STAT3-ΔNTD-eGFP, and full length STAT3 constructs (TMRstar-STAT3 and STAT3-TMRstar) to verify the previous findings from 2f-FCS experiments (Figure 32).

.

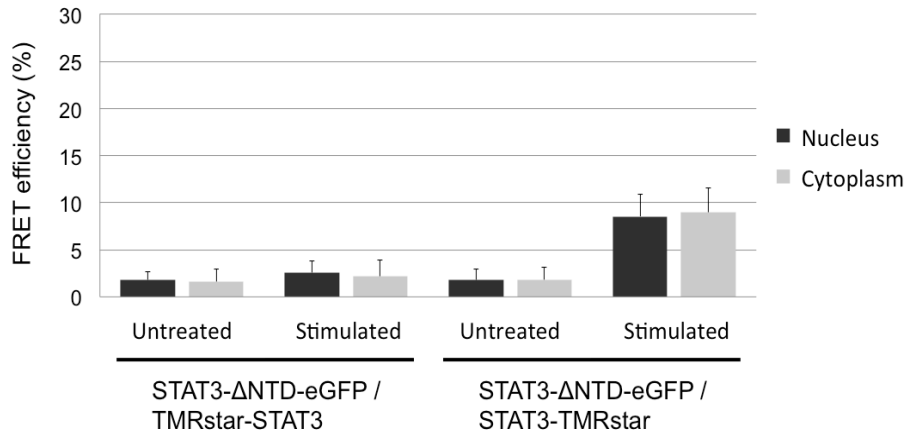


Figure 32. Dimerization study of N-terminally deleted STAT3 with wild type form. No significant FRET signal was detectable between N-terminally truncated and full length STAT3 constructs prior to activation, indicating the importance of the N-terminal region in dimerization of latent STAT3. After stimulation the increased FRET efficiency demonstrates the active dimer formation. (N: 34-40 cells)

No significant FRET efficiency was detectable prior to stimulation, confirming the defect of N-terminally deleted STAT3 in stable dimer formation under latent conditions.
After cytokine treatment an increased FRET signal between the C-terminally labelled constructs (nucleus: 8.55±2.31%, cytoplasm: 8.94±2.65%) demonstrated the capability of the NTD deletion mutant to form active dimers. However this dimerization is not visible between the reciprocally labelled constructs (nucleus: 2.54±1.23%, cytoplasm: 2.19±1.73%), possibly due to the structural consequence of the domain deletion.

In summary, 2f-FCS and FRET measurements identified the N-terminal domain of STAT3 to be crucial for the formation of latent dimers (Figure 33).

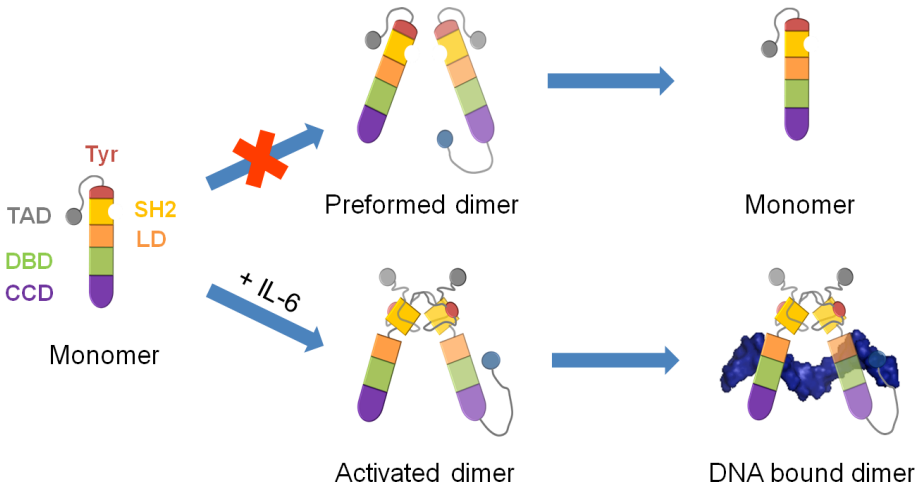


Figure 33. Deletion of the N-terminal domain prevents the formation of latent STAT3 dimers. Truncation of the N-terminal domain inhibits the association of STAT3 monomers in latent state, but does not affect the phosphorylation driven dimerization and DNA-binding in response to cytokine stimulation (for more details see in Ref. [139]).

3.5. Characterization of N-terminal domain mediated interactions

To study the function of N-terminal domain in dimerization and tetramerization of STAT3, we generated a construct which encodes the N-terminal fragment of STAT3 (NTD) and for fluorescence detection, fused to a SNAP-tag and reacted with the red fluorophore TMRstar (TMRstar-NTD).

3.5.1. Homotypic N-terminal domain interactions

In the first experiments we ensured that the isolated N-terminal fragment is functional and capable to interact with full length STAT3.
HeLa cells were transfected with constructs encoding TMRstar-NTD and eGFP-STAT3 or STAT3-eGFP and analyzed by FRET approach (Figure 34). A strong FRET signal was detectable (nucleus: 9.34±3.62%, cytoplasm: 8.72±2.94%) when the donor fluorophore was localized at the N-terminal end of the full length protein.

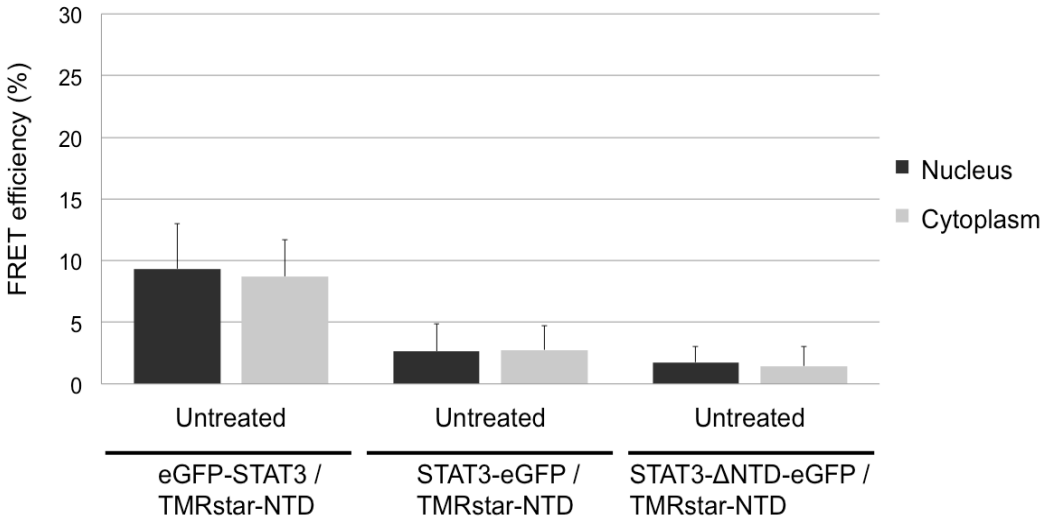


Figure 34. FRET efficiencies (%) of TMRstar-NTD with different STAT3-eGFP constructs. FRET results show the capability of the isolated N-terminal construct to interact with STAT3, and this interaction is driven in a homotypic manner between the N-terminal domains. (N: 30 cells)

In contrast, measurements on STAT3-eGFP / TMRstar-NTD resulted in low FRET signals (nucleus: 2.64±2.23%, cytoplasm: 2.76±1.94%) indicating that the interaction is localized at the N-terminal region of STAT3.
Control measurements on N-terminally deleted STAT3 (STAT3-ΔNTD-eGFP), revealed no significant FRET between the two constructs (nucleus: 1.76±1.25%, cytoplasm: 1.45±1.57%), indicating that no other STAT3 domains are involved in the N-terminal interactions.
This is in good agreement with GST pull-down assays between N-terminal and other STAT3 domain fragments [41], where also no visible interaction was detectable with other structural domains of STAT3.
The results demonstrate the capability of the TMRstar-NTD construct to interact with full lenght STAT3, and FRET measurements are marking the N-terminal domain as the interaction surface.
These findings are in good agreement with previous publications showing the tendence of N-domains of STATs to dimerize with itself [137].

To further verify and investigate the participation of N-terminal domain homotypic interaction in preformed dimer formation, a native gel analysis was performed (Figure 35).

HeLa cells were transfected with STAT3-YFP and increasing amounts of SNAP-NTD encoding expression vector (2-4-8 µg). Cells were left unstimulated, lysed, and following the electrophoresis, the gel was analyzed with a fluorescence scanner to visualize the STAT3-YFP signal.

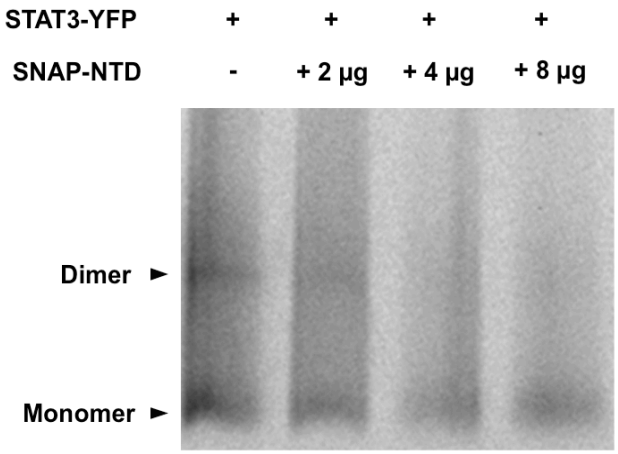


Figure 35. Inhibition of latent dimer formations visualized by native gel electrophoresis. The increased expresssion of the isolated N-terminal domain construct (SNAP-NTD) affects dimer formations of unphosphorylated full lenght STAT3.

The STAT3-YFP alone transfected lysates show clearly two bands, representing the dimer and monomer fraction of STAT3-YFP. Transfection of increasing amounts of expression vector encoding SNAP-NTD, lead to the inhibition of preformed dimer formation, as it is visible from the disappearance of dimer bands.

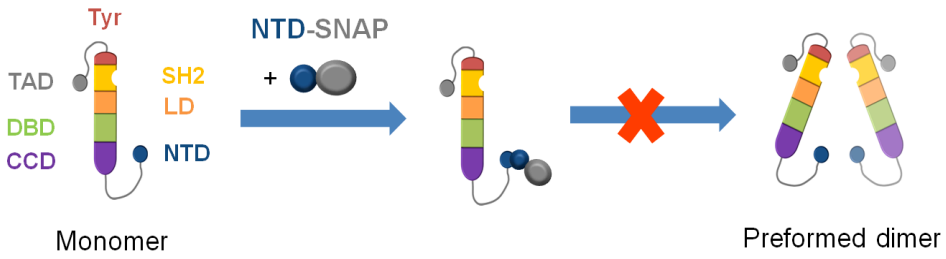


Figure 36. Dissociation of preformed dimers with isolated N-terminal domain. Isolated NTD (SNAP-NTD) directly interacts with the N-terminal region of full length STAT3. This interaction prevents the formation of NTD-NTD interaction for stabilizing the dimer structure, resulting in a monomeric latent STAT3.

The results are demonstrating the functionality of the isolated NTD to inhibit the dimerization of latent STAT3 molecules. This inhibition involves the direct interaction with the N-terminal domain of STAT3, which leads to the disruption of dimerization by interference with the NTD-NTD interdomain interactions (Figure 36).

3.5.2. Importance of L78 residue in dimerization of N-terminal domains

In the next step we decided to identify the critical amino acid residue which plays a crucial role in promoting NTD-NTD interaction and stabilizing the preformed dimers.
For this purpose, we generated a point mutant construct, targeting the somatic mutation site found in human inflammatory hepatocellular adenomas (IHCAs) in the N-terminal domain of STAT3 at position leucine 78 [58] (Figure 7).
Similar to the mutation found in IHCA [58] we generated a L78R mutation in the N-terminal domain of STAT3. As in case of the wild type construct we fused a SNAP-tag to the mutated NTD and tested the interaction capability with full length STAT3 using FRET analysis (Figure 37).

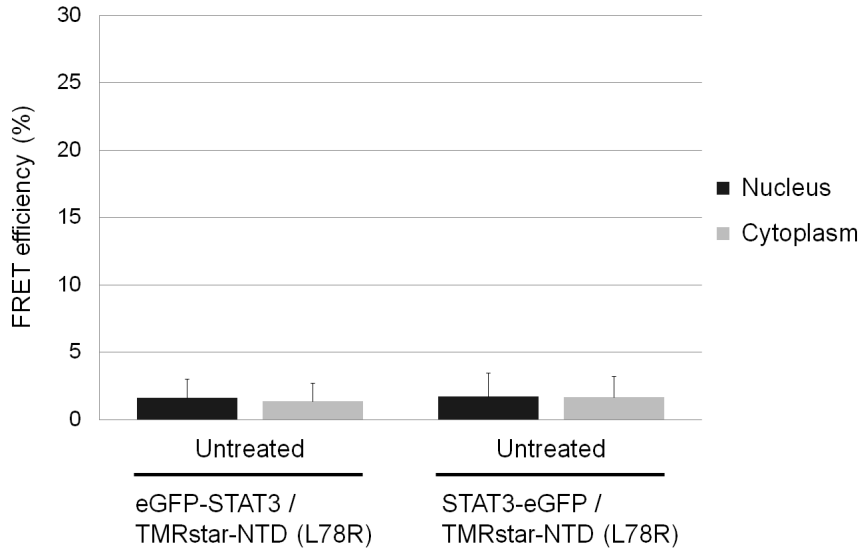


Figure 37. L78 mutated N-terminal domain does not interact with STAT3. A single amino acid mutation in the N-terminal domain leads to the destruction of NTD-NTD interdomain interaction. The detectable FRET efficiencies in both cases are undistinguishable from the background, eGFP-STAT3 / TMRstar-NTD L78R (nucleus: 1.62 ±1.37%, cytoplasm: 1.37 ±1.31%) and STAT3-eGFP / TMRstar-NTD L78R (nucleus: 1.70 ±1.74%, cytoplasm: 1.65 ±1.56%). (N: 30 cells)

This single mutation in the N-terminal fragment leads to the complete loss of FRET signal between the NTDs of STAT3 (nucleus: 1.62 ±1.37%, cytoplasm: 1.37 ±1.31%) in comparison with the previously measured wild type form (nucleus: 9.34±3.62%, cytoplasm: 8.72±2.94%, Figure 34).
The FRET results from L78R mutated N-terminal domain represent the direct evidence of L78 residue importance in promoting homotypic NTD-NTD interactions between the two domains.
Involvement of the L78 residue in the dimerization of N-terminal domains indicates the existence of a similar dimer interface in case of STAT3, which was previously proposed for STAT1, where the NTDs carrying the L78 mutation were properly folded but monomer fractions [140].

3.5.3. Importance of L78 residue in tetramerization

The cooperative binding of STAT dimers (tetramer formation) on specific DNA target sites is mediated by homotypic interactions between N-terminal domains [141, 142].
Tetramerization of STAT3 was shown to be essential for the maximal transcriptional activation of the α2-macroglobulin gene promoter [35].
As we showed previously (section 3.5.1.), the construct encoding the N-terminal domain of STAT3 fused to a SNAP-tag (SNAP-NTD) are capable to interact with full lenght STAT3 and to inhibit the dimerization of latent STAT3 by preventing NTD-NTD interdomain interactions. We were interested in this inhibitory effect in case of tetramer formations (Figure 38).

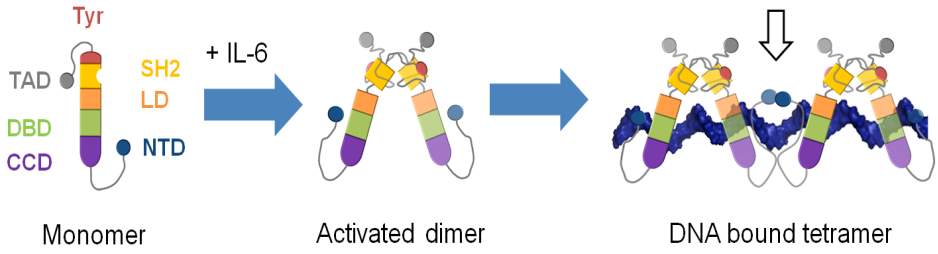


Figure 38. Tetramerization of STAT3. Phosphorylated STAT3 dimers are able to form stable tetramers on specific DNA sequences, mediated by homotypic interactions between the N-terminal domains of one dimer and the N-terminal domains from the other dimer (indicated by white arrow), and were found to be essential for the maximal activation of specific gene promoters.

STAT3 tetramerization is analyzed by an α2-macroglobulin promoter assay. HepG2 cells were transfected with the reporter construct and with expression vectors encoding SNAP-NTD, N-terminal domain construct carrying the L78R mutation (SNAP-NTD L78R) or with or 4 μg empty vector (Mock).

Using wild type NTD, a significant downregulation of the α2-macroglobulin promoter was detectable compared to non-transfected or empty-vector transfected samples (Figure 39A). In agreement with our results, the same effect was demonstrated with the use of a STAT3 N-terminal domain based inhibitor peptide (STAT3-Hel2A) on an APRE luciferase reporter [129]. In contrast, this inhibition disappeared when the N-terminal domain was mutated at the L78 position (Figure 39B).

These results demonstrate the importance of the L78R residue in N-terminal domain driven tetramerization of STAT3, indicating the involvement of a similar structural interface in this procedure as in dimerization of latent STAT3.

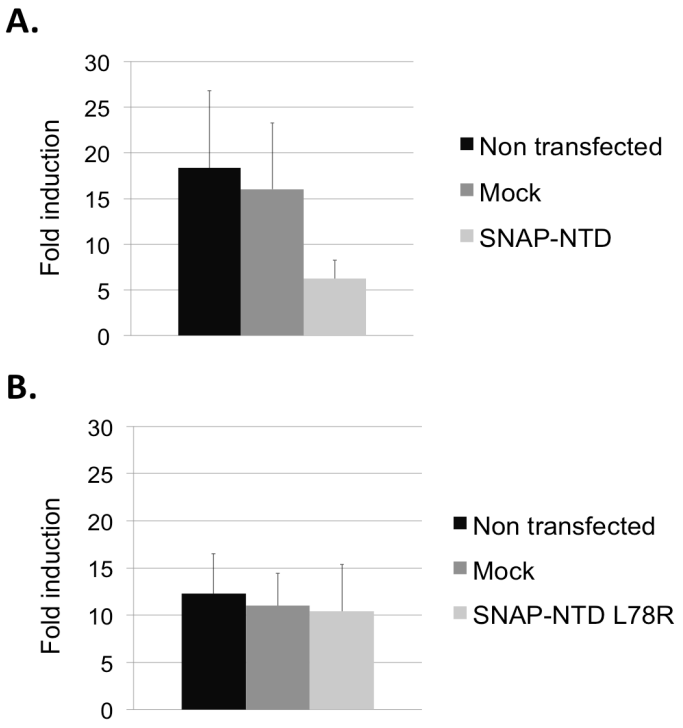


Figure 39. (A) Inhibition of α2-macroglobulin promoter activity by SNAP-NTD. Cotransfection of wild type N-terminal fragment of STAT3 leads to the prevention of tetramer complexes on α2-macroglobulin promoter, as detectable as a decreased induction of the promoter. **(B) L78R mutation in the N-terminal domain erases the inhibitory effect of NTD.** The N-terminal fragment carrying a specific point mutation (L78R) is not capable to inhibit STAT3-mediated gene induction. Induction of α2-macroglobulin promoter showed no difference compared to non transfected or empty vector transfected sample ($p=0.645$ and $p=0.877$ respectively).

3.6. Importance of L78R residue in dimerization of latent STAT3

Our previous findings highlighted the importance of N-terminal domain interactions in stabilizing the preformed STAT3 dimer. We demonstrated the relevance of the L78 residue in this dimer interface, as well as its importance in STAT3 tetramer formation. To elaborate these findings, we introduced this single mutation to full length STAT3 and applied the mutated protein for further analysis. The results from L78R mutated STAT3 are described in this section.

3.6.1. Characterization of N-terminally mutated STAT3(L78R) constructs

For further investigations, two STAT3 constructs were generated carrying the specific point mutation at leucine L78 in the N-terminal domain: SNAP-STAT3(L78R) and STAT3(L78R)-SNAP (Figure 40).

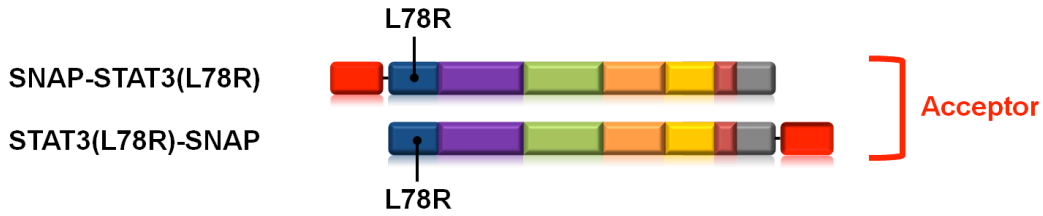


Figure 40. Mutated STAT3 acceptor constructs for FRET imaging. The SNAP-tag as a labelling site is located N- or C-terminally on the host molecule carrying the specific L78R amino acid substitution in the N-terminal region.

To test the functionality and expression of the mutant STAT3 fusion constructs, HeLa cells were transfected with plasmids encoding SNAP-STAT3(L78R) or STAT3(L78R)-SNAP and stimulated with IL-6 and soluble IL-6 receptor (sR) or left untreated. The cells were lysed and analyzed using western blot technique (Figure 41A).
Both constructs showed specific phosphorylation on Tyr705 residue after cytokine addition as a hallmark of STAT3 activation, and both are expressed in HeLa cells as it is detected after reprobing with an antibody against STAT3 protein (Figure 41A lower panel).

Additionally, nuclear accumulation of the above mentioned fusion proteins was studied by live cell imaging (Figure 41B).
Both constructs, SNAP-STAT3(L78R) and STAT3(L78R)-SNAP (labelled with TMRstar substrate) responded with nuclear accumulation to cytokine treatment, showing that the mutation in the N-terminal region did not affect the transport of the host molecule.
Taken together, results from the characterization of L78R mutated STAT3 indicate that the fusion protein constructs carrying the amino acid L78R substitution in the N-terminal domain and labelled with SNAP-tag are functional and can be used for further investigations.

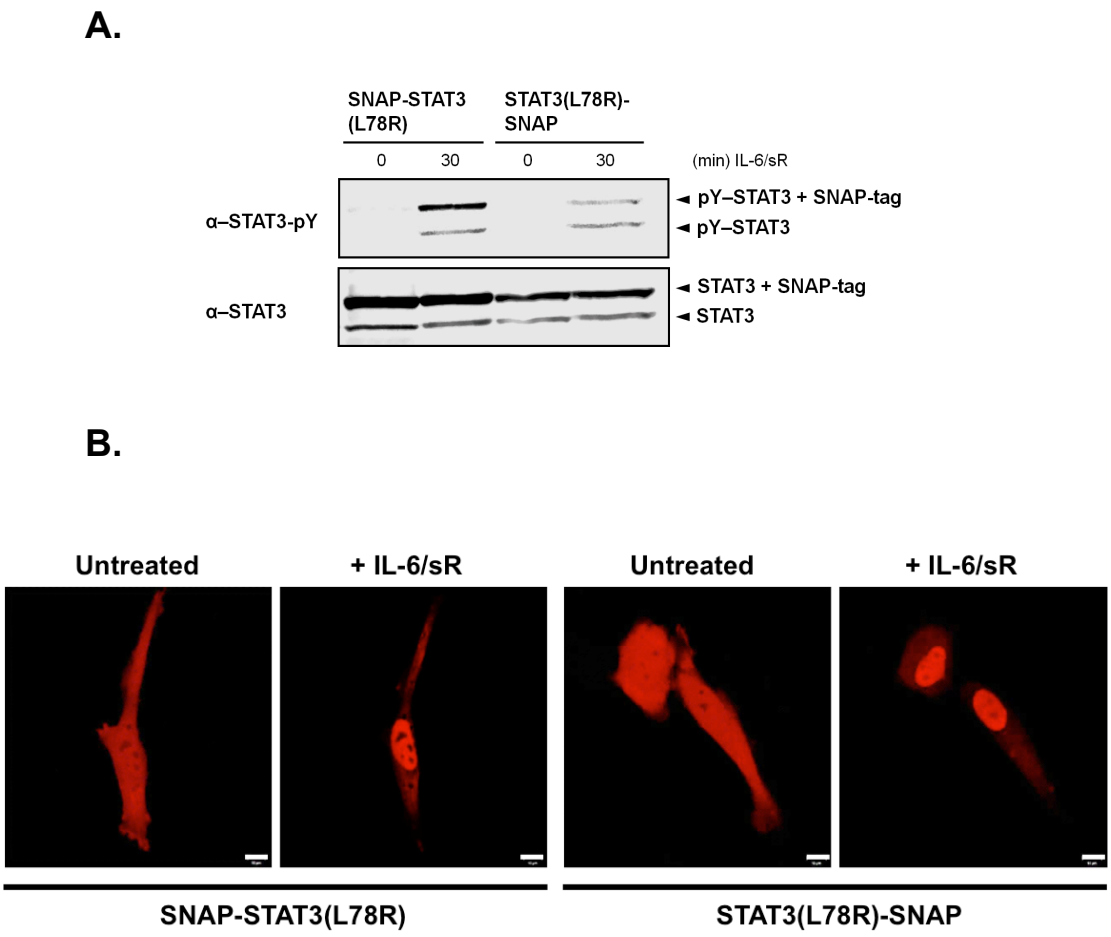


Figure 41. (A) Functional analysis of N-terminally mutated STAT3 constructs. HeLa cells were transfected with the indicated expression vectors encoding SNAP-STAT3(L78R) or STAT3(L78R)-SNAP. Cells were stimulated with 20 ng/ml IL-6 and 500 ng/ml soluble IL-6 receptor for 30 minutes or left unstimulated. Lysates were analyzed by western blotting using STAT3 phosphotyrosine 705 (STAT3-pY) and STAT3 specific antibodies. **(B) Ligand induced nuclear accumulation of L78 mutated STAT3 fusion proteins.** Localization of STAT3-SNAP constructs (fluorescently labelled with TMRstar) was followed in real time after stimulation with 20 ng/ml IL-6 and 500 ng/ml soluble IL-6 receptor using confocal microscopy in living HeLa cells. Bars, 10 μm.

3.6.2. L78R mutation prevents the dimerization of latent STAT3 *in vitro* and *in vivo*

To analyze the capability of L78R mutated STAT3 constructs to form stable dimers prior to cytokine addition, FRET was measured similar to wild type measurements on three different FRET pair combinations as: eGFP-STAT3 / TMRstar-STAT3(L78R), eGFP-STAT3 / STAT3(L78R)-TMRstar and STAT3-eGFP / STAT3(L78R)-TMRstar (Figure 42).

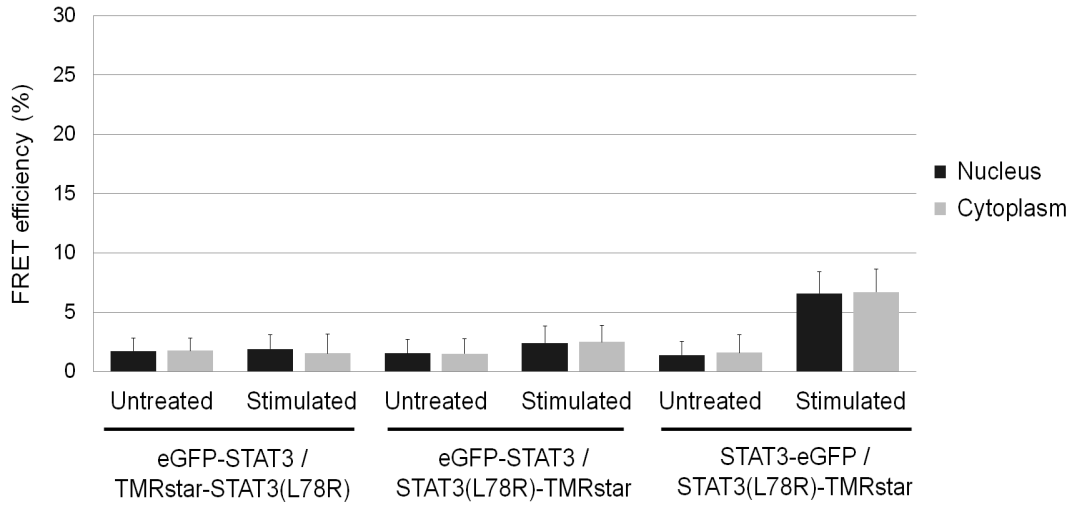


Figure 42. Summary of FRET results on L78R mutated STAT3 molecules. HeLa cells were transfected with the indicated donor/acceptor pairs, labelled with TMRstar substrate, stimulated with IL-6 and soluble IL-6 receptor or left untreated, fixed and used for FRET imaging. (N: 35 cells)

In all three cases, no significant FRET signal was detectable prior to stimulation. FRET efficiencies are: eGFP-STAT3 / TMRstar- STAT3(L78R) (nucleus: 1.74±1.11%, cytoplasm: 1.76±1.08%), eGFP-STAT3 / STAT3(L78R)-TMRstar (nucleus: 1.55±1.15%, cytoplasm: 1.53±1.23%) and STAT3-eGFP / STAT3(L78R)-TMRstar (nucleus: 1.42±1.15%, cytoplasm: 1.60±1.54%). The results are clearly indicating the disability of L78R mutated STAT3 molecules to form dimers in latent state.

Increased FRET efficiency was detectable after cytokine addition, as is clearly visible in the measurements on C-terminally labelled constructs, STAT3-eGFP / STAT3(L78R)-TMRstar (nucleus: 6.61 ±1.82%, cytoplasm: 6.70 ±1.93%) indicating the existence of phosphorylated dimer structures, demonstrating that the L78R mutation does not prevent the formation of activated STAT3 dimers.

To summarize our FRET analysis on L78R mutated STAT3 constructs, the results revealed the importance of the L78 residue in the N-terminal domain, for promoting NTD-NTD interaction and stabilizing the preformed dimers.
As in case of wild type STAT3, the *in vitro* findings on fixed cells were repeated and confirmed in living cell experiments (Figure 43).

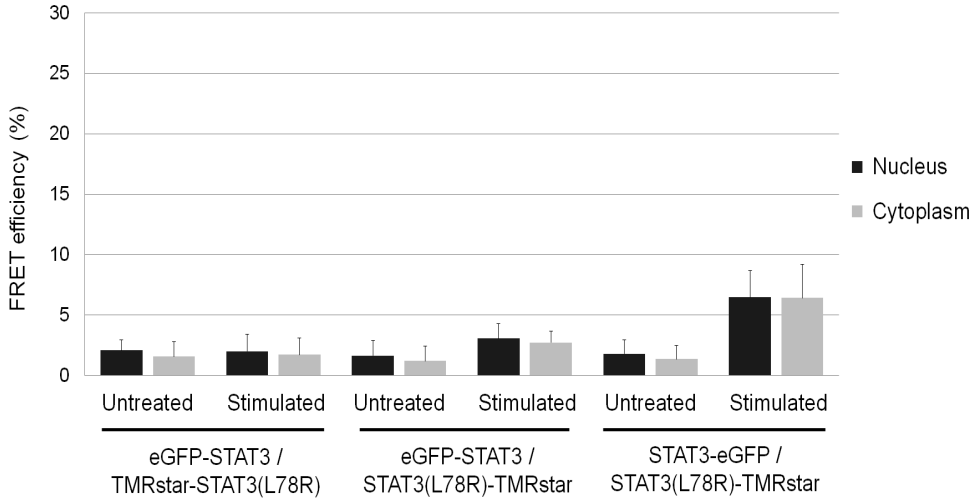


Figure 43. Live cell FRET measurements on L78R mutated STAT3 molecules. HeLa cells were transfected with the indicated STAT3 constructs, labelled with TMRstar substrate, measured and imaged at 37°C and 5% CO_2. No significant FRET was detectable in all cases prior to stimulation, indicating the *in vivo* incapability of the L78R mutated STAT3 to form dimers prior to cytokine addition. (N:14-20 cells)

Similar to fixed samples, no preformed dimerization (significant FRET efficiency) was detectable in latent state in all measured samples. The measured FRET efficiencies are: eGFP-STAT3 / TMRstar- STAT3(L78R) (nucleus:2.08±0.85%,cytoplasm:1.56±1.23%),eGFP-STAT3 / STAT3(L78R)-TMRstar (nucleus: 1.64±1.23%, cytoplasm: 1.21±1.22%) and STAT3-eGFP / STAT3(L78R)-TMRstar (nucleus: 1.80±1.15%, cytoplasm: 1.35±1.12%). Stimulation leads to the dimerization and nuclear translocation of the constructs as it is detected as a slightly increased FRET signal between eGFP-STAT3 / STAT3(L78R)-TMRstar constructs and more clearly visible between C-terminally labelled constructs, STAT3-eGFP/STAT3(L78R)-TMRstar (nucleus: 6.48±2.21%, cytoplasm: 6.42±2.75%).
In summary, fixed sample and living cell measurements supported our conclusion, that the preformed STAT3 dimers are mostly stabilized by homotypic interactions driven by the N-terminal domains, and a mutation targeting this interface (L78R) prevents these dimer formations.

3.7. Function of preformed dimers in STAT3 activation

We identified the N-terminally located amino acid L78, as a key residue for promoting dimerization, tetramerization and NTD-NTD interaction between STAT3 monomers and dimers.
In this section we would like to experimentally characterize the possible functions of preformed STAT3 dimers in the activation or deactivation cycle of JAK/STAT3 signalling.
From intermolecular FRET measurements on wild type STAT3, we propose the existence of a non- or deactivated STAT3 dimer population in the cytoplasmic compartment after cytokine stimulation, which shows similar structural arrangement as the preassociated monomer forms (Figure 44).

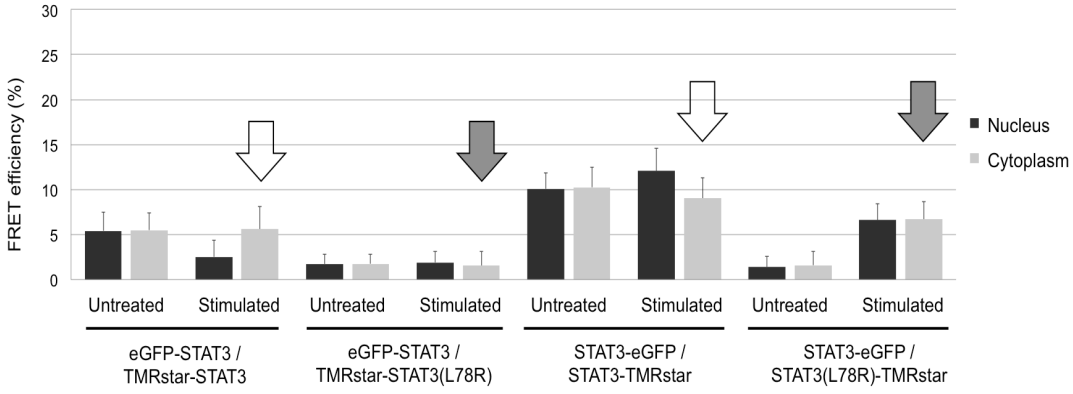


Figure 44. FRET on wild type STAT3 versus L78R STAT3. After 30 minutes of cytokine stimulation, a significant difference (unfilled arrows) was detectable between the cytoplasmic and nuclear fractions of activated wild type STAT3 dimers. This difference disappeared (filled arrows) by introducing the L78R mutation in the N-terminal domain of STAT3, indicating the importance of N-terminal interactions in promoting these dimer formations.

Comparing the results from wild type form and L78R mutated STAT3, which is unable to form stable dimers in latent state, we are able to analyze and visualize the effect of blocking dimerization of latent STAT3 on dimerization of activated STAT3 (Figure 44). As it is clearly visible, disrupting the capability of STAT3 to form dimers based on N-terminal homotypic interactions, the differences in FRET efficiencies of activated STAT3 between cytoplasmic and nuclear compartments are not detectable anymore: eGFP-STAT3 / TMRstar-STAT3 after stimulation (nucleus: 2.53±1.87%, cytoplasm: 5.61±2.53%) versus eGFP-STAT3 / TMRstar-STAT3(L78R) (nucleus: 1.91±1.22%, cytoplasm: 1.55±1.6%).

These disappeared FRET differences are also visible from measurements on C-terminally labelled constructs: STAT3-eGFP / STAT3-TMRstar after stimulation (nucleus: 12.09±2.52%, cytoplasm: 9.03±2.29%) compared to STAT3-eGFP / STAT3(L78R)-TMRstar (nucleus: 6.61±1.82%, cytoplasm: 6.70±1.93%). These results suggest the existence of NTD-dependent non-activated STAT3 dimers after cytokine addition, assuming the capability of these dimers to by-pass the activation.

It is well described in context of STAT1, that these N-terminal interactions are involved in the reorientation of monomers in the activated dimer form to promote dephosphorylation [75]. According to these findings, we tested the dependence of the latent dimer form on the dephosphorylation mechanism. Cells were transfected with STAT3-eGFP / STAT3-TMRstar constructs, pre-treated with phosphatase inhibitors, Na-vanadate or Halt protease and phosphatase inhibitor cocktail for 15 minutes and stimulated with IL-6 and sR for 30 minutes, fixed and imaged by confocal microscopy (Figure 45). Inhibition of cell phosphatases caused an overall reduction of FRET signals, however the non-activated dimers were still detectable in cytoplasmic fraction (Na-vanadate: 4.54±1.45%, Halt inhibitor cocktail: 4.62±1.48%). These results demonstrate that preformed STAT3 dimers at some part are connected (but not necessary) to the inactivation of STAT3 molecules, indicating the ability of dephosphorylated monomers to dimerize after deactivation.

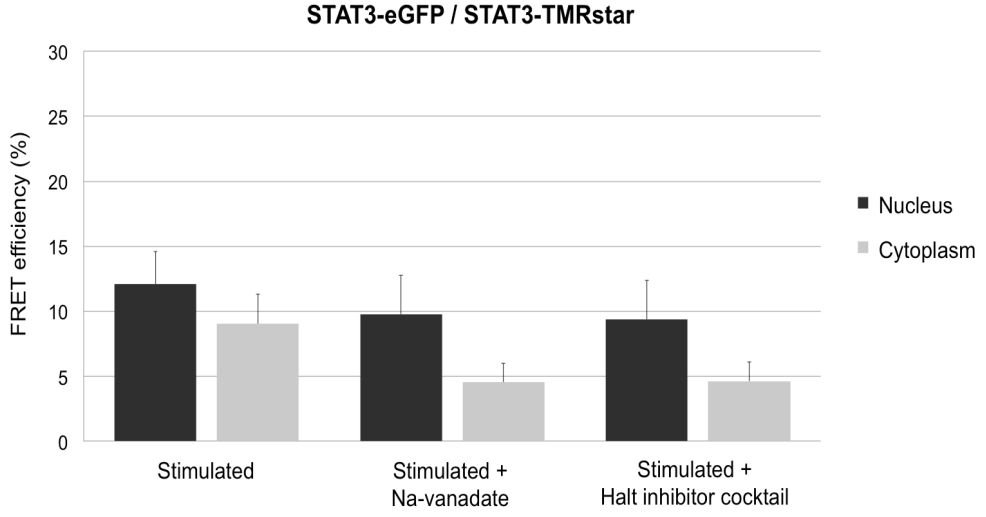


Figure 45. Effect of phosphatase inhibition on FRET efficiencies between STAT3-eGFP and STAT3-TMRstar. HeLa cells were transfected with STAT3-eGFP/STAT3-TMRstar FRET pairs, pretreated for 15 minutes with Na-vanadate (1mM) or Halt inhibitor cocktail (1:100), stimulated, fixed and analyzed with confocal microscopy. (N: 15-20 cells)

These findings are in good agreement with previous reports on N-terminally deleted STAT3, where the truncated mutant showed similar dephosphorylation kinetics as the wild type form [143].
Together with our data, these findings demonstrate the ability of dephosphorylated STAT3 monomers to re-dimerize through NTD-NTD interactions, however this formation is not necessary for the dephosphorylation of activated dimers.
Furthermore, we tested the involvement of preformed dimers in STAT3 activation. Cells were transfected with wild type (TMRstar-STAT3) or the L78R mutant form, left untreated or stimulated for 30, 60 and 120 minutes and analyzed by immunoblotting (Figure 46).
L78R mutated STAT3 showed a reduced expression compared to wild type, as it is visualized from reblotting with two different antibodies against STAT3 (Figure 46 second and third panel). A similar difference in the expression pattern was detected in case of the STAT5a F81A mutant in 293T cells [144]. However the pTyr 705 signal (Figure 46 first panel) showed almost comparable level of phosphorylation.

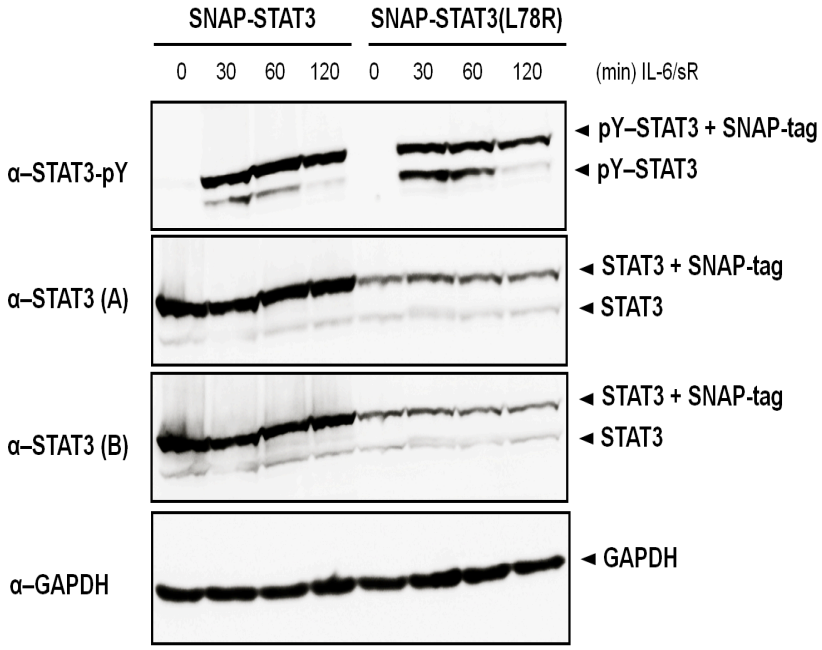


Figure 46. Disruption of preformed dimers leads to a stronger STAT3 activation. HeLa cells were transfected with the indicated expression vectors encoding SNAP-STAT3 or SNAP-STAT3(L78R). Cells were stimulated with 20 ng/ml IL-6 and 500 ng/ml soluble IL-6 receptor for 30, 60 and 120 minutes, or left unstimulated. Lysates were analyzed by western blotting using STAT3 phosphotyrosine 705 (STAT3-pY) and STAT3 specific antibodies (A: against C-terminal domain of STAT3, B: against N-terminal domain) and GAPDH as a loading control.

This robust activation was also visible in case of N-terminally deleted STAT3 forms [143, 145].
This difference is even more visible on endogenous STAT3 (Figure 46 first panel), where the coexpression of L78R mutant STAT3 leads to an enhanced phosphorylation signal, indicating the more effective activation of STAT3 when the preformed dimers are disrupted.

In summary, the results based on wild type and L78R mutant STAT3 showed the involvement of preformed dimers in the negative regulation of STAT3 activation.
This effect could be described by the preassociated dimer structure, which is driven by N-terminal domain interactions and possibly additionally stabilized by other domains (SH2-domain) [70], resulting in a conformation which avoids STAT3 recruitment to the receptor and keeps the molecules in the unstimulated state (Figure 47).

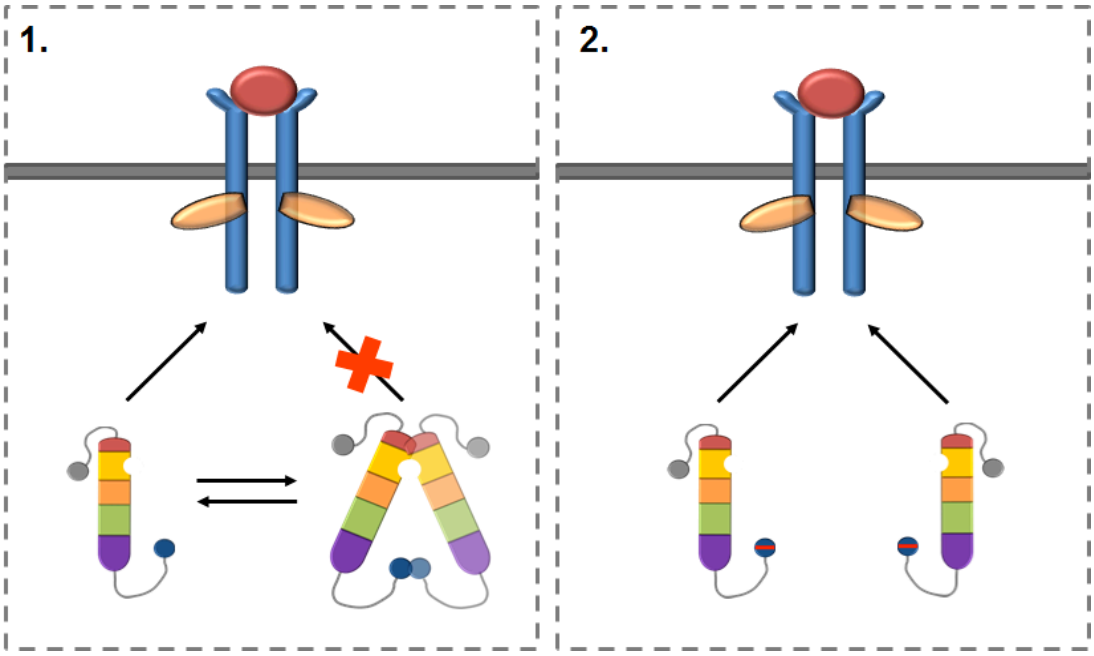


Figure 47. Function of preformed dimerization in STAT3 activation. In the first scenario (1), STAT3 is able to form stable dimers in latent state. This dimer formation is stabilized by interactions between N-terminal domains and additional interdomain interactions involving the SH2-domains of STAT3. This structural organization prevents the recruitment to the receptor. In contrast (2), when preformed dimerization is blocked (by a mutation in N-terminal region, highlighted in red) the STAT3 activation is more effective.

3.8. Intramolecular FRET measurements on STAT3

From the above data we concluded, that latent STAT3 dimers are hindered in receptor-mediated phosphorylation and activation. We proposed additional interactions involving the SH2-domains that drive the dimers into a conformation which blocks the proteins from receptor binding. In this section we focused on the role of the SH2-domain in latent dimerization of STAT3.

Detecting intramolecular FRET between donor and acceptor fluorophores, localized at the same host molecule is a unique way to follow conformational changes of the target molecules [146]. We applied this intramolecular way of FRET detection to analyze the conformation of an SH2 domain mutant STAT3, which carries an arginine to glutamine substitution at amino acid position 609 (Figure 48).
This specific mutation has a strong influence on the overall functionality of STAT3 molecule and leads to a non functional SH2 domain [147], preventing the phosphorylation of STAT3 [148].
Additionally the mutated STAT3(R609Q) protein is unable to form stable dimers prior or after stimulation [70, 149], representing a pure monomer STAT3 population.

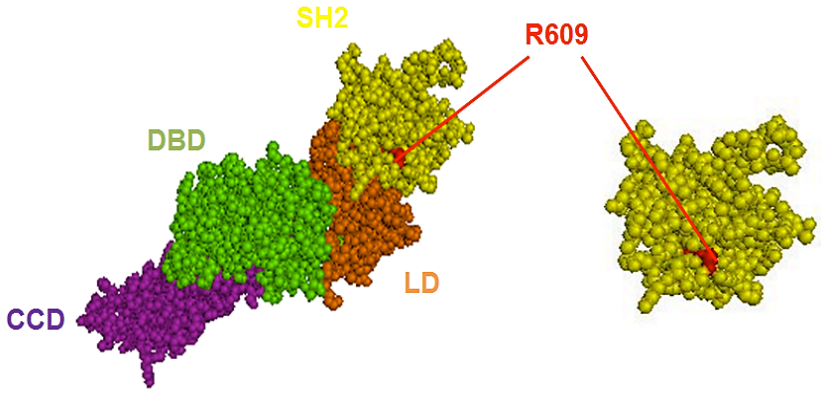


Figure 48. Mutation of R609 residue targets the SH2 domain of STAT3. R609 residue is critical (with K591, S611 and S613) to form polar interactions with phosphotyrosine 705 motif [15]. Mutation of this residue inhibits the dimer formation of STAT3 both in non-activated and activated state. (RCSB Protein Data Bank accession number for STAT3 is 1BG1)

Our aim was to analyze the effect of R609Q mutation on the overall STAT3 structure, and to find a structural answer to the defective dimerization. For measuring intramolecular FRET, two double labelled STAT3 constructs were generated: eGFP-STAT3-SNAP and eGFP-STAT3(R609Q)-SNAP (Figure 49).

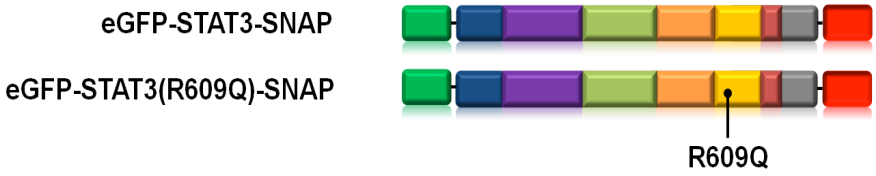


Figure 49. STAT3 constructs used for intramolecular FRET measurements. To generate samples for intramolecular FRET analysis, the donor (eGFP, green) and acceptor (SNAP-tag coupled with TMRstar substrate, red) were fused on the same host molecule N- and C-terminally, respectively.

FRET efficiencies from measurements on double tagged wild type STAT3 (Figure 50) prior (nucleus: 6.68±1.24%, cytoplasm: 6.48±1.39%) or after cytokine stimulation (nucleus: 11.39±1.90%, cytoplasm: 13.20±2.78%), showed similar results and tendence as the intermolecular FRET results on the eGFP-STAT3 / STAT3-TMRstar pair prior or after activation (Figure 26).

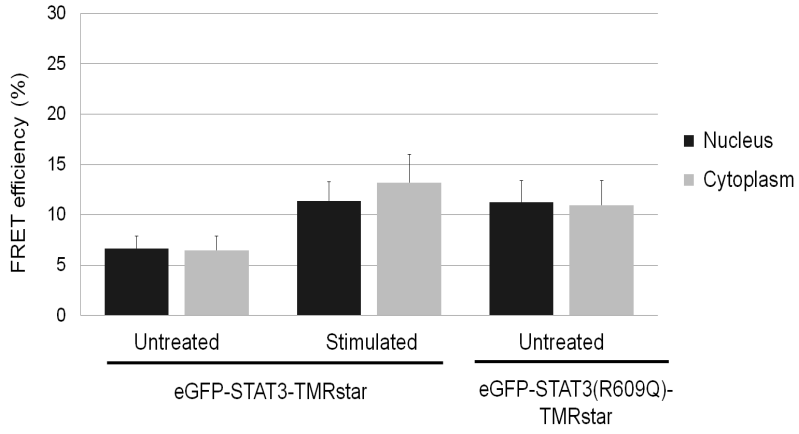


Figure 50. Summary of intramolecular FRET measurements on wild type and R609Q mutated STAT3. Similar to intermolecular FRET results an increased efficiency was detectable after cytokine addition, indicating a more sensitive detection of intermolecular FRET signal. The R609Q mutated monomer STAT3 form showed similar FRET efficiencies as the activated STAT3, indicating the similar orientation of the C- and N-terminal domains in mutant monomer as in activated dimer form. (N:30 cells)

In the measurements of double-labelled wild type STAT3 we cannot exclude the intermolecular FRET signal from our detection system. However, the R609Q mutant form which is a pure monomer form, showed high intramolecular FRET efficiency values (nucleus: 11.27±2.16, cytoplasm: 10.95±2.45) similar to the activated wild type form, indicating the same structural organization of this mutant monomer form as the activated dimer (Figure 51).

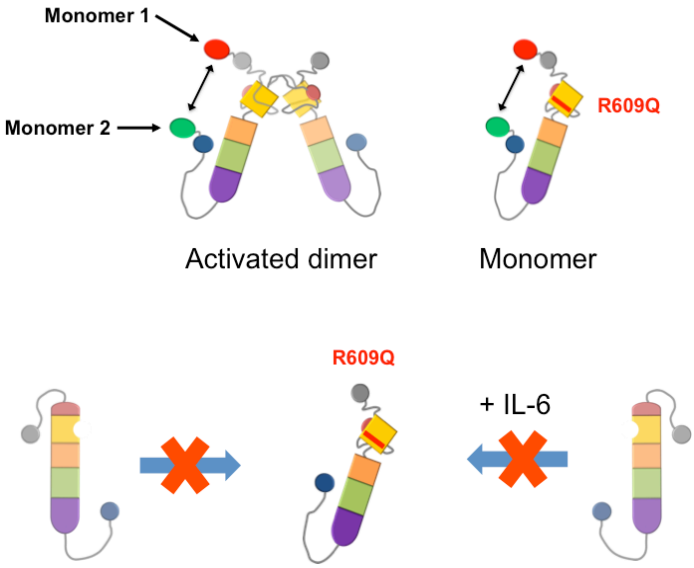


Figure 51. Effect of R609 mutation on STAT3 structure. Mutation of the R609 residue drives the STAT3 monomer form to a similar structure organization as activated dimer. This modification in the SH2 domain leads to the complete inability of STAT3 to form dimers prior or after cytokine addition. Proposed localizations of the fluorophores in activated dimer and R609Q mutated STAT3 structures are highlighted in green (donor, eGFP) and red (acceptor, TMRstar).

These results suggest, that mutation of the R609 residue in the SH2 domain, not only prevents the interaction between pTyr motif and the binding pocket in SH2 domain, but leads to a complete reorganization of the SH2 fragment (detected as high intramolecular FRET efficiency between the N- and C-terminal domains), disrupting the capability of the SH2 domain to additionally stabilize the preformed dimers.
The R609Q mutant reflects a STAT3 form, which structurally mimics the activated state, driving the molecule structurally unable to interact with activated and latent STAT3 monomer forms (Figure 51).

4. Summary and discussion

4.1. STAT3 dimers prior to activation

One of our major goals was to follow the association of nonphosphorylated STAT3 molecules and to structurally identify which regions and domains are involved in the stabilization of this dimer.
Our measurements using dual focus fluorescence correlation spectroscopy (2f-FCS) on N-terminally truncated STAT3 (STAT3-ΔNTD) showed that deletion of the N-terminal domain leads to the abrogation of latent dimers (section 3.4.1.). This inhibited association of unphosphorylated monomers was also confirmed by Förster resonance energy transfer (FRET) and proposes the contribution of the NTD in promoting dimerization of latent STAT3 molecules (section 3.4.2.).

Results from studies on STAT1 [135] and STAT4 [34] demonstrated the homotypic interactions of amino terminal domains in promoting dimerization and polymerization of these STAT forms.

Our results on constructs encoding only the N-terminal fragment of STAT3 (SNAP-NTD) revealed the capability of these domains to specifically interact with each other, and no cross reaction was detectable involving other domains of STAT3 (section 3.5.1.). These findings are in good agreement with previously published data based on other STAT-family members [73, 137].
Native gel electrophoresis (section 3.5.1.) showed that dimerization of nonphosphorylated STAT3 can be inhibited by the coexpression of wild type N-terminal domain (SNAP-NTD) and demonstrated that these preformed dimers are mostly stabilized by homotypic NTD-NTD interactions, similar to other members of the STAT family.
Additionally, we focused on the critical residue in the N-terminal domain, which is involved in mediating and stabilizing the homotypic interaction of these domains. Based on the somatic mutations found in inflammatory hepatocellular tumors [58] targeting the NTDs (L78 residue), we generated a construct encoding the N-terminal fragment with a L78R amino acid substitution (SNAP-NTD L78R) and tested how this single mutation affects the dimerization of N-terminal domains (section 3.5.2.). Compared with wild type form, no interaction was detectable with full length STAT3 protein, and suggested the L78 residue as a promising target for further investigations.

To confirm our findings from the isolated N-terminal domains (SNAP-NTD constructs), we generated an L78R mutated STAT3 fusion protein (section 3.6.1.) to analyze how the full length, but N-terminally mutated protein behaves. FRET measurements on L78R mutated STAT3 (section 3.6.2.) showed no detectable dimers prior to activation (*in vitro* and *in vivo*) and confirmed the L78 residue importance in forming the NTD-NTD interaction.

These results suggest the existence of a similar NTD-NTD interaction interface in context of STAT3, which was previously proposed for STAT4 [140] where the hydrophobic residues L77 and L78 (Figure 52) are involved in the homodimerization of these domains.

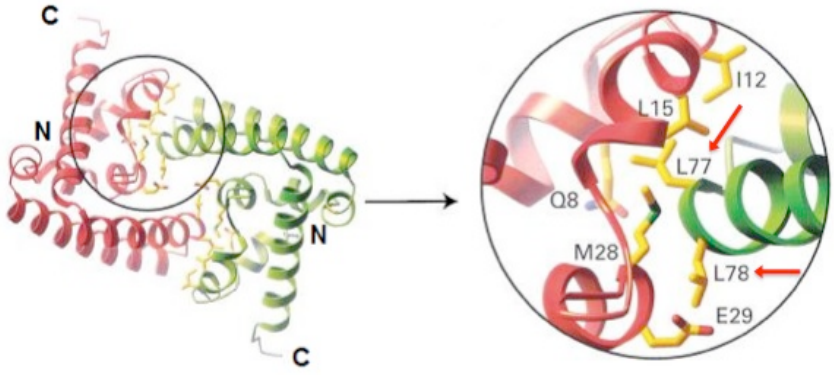


Figure 52. The alternate N-domain dimer of STAT4. This dimer interface is suggested by crystal packing. Proteins containing mutations L77A and L78A (indicated by arrows) were monomer forms in analytical ultracentrifugation studies (adopted from Ref. [140]).

To get information, how the monomers are oriented (with respect to each other) in the preformed dimer structure, we performed FRET measurements on differently combined STAT3 constructs carrying the fluorophores N- or C-terminally (Figure 20).
Measurements on STAT3 when both (donor and acceptor) fluorophores are fused to the N-terminal end of the host molecule (section 3.3.1.) revealed the closely oriented N-domains as evident from a positive FRET signal.

Similar results were obtained in case of STAT5a [131], which supports the theory of N-terminal domain driven stabilization of latent STAT3 dimers.

Although the dimerization of NTDs suggests the close proximity of donor and acceptor fluorophores, the detected FRET signal between N-terminally labelled full length proteins was relatively low (nucleus: 5.42±2.05%, cytoplasm: 5.50±1.91%, Figure 53), similar to studies on STAT5a [131].

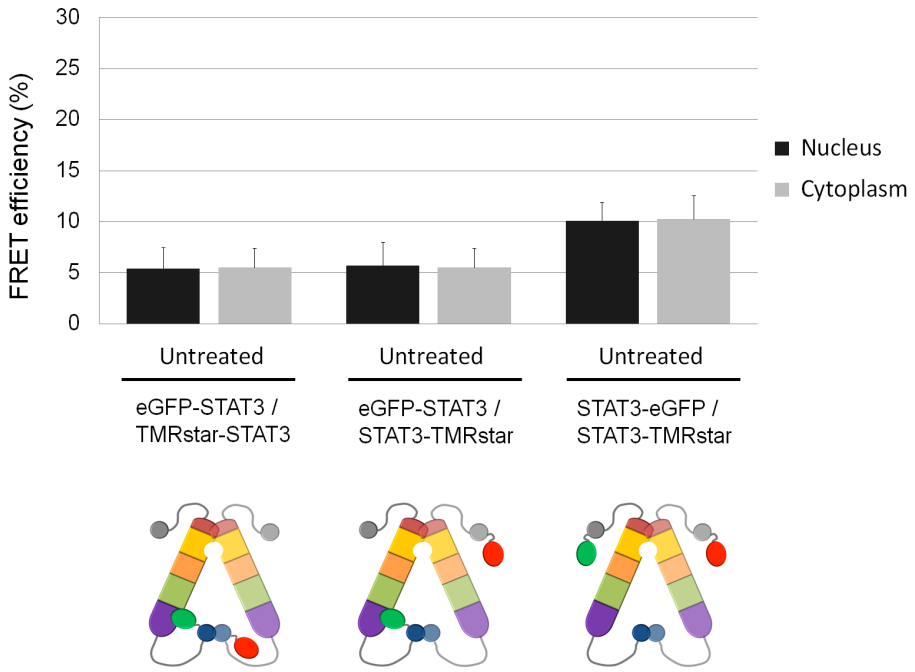


Figure 53. Summary of FRET results on wild type STAT3 in unstimulated state. The figure represents the differently combined FRET donor and acceptor pairs with the measured FRET efficiencies in nuclear and cytoplasmic regions. The proposed localizations of the fluorophores in preformed dimer structure is highlighted in green (donor, eGFP) and red (acceptor, TMRstar).

This low FRET efficiency could possibly be due to the structural background of the N-terminal dimerization interface. As it is visible in case of STAT4 (Figure 52), the reconsidered dimer interface of NTDs identified the importance of L77 and L78 residues. In this organization, the N-terminal residues of NTDs are distantly located which could cause at some point this reduced FRET efficiency.

The other point that possibly interferes with the FRET signal includes the effect of N-terminal domains interaction on the orientation of fluorophore dipoles.

As it is well described in previous reports [87], FRET coupling directly depends on the angle between donor and acceptor fluorophores, and the parallel oriented donor and acceptor molecules yield higher FRET signal, compared to the perpendicular oriented fluorophores. These orientation changes (or not optimal orientation of fluorophores), as a consequence of N-domain interactions, could additionally affect the FRET efficiency.

FRET measurements on reciprocally (N- and C-terminally) labelled STAT3 molecules confirmed the distant localization of the two domains (Figure 53).
Interestingly, we have found the close orientations of carboxy-terminal domains of STAT3 with FRET efficiencies (%) of 10.09 (±1.79) and 10.26 (±2.26) in the nuclear and cytoplasmic region respectively. Compared with transfer efficiency of the positive control (17.55±4.84%), the measured FRET signal indicates the closely localized C-terminal domains in preformed dimer structure. These findings strongly indicate the parallel oriented monomers in preformed dimer state, instead of antiparallel formation which was described for STAT1 (section 1.6.1 and [75]). This formation could structurally explain how unphosphorylated STAT3 molecules might be involved in gene expression activation [150] or capable of DNA-binding [151] in latent state.

As it is known from previous publications, STAT3 (compared with STAT1 and STAT4) forms N-domain dimers with low affinity [73], proposing the involvement of other structural regions in dimer stabilization. Crystal structure of unphosphorylated STAT3 (lacking the NTD and transactivation domain) revealed no evidence of other structural domains being involved in preformed dimer formation such as coiled-coil domain or DNA-binding domain (in contrast to STAT1 and STAT5) [136].

Our measurements on C-terminally truncated STAT3 molecules showed, that deletion of the transactivation domain does not affect the formation of preformed dimers (Supporting material Figures S2 and S3), as it is detected as significant FRET signals between the N- and C-terminal (nucleus: 8.46±2.74%, cytoplasm: 8.37±2.41%) as well as between C-terminal ends of the dimer (nucleus: 4.75±1.86%, cytoplasm: 4.66±1.89%).

FRET studies on SH2-mutated STAT3 form, STAT3(R609Q), revealed the need of an intact SH2 domain for preformed dimerization, and highlighted the possibility of SH2 homotypic interactions prior to activation [70].

Our intramolecular FRET measurements on R609Q mutated STAT3 (section 3.8.) indicate that this single mutation strongly affects the overall structure of the SH2 domain (not only the interacting regions with phosphotyrosine motif), resulting in a monomer form, which mimics the structural organization of the activated STAT3 dimer (Figure 51). This modification possibly interferes with regions in the SH2 domain which are involved in dimerization of latent STAT3, by generating an additional stabilizator interface between the SH2 fragments.

Supporting this hypothesis, previously published data from isolated STAT3 SH2 domains showed the ability of the domain fragments to dimerize with itself, and even more interestingly these dimerized SH2 domains were unable to interact with phosphopeptides [152].

This dimerization of SH2 domains independent from phosphopeptide binding could structurally explain, why the inhibition of preformed dimers leads to an increased STAT3 phosphorylation (Figure 46) and additionally could support the existence of non activated dimers in the cytoplasmic region after cytokine treatment, while the activated STAT3 dimers are mostly located in the nuclear compartment.
In summary, our findings identify the SH2 domain as a secondary stabilizer domain in dimerization of latent STAT3. This parallel dimer, formed by the interaction of N-terminal domains, allows the SH2 domains to get into a closer proximity and to additionally stabilize the dimer by interdomain connections between the SH2 fragments. This dimer formation (Figure 47) avoids the monomers from receptor binding and subsequently from phosphorylation, representing the preformed STAT3 dimers as regulators of the cytokine driven activation of STAT3.

In contrast to STAT1, NTD driven association of monomers is not required for the dephosphorylation of STAT3 since N-terminally deleted STAT3 responds similar to IL-6 treatment and displays the same dephosphorylation kinetics as wild type form [143].

However our measurements after phosphatase inhibitor treatment, showed a decreased FRET signal (Figure 45) in cytoplasmic region after cytokine addition indicating that dephosphorylated and inactivated STAT3 molecules are able to re-dimerize by the N-terminal domains in a latent formation.

This dimer organization is not required for the dephosphorylation mechanism (in contrast to STAT1) but could possibly regulate the hyperactivation of STAT3, by keeping the monomers in a non-activable dimer state. This could structurally explain why the constitutively activated mutations oftenly targets the SH2-domain and in case of inflammatory hepatocellular adenomas (IHCAs), the N-terminal fragment of STAT3 (section 1.5.3., Figure 6 and Figure 7)

4.2. Activated STAT3 dimers and tetramers

After cytokine stimulation, phosphorylated STAT3 monomers associated in an activated dimer form, which is stabilized by the reciprocal interactions between a phosphorylated tyrosine residue (pTyr705) of one, and the SH2 domain of the other monomer [39]. The phosphorylated dimers are transported to the nuclear compartment, bind to specific DNA sequences and activate the cytokine driven target gene expression [16].

We analyzed the dimer formation after cytokine treatment, to detect the possible structural differences between preformed and activated dimer structures.

N-terminally labelled STAT3 constructs (section 3.3.1.) in the nucleus, loose FRET signal between the N-terminal regions, indicating the separation of N-terminal domains upon activation, which leads to a structural rearrangement of the dimers to form the transcriptionally active conformation (Figure 25 and 54) where the N-terminal regions of each monomer are distantly located [15].
However the cytoplasmic fraction showed a similar FRET signal as the unstimulated sample, indicating the existence of a non-activated STAT3 dimer fraction in the cytoplasmic region (Figure 54, eGFP-STAT3 / TMRstar-STAT3, cytoplasm).
Measurements on reciprocally tagged STAT3 constructs showed an increased FRET signal after stimulation, compared with untreated cells, indicating the closer orientation of the two separate domains in the activated dimer. This closely oriented N- and C-terminal ends from two different monomers could be structurally explained by the reciprocally oriented C-terminal ends, as a consequence of pTyr705-SH2 interaction, as well as by the relocated N-terminal domains, which is caused by the disruption of NTD-NTD interactions.

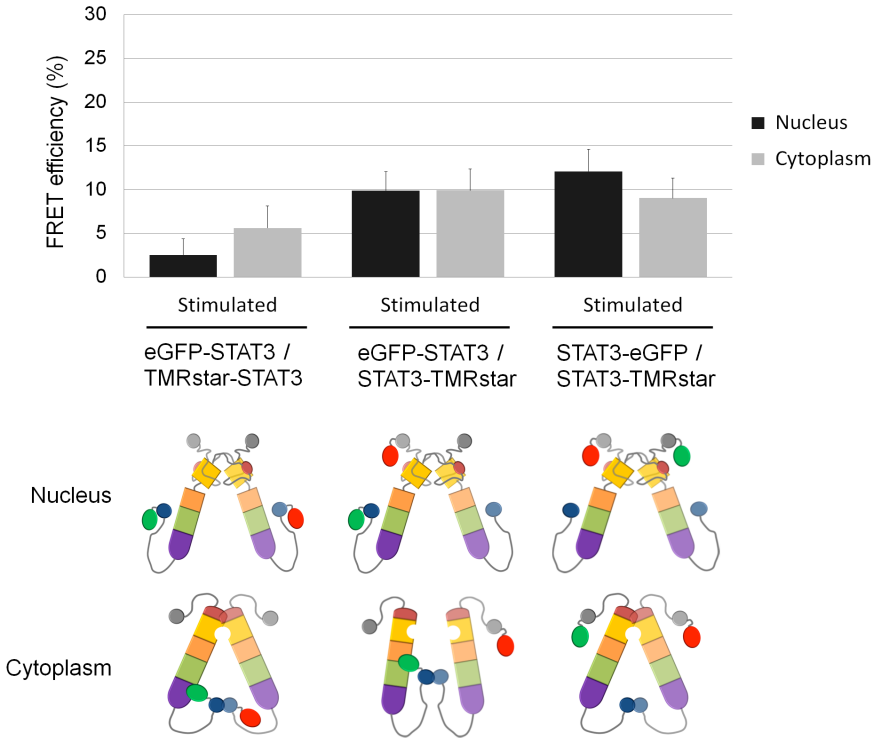


Figure 54. Summary of FRET results on wild type STAT3 in activated state. The figure represents the differently combined FRET donor and acceptor pairs with measured FRET efficiencies in nuclear and cytoplasmic regions. Proposed localizations of the fluorophores in activated dimer structures are highlighted in green (donor, eGFP) and red (acceptor, TMRstar).

We cannot detect any differences in FRET signals between nuclear and cytoplasmic fraction for the constructs eGFP-STAT3 / STAT3-TMRstar, indicating the existence of an intermediate dimer formation from de-activated molecules which is stabilized by N-terminal interactions in a structural orientation where the N- and C-terminal domains are closely localized (Figure 54, eGFP-STAT3 / STAT3-TMRstar, cytoplasm).
FRET results from STAT3-eGFP / STAT3-TMRstar showed increased transfer efficiency upon cytokine stimulation, compared to unstimulated sample, similar to publications by others [70, 134] as a consequence of SH2-domain mediated dimer formation (Figure 54, STAT3-eGFP / STAT3-TMRstar, nucleus), where the reduced FRET signal in the cytoplasmic region represents the non-activated/de-activated dimer forms.

To confirm our results the measurements were additionally performed in living cells (section 3.3.4., Figure 30B).

The formation of STAT3 oligomers as tetramers on specific DNA target sites is a well described phenomenon, which is mediated by homotypic interaction of N-terminal domains [141, 142]. Tetramerization of STAT3 was shown to be essential for the maximal transcriptional activation of the α2-macroglobulin gene promoter, and this cooperation was also stabilized by interactions between the N-terminal fragments [35].

We analyzed the inhibition of N-domain interactions on the activation of the α2-macroglobulin promoter (section 3.5.3.) with the expression of a plasmid construct encoding the N-terminal fragment of STAT3 (SNAP-NTD). Using wild type NTD, we were able to downregulate the promoter activation, most probably by the inhibition of N-domain interactions, which results in the disruption of tetramer formations (Figure 36).

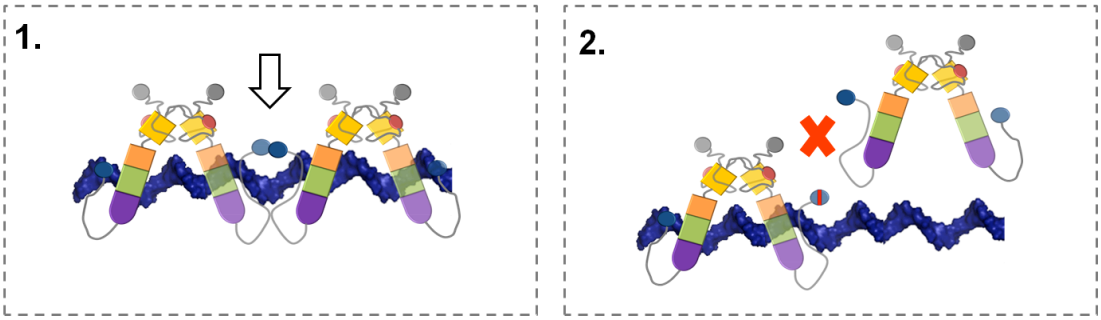


Figure 55. Tetramerization of STAT3 molecules on DNA. (1) STAT3 tetramers on specific DNA sequences are stabilized by homotypic N-terminal interactions (indicated by the arrow) **(2)** Disrupting the NTD-NTD interactions by mutating the L78 residue, destabilizes the tetramer formation.

In contrast, this inhibition disappeared when the N-terminal domain was mutated at L78 position (Figure 39). These findings suggest a similar NTD-NTD interaction interface involved in latent dimer formation, as well in tetramerization of STAT3, representing a possible target for inhibitor design against the oligomerized STAT3 molecules (Figure 55).

In context of oligomerization it is still an open question is how the N-terminal domains contribute to STAT3 body formations (section 1.6.2). Previous report on STAT1 paracrystals [83] showed the involvement of mutual N-domain and pTyr-SH2 domain interactions in the assembly of the proteins However, in our hands the N-terminally deleted or L78R mutated STAT3 molecules were still able to form nuclear bodies after cytokine stimulation.

4.3. STAT3 dimer formations in the JAK/STAT3 pathway

Our FRET results demonstrated the existence of stable, unphosphorylated STAT3 dimers in latent state (Figure 53 and 56) which is in good agreement with previously published results [67, 69, 70].
We found that dimer formation is dominated by homotypic interactions between the N-terminal domains, similar to other STATs [135, 140] and additionally we identified the L78 residue to be important in promoting the association of the NTDs (section 3.5.2.).

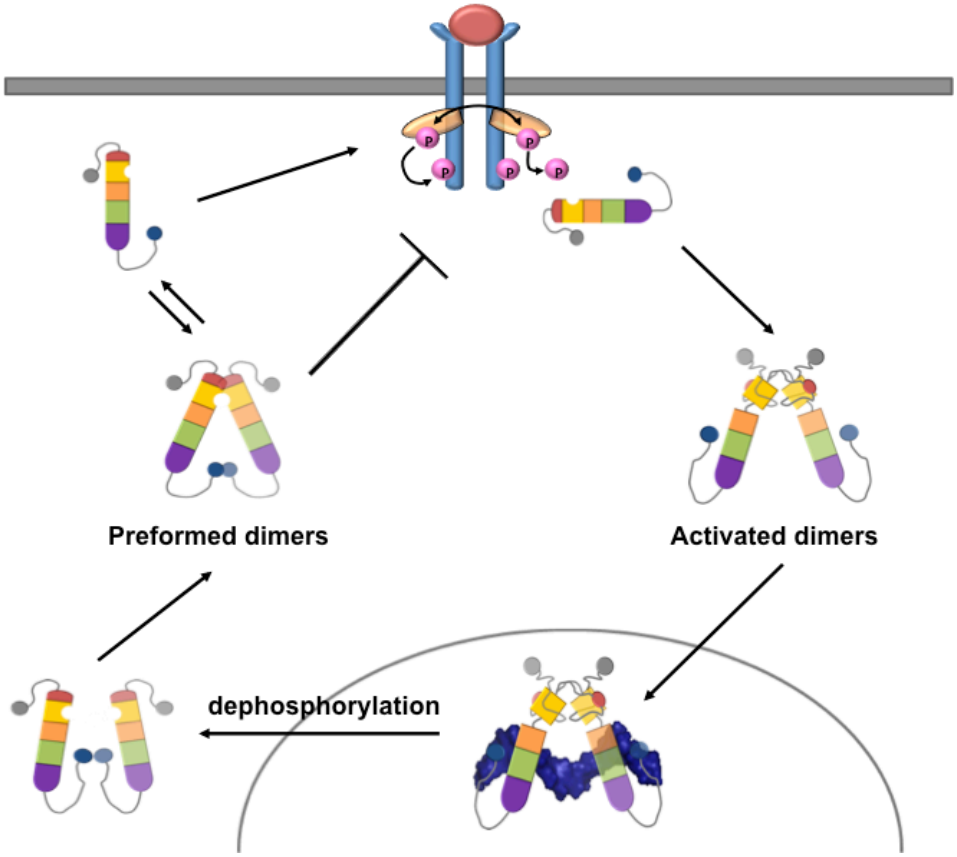


Figure 56. Preformed and activated STAT3 dimers in the JAK/STAT3 pathway. Monomers are associated in latent state (preformed dimers) in a parallel orientation. This dimer is mostly stabilized by homotypic interactions between the N-terminal domains, and orientates the monomers in a form, which structurally allows the separate SH2 domains to interact with each other (additional stabilization) avoiding the monomers from activation (receptor binding). The phosphorylated monomers are associated in an activated dimer form (stabilized by pTyr-SH2 interactions) and translocated to the nuclear compartment where they bind to specific DNA sequences. After inactivation (dephosphorylation) STAT3 is transported to the cytoplasmic region, and through an intermediate state, forms latent dimers or monomers.

This interaction between N-terminal regions, drives the two monomers into a parallel orientation which is stabilized by the SH2 domains. This dimer form is structurally inhibited from activation (receptor binding) (Figure 47 and Figure 56).
Activated and phosphorylated STAT3 monomers also dimerize in a parallel manner, which is driven and stabilized by pTyr-SH2 reciprocal interactions. This activated form translocates to the nucleus and binds to DNA. After dephosphorylation, the molecules return to the cytoplasm and are stabilized through an intermediate state in a latent parallel dimer form (Figure 56).

5. Conclusions and perspectives

The central aim of our study was to investigate STAT3 dimerization in latent and activated state with single molecule spectroscopy and advanced microscopy methods as 2f-FCS or acceptor photobleaching FRET.

In this study we demonstrated the importance of the N-terminal domain in the dimerization of latent STAT3 (section 3.4) as well as the role of homotypic interactions of NTDs in the stabilization of these dimer forms (section 3.5.1).

We identified the relevance of the L78 residue in promoting these interactions (section 3.5.2 and section 3.6.2), and additionally the participitation of this dimer interface in tetramerization of STAT3 on the α2-macroglobulin promoter (section 3.5.3).

We identified the role of preassociated STAT3 dimers in the negative regulation of STAT3 activation (section 3.7) and we proposed the SH2 domain involvement as additional stabilizators in formation of latent dimers (section 3.8).

From our FRET results we concluded the parallel association of the non-activated and activated dimer forms, however the dimeric complexes are stabilized by diverse interdomain interactions (Figure 56).

Although our findings indicate the existence of a similar N-terminal domain dimer interface in context of STAT3, as in case of other STAT family members, this does not rule out the divergent structural organization of NTD dimers.

This possibility should be analyzed by crystallographic studies on NTD-dimers of STAT3. More detailed knowledge of NTD-dimer interface(s) of STAT3 is indispensable for successful inhibitor design against these interaction surfaces.

Based on our results we proposed the SH2-SH2 interaction as a secondary stabilizer interface in preformed dimerization. This hypothesis should be refined by point mutation studies on the SH2 domain based on the somatic mutations found in several diseases such as hyperimmunoglobulin-E syndrome (HIES), large granular lymphocytic leukaemia (LGL leukaemia) or in inflammatory hepatocellular adenomas (IHCAs) (section 1.5.3) to identify key residues in promoting SH2 homotypic interactions and structurally answer the effect of these mutations on formation of latent dimers, or on the overall STAT3 structure.

The work presented here proposes the structurally similar organizations of preformed and activated dimer forms (parallel arrangements). The activation requires only a slight turn of the monomers in respect to each other in the phosphorylated dimer form as a consequence of pTyr-SH2 interaction formation.

In context of inhibitor design it could be interesting how STAT3 molecules can be kept in „preformed“ state avoiding the molecules from activation, or the other way around is there a possiblity to turn or force the activated STAT3 dimers to an inactive dimer form.

Another important issue is to analyze the function of the N-terminally mutated STAT3 in mouse models, which could possibly explain the roles of the N-terminal domain in diverse biological functions.

In case of tetramerization or oligomerization of STAT3, there are still some interesting questions to answer, as is tetramerization only formed on specific DNA sequences and restricted to tandem STAT3 binding sites, or also possible on single canonical sites, as it is proposed for STAT1 [144].

References

1. Compston, A. and A. Coles, *Multiple sclerosis.* Lancet, 2008. **372** 1502-17.
2. Cohen, S., P.E. Bigazzi, and T. Yoshida, *Commentary. Similarities of T cell function in cell-mediated immunity and antibody production.* Cell Immunol, 1974. **12** 150-9.
3. Tayal, V. and B.S. Kalra, *Cytokines and anti-cytokines as therapeutics - An update.* European Journal of Pharmacology, 2008. **579** 1-12.
4. Jones, S.A., J. Scheller, and S. Rose-John, *Therapeutic strategies for the clinical blockade of IL-6/gp130 signaling.* J Clin Invest, 2011. **121** 3375-83.
5. Schwache, D. and G. Muller-Newen, *Receptor fusion proteins for the inhibition of cytokines.* Eur J Cell Biol, 2012. **91** 428-34.
6. Papanicolaou, D.A. and A.N. Vgontzas, *Interleukin-6: the endocrine cytokine.* J Clin Endocrinol Metab, 2000. **85** 1331-3.
7. Dinarello, C.A., *Role of pro- and anti-inflammatory cytokines during inflammation: experimental and clinical findings.* Journal of Biological Regulators and Homeostatic Agents, 1997. **11** 91-103.
8. Heinrich, P.C., I. Behrmann, S. Haan, H.M. Hermanns, G. Muller-Newen, and F. Schaper, *Principles of interleukin (IL)-6-type cytokine signalling and its regulation.* Biochem J, 2003. **374** 1-20.
9. Bazan, J.F., *A novel family of growth factor receptors: a common binding domain in the growth hormone, prolactin, erythropoietin and IL-6 receptors, and the p75 IL-2 receptor beta-chain.* Biochem Biophys Res Commun, 1989. **164** 788-95.
10. Garbers, C., H.M. Hermanns, F. Schaper, G. Muller-Newen, J. Grotzinger, S. Rose-John, and J. Scheller, *Plasticity and cross-talk of Interleukin 6-type cytokines.* Cytokine Growth Factor Rev, 2012. **23** 85-97.
11. Pflanz, S., J.C. Timans, J. Cheung, R. Rosales, H. Kanzler, J. Gilbert, L. Hibbert, T. Churakova, M. Travis, E. Vaisberg, W.M. Blumenschein, J.D. Mattson, J.L. Wagner, W. To, S. Zurawski, T.K. McClanahan, D.M. Gorman, J.F. Bazan, R. de Waal Malefyt, D. Rennick, and R.A. Kastelein, *IL-27, a heterodimeric cytokine composed of EBI3 and p28 protein, induces proliferation of naive CD4(+) T cells.* Immunity, 2002. **16** 779-90.
12. Rawlings, J.S., K.M. Rosler, and D.A. Harrison, *The JAK/STAT signaling pathway.* J Cell Sci, 2004. **117** 1281-3.
13. Levy, D.E. and J.E. Darnell, Jr., *Stats: transcriptional control and biological impact.* Nat Rev Mol Cell Biol, 2002. **3** 651-62.
14. Winston, L.A. and T. Hunter, *Intracellular signalling: putting JAKs on the kinase MAP.* Curr Biol, 1996. **6** 668-71.
15. Becker, S., B. Groner, and C.W. Muller, *Three-dimensional structure of the Stat3beta homodimer bound to DNA.* Nature, 1998. **394** 145-51.
16. Darnell, J.E., Jr., *STATs and gene regulation.* Science, 1997. **277** 1630-5.
17. Mohr, A., N. Chatain, T. Domoszlai, N. Rinis, M. Sommerauer, M. Vogt, and G. Muller-Newen, *Dynamics and non-canonical aspects of JAK/STAT signalling.* Eur J Cell Biol, 2012. **91** 524-32.
18. Santos, C.I. and A.P. Costa-Pereira, *Signal transducers and activators of transcription-from cytokine signalling to cancer biology.* Biochim Biophys Acta, 2011. **1816** 38-49.

19. Li, W.X., *Canonical and non-canonical JAK-STAT signaling.* Trends Cell Biol, 2008. **18** 545-51.
20. Ng, D.C., B.H. Lin, C.P. Lim, G. Huang, T. Zhang, V. Poli, and X. Cao, *Stat3 regulates microtubules by antagonizing the depolymerization activity of stathmin.* J Cell Biol, 2006. **172** 245-57.
21. Gough, D.J., A. Corlett, K. Schlessinger, J. Wegrzyn, A.C. Larner, and D.E. Levy, *Mitochondrial STAT3 supports Ras-dependent oncogenic transformation.* Science, 2009. **324** 1713-6.
22. Stark, G.R. and J.E. Darnell, *The JAK-STAT Pathway at Twenty.* Immunity, 2012. **36** 503-514.
23. Darnell, J.E., Jr., I.M. Kerr, and G.R. Stark, *Jak-STAT pathways and transcriptional activation in response to IFNs and other extracellular signaling proteins.* Science, 1994. **264** 1415-21.
24. Copeland, N.G., D.J. Gilbert, C. Schindler, Z. Zhong, Z. Wen, J.E. Darnell, Jr., A.L. Mui, A. Miyajima, F.W. Quelle, J.N. Ihle, and et al., *Distribution of the mammalian Stat gene family in mouse chromosomes.* Genomics, 1995. **29** 225-8.
25. Benekli, M., M.R. Baer, H. Baumann, and M. Wetzler, *Signal transducer and activator of transcription proteins in leukemias.* Blood, 2003. **101** 2940-54.
26. O'Sullivan, L.A., C. Liongue, R.S. Lewis, S.E. Stephenson, and A.C. Ward, *Cytokine receptor signaling through the Jak-Stat-Socs pathway in disease.* Mol Immunol, 2007. **44** 2497-506.
27. Bowman, T., R. Garcia, J. Turkson, and R. Jove, *STATs in oncogenesis.* Oncogene, 2000. **19** 2474-88.
28. Lim, C.P. and X. Cao, *Structure, function, and regulation of STAT proteins.* Mol Biosyst, 2006. **2** 536-50.
29. Soler-Lopez, M., C. Petosa, M. Fukuzawa, R. Ravelli, J.G. Williams, and C.W. Muller, *Structure of an activated Dictyostelium STAT in its DNA-unbound form.* Mol Cell, 2004. **13** 791-804.
30. Wegenka, U.M., J. Buschmann, C. Lutticken, P.C. Heinrich, and F. Horn, *Acute-phase response factor, a nuclear factor binding to acute-phase response elements, is rapidly activated by interleukin-6 at the posttranslational level.* Mol Cell Biol, 1993. **13** 276-88.
31. Zhong, Z., Z. Wen, and J.E. Darnell, Jr., *Stat3: a STAT family member activated by tyrosine phosphorylation in response to epidermal growth factor and interleukin-6.* Science, 1994. **264** 95-8.
32. Akira, S., Y. Nishio, M. Inoue, X.J. Wang, S. Wei, T. Matsusaka, K. Yoshida, T. Sudo, M. Naruto, and T. Kishimoto, *Molecular cloning of APRF, a novel IFN-stimulated gene factor 3 p91-related transcription factor involved in the gp130-mediated signaling pathway.* Cell, 1994. **77** 63-71.
33. Hou, T., S. Ray, C. Lee, and A.R. Brasier, *The STAT3 NH2-terminal domain stabilizes enhanceosome assembly by interacting with the p300 bromodomain.* J Biol Chem, 2008. **283** 30725-34.
34. Vinkemeier, U., I. Moarefi, J.E. Darnell, Jr., and J. Kuriyan, *Structure of the amino-terminal protein interaction domain of STAT-4.* Science, 1998. **279** 1048-52.
35. Zhang, X. and J.E. Darnell, Jr., *Functional importance of Stat3 tetramerization in activation of the alpha 2-macroglobulin gene.* J Biol Chem, 2001. **276** 33576-81.

36. Zhang, X., M.H. Wrzeszczynska, C.M. Horvath, and J.E. Darnell, Jr., *Interacting regions in Stat3 and c-Jun that participate in cooperative transcriptional activation.* Mol Cell Biol, 1999. **19** 7138-46.
37. Zhang, T., W.H. Kee, K.T. Seow, W. Fung, and X. Cao, *The coiled-coil domain of Stat3 is essential for its SH2 domain-mediated receptor binding and subsequent activation induced by epidermal growth factor and interleukin-6.* Mol Cell Biol, 2000. **20** 7132-9.
38. Greenlund, A.C., M.A. Farrar, B.L. Viviano, and R.D. Schreiber, *Ligand-induced IFN gamma receptor tyrosine phosphorylation couples the receptor to its signal transduction system (p91).* EMBO J, 1994. **13** 1591-600.
39. Shuai, K., C.M. Horvath, L.H. Huang, S.A. Qureshi, D. Cowburn, and J.E. Darnell, Jr., *Interferon activation of the transcription factor Stat91 involves dimerization through SH2-phosphotyrosyl peptide interactions.* Cell, 1994. **76** 821-8.
40. Schuringa, J.J., H. Schepers, E. Vellenga, and W. Kruijer, *Ser727-dependent transcriptional activation by association of p300 with STAT3 upon IL-6 stimulation.* FEBS Lett, 2001. **495** 71-6.
41. Zhang, T., K.T. Seow, C.T. Ong, and X. Cao, *Interdomain interaction of Stat3 regulates its Src homology 2 domain-mediated receptor binding activity.* J Biol Chem, 2002. **277** 17556-63.
42. Hevehan, D.L., W.M. Miller, and E.T. Papoutsakis, *Differential expression and phosphorylation of distinct STAT3 proteins during granulocytic differentiation.* Blood, 2002. **99** 1627-37.
43. Aggarwal, B.B., A.B. Kunnumakkara, K.B. Harikumar, S.R. Gupta, S.T. Tharakan, C. Koca, S. Dey, and B. Sung, *Signal transducer and activator of transcription-3, inflammation, and cancer: how intimate is the relationship?* Ann N Y Acad Sci, 2009. **1171** 59-76.
44. Wen, Z., Z. Zhong, and J.E. Darnell, Jr., *Maximal activation of transcription by Stat1 and Stat3 requires both tyrosine and serine phosphorylation.* Cell, 1995. **82** 241-50.
45. Lim, C.P. and X. Cao, *Serine phosphorylation and negative regulation of Stat3 by JNK.* J Biol Chem, 1999. **274** 31055-61.
46. Hazan-Halevy, I., D. Harris, Z. Liu, J. Liu, P. Li, X. Chen, S. Shanker, A. Ferrajoli, M.J. Keating, and Z. Estrov, *STAT3 is constitutively phosphorylated on serine 727 residues, binds DNA, and activates transcription in CLL cells.* Blood, 2010. **115** 2852-63.
47. Yuan, Z.L., Y.J. Guan, D. Chatterjee, and Y.E. Chin, *Stat3 dimerization regulated by reversible acetylation of a single lysine residue.* Science, 2005. **307** 269-73.
48. Wormald, S. and D.J. Hilton, *Inhibitors of cytokine signal transduction.* J Biol Chem, 2004. **279** 821-4.
49. Jackson, P.K., *A new RING for SUMO: wrestling transcriptional responses into nuclear bodies with PIAS family E3 SUMO ligases.* Genes Dev, 2001. **15** 3053-8.
50. Chung, C.D., J. Liao, B. Liu, X. Rao, P. Jay, P. Berta, and K. Shuai, *Specific inhibition of Stat3 signal transduction by PIAS3.* Science, 1997. **278** 1803-5.
51. Kim, D.J., M.L. Tremblay, and J. Digiovanni, *Protein tyrosine phosphatases, TC-PTP, SHP1, and SHP2, cooperate in rapid dephosphorylation of Stat3 in keratinocytes following UVB irradiation.* PLoS One, 2010. **5** 10290.

52. Perry, E., R. Tsruya, P. Levitsky, O. Pomp, M. Taller, S. Weisberg, W. Parris, S. Kulkarni, H. Malovani, T. Pawson, S. Shpungin, and U. Nir, *TMF/ARA160 is a BC-box-containing protein that mediates the degradation of Stat3.* Oncogene, 2004. **23** 8908-19.
53. Daino, H., I. Matsumura, K. Takada, J. Odajima, H. Tanaka, S. Ueda, H. Shibayama, H. Ikeda, M. Hibi, T. Machii, T. Hirano, and Y. Kanakura, *Induction of apoptosis by extracellular ubiquitin in human hematopoietic cells: possible involvement of STAT3 degradation by proteasome pathway in interleukin 6-dependent hematopoietic cells.* Blood, 2000. **95** 2577-85.
54. Minegishi, Y., M. Saito, S. Tsuchiya, I. Tsuge, H. Takada, T. Hara, N. Kawamura, T. Ariga, S. Pasic, O. Stojkovic, A. Metin, and H. Karasuyama, *Dominant-negative mutations in the DNA-binding domain of STAT3 cause hyper-IgE syndrome.* Nature, 2007. **448** 1058-62.
55. He, J., J. Shi, X. Xu, W. Zhang, Y. Wang, X. Chen, Y. Du, N. Zhu, J. Zhang, Q. Wang, and J. Yang, *STAT3 mutations correlated with hyper-IgE syndrome lead to blockage of IL-6/STAT3 signalling pathway.* J Biosci, 2012. **37** 243-57.
56. Tangye, S.G., M.C. Cook, and D.A. Fulcher, *Insights into the role of STAT3 in human lymphocyte differentiation as revealed by the hyper-IgE syndrome.* J Immunol, 2009. **182** 21-8.
57. Koskela, H.L., S. Eldfors, P. Ellonen, A.J. van Adrichem, H. Kuusanmaki, E.I. Andersson, S. Lagstrom, M.J. Clemente, T. Olson, S.E. Jalkanen, M.M. Majumder, H. Almusa, H. Edgren, M. Lepisto, P. Mattila, K. Guinta, P. Koistinen, T. Kuittinen, K. Penttinen, A. Parsons, J. Knowles, J. Saarela, K. Wennerberg, O. Kallioniemi, K. Porkka, T.P. Loughran, Jr., C.A. Heckman, J.P. Maciejewski, and S. Mustjoki, *Somatic STAT3 mutations in large granular lymphocytic leukemia.* N Engl J Med, 2012. **366** 1905-13.
58. Pilati, C., M. Amessou, M.P. Bihl, C. Balabaud, J.T. Nhieu, V. Paradis, J.C. Nault, T. Izard, P. Bioulac-Sage, G. Couchy, K. Poussin, and J. Zucman-Rossi, *Somatic mutations activating STAT3 in human inflammatory hepatocellular adenomas.* J Exp Med, 2011. **208** 1359-66.
59. Yu, H. and R. Jove, *The stats of cancer - New molecular targets come of age.* Nature Reviews Cancer, 2004. **4** 97-105.
60. Debnath, B., S. Xu, and N. Neamati, *Small Molecule Inhibitors of Signal Transducer and Activator of Transcription 3 (Stat3) Protein.* J Med Chem, 2012.
61. Krause, A., N. Scaletta, J.D. Ji, and L.B. Ivashkiv, *Rheumatoid arthritis synoviocyte survival is dependent on Stat3.* J Immunol, 2002. **169** 6610-6.
62. Sano, S., K.S. Chan, S. Carbajal, J. Clifford, M. Peavey, K. Kiguchi, S. Itami, B.J. Nickoloff, and J. DiGiovanni, *Stat3 links activated keratinocytes and immunocytes required for development of psoriasis in a novel transgenic mouse model.* Nat Med, 2005. **11** 43-9.
63. Sugimoto, K., *Role of STAT3 in inflammatory bowel disease.* World J Gastroenterol, 2008. **14** 5110-4.
64. Gharavi, N.M., J.A. Alva, K.P. Mouillesseaux, C. Lai, M. Yeh, W. Yeung, J. Johnson, W.L. Szeto, L. Hong, M. Fishbein, L. Wei, L.M. Pfeffer, and J.A. Berliner, *Role of the Jak/STAT pathway in the regulation of interleukin-8 transcription by oxidized phospholipids in vitro and in atherosclerosis in vivo.* J Biol Chem, 2007. **282** 31460-8.

65. Bach, E.A., M. Aguet, and R.D. Schreiber, *The IFN gamma receptor: a paradigm for cytokine receptor signaling.* Annu Rev Immunol, 1997. **15** 563-91.
66. Stancato, L.F., M. David, C. Carter-Su, A.C. Larner, and W.B. Pratt, *Preassociation of STAT1 with STAT2 and STAT3 in separate signalling complexes prior to cytokine stimulation.* J Biol Chem, 1996. **271** 4134-7.
67. Haan, S., M. Kortylewski, I. Behrmann, W. Muller-Esterl, P.C. Heinrich, and F. Schaper, *Cytoplasmic STAT proteins associate prior to activation.* Biochem J, 2000. **345** 417-21.
68. Braunstein, J., S. Brutsaert, R. Olson, and C. Schindler, *STATs dimerize in the absence of phosphorylation.* J Biol Chem, 2003. **278** 34133-40.
69. Schroder, M., K.M. Kroeger, H.D. Volk, K.A. Eidne, and G. Grutz, *Preassociation of nonactivated STAT3 molecules demonstrated in living cells using bioluminescence resonance energy transfer: a new model of STAT activation?* J Leukoc Biol, 2004. **75** 792-7.
70. Kretzschmar, A.K., M.C. Dinger, C. Henze, K. Brocke-Heidrich, and F. Horn, *Analysis of Stat3 (signal transducer and activator of transcription 3) dimerization by fluorescence resonance energy transfer in living cells.* Biochem J, 2004. **377** 289-97.
71. Pranada, A.L., S. Metz, A. Herrmann, P.C. Heinrich, and G. Muller-Newen, *Real time analysis of STAT3 nucleocytoplasmic shuttling.* J Biol Chem, 2004. **279** 15114-23.
72. Meyer, T. and U. Vinkemeier, *Nucleocytoplasmic shuttling of STAT transcription factors.* Eur J Biochem, 2004. **271** 4606-12.
73. Wenta, N., H. Strauss, S. Meyer, and U. Vinkemeier, *Tyrosine phosphorylation regulates the partitioning of STAT1 between different dimer conformations.* Proc Natl Acad Sci U S A, 2008. **105** 9238-43.
74. Zhong, M., M.A. Henriksen, K. Takeuchi, O. Schaefer, B. Liu, J. ten Hoeve, Z. Ren, X. Mao, X. Chen, K. Shuai, and J.E. Darnell, Jr., *Implications of an antiparallel dimeric structure of nonphosphorylated STAT1 for the activation-inactivation cycle.* Proc Natl Acad Sci U S A, 2005. **102** 3966-71.
75. Mertens, C., M. Zhong, R. Krishnaraj, W. Zou, X. Chen, and J.E. Darnell, Jr., *Dephosphorylation of phosphotyrosine on STAT1 dimers requires extensive spatial reorientation of the monomers facilitated by the N-terminal domain.* Genes Dev, 2006. **20** 3372-81.
76. Ihle, J.N., *STATs: signal transducers and activators of transcription.* Cell, 1996. **84** 331-4.
77. Lin, J.X., P. Li, D. Liu, H.T. Jin, J. He, M. Ata Ur Rasheed, Y. Rochman, L. Wang, K. Cui, C. Liu, B.L. Kelsall, R. Ahmed, and W.J. Leonard, *Critical Role of STAT5 transcription factor tetramerization for cytokine responses and normal immune function.* Immunity, 2012. **36** 586-99.
78. Ndubuisi, M.I., G.G. Guo, V.A. Fried, J.D. Etlinger, and P.B. Sehgal, *Cellular physiology of STAT3: Where's the cytoplasmic monomer?* J Biol Chem, 1999. **274** 25499-509.
79. Watanabe, K., K. Saito, M. Kinjo, T. Matsuda, M. Tamura, S. Kon, T. Miyazaki, and T. Uede, *Molecular dynamics of STAT3 on IL-6 signaling pathway in living cells.* Biochem Biophys Res Commun, 2004. **324** 1264-73.

80. Shah, M., K. Patel, V.A. Fried, and P.B. Sehgal, *Interactions of STAT3 with caveolin-1 and heat shock protein 90 in plasma membrane raft and cytosolic complexes. Preservation of cytokine signaling during fever.* J Biol Chem, 2002. **277** 45662-9.
81. Herrmann, A., U. Sommer, A.L. Pranada, B. Giese, A. Kuster, S. Haan, W. Becker, P.C. Heinrich, and G. Muller-Newen, *STAT3 is enriched in nuclear bodies.* J Cell Sci, 2004. **117** 339-49.
82. Martincuks, A., *Cross-talk and subcellular localization of NF-κB and STAT3.* Master thesis, 2012.
83. Droescher, M., A. Begitt, A. Marg, M. Zacharias, and U. Vinkemeier, *Cytokine-induced paracrystals prolong the activity of signal transducers and activators of transcription (STAT) and provide a model for the regulation of protein solubility by small ubiquitin-like modifier (SUMO).* J Biol Chem, 2011. **286** 18731-46.
84. Howe, C.L. and W.C. Mobley, *Signaling endosome hypothesis: A cellular mechanism for long distance communication.* J Neurobiol, 2004. **58** 207-16.
85. Howe, C.L., *Modeling the signaling endosome hypothesis: why a drive to the nucleus is better than a (random) walk.* Theor Biol Med Model, 2005. **2** 43.
86. Haustein, E. and P. Schwille, *Single-molecule spectroscopic methods.* Curr Opin Struct Biol, 2004. **14** 531-40.
87. Ishikawa-Ankerhold, H.C., R. Ankerhold, and G.P. Drummen, *Advanced fluorescence microscopy techniques--FRAP, FLIP, FLAP, FRET and FLIM.* Molecules, 2012. **17** 4047-132.
88. Magde, D., W.W. Webb, and E. Elson, *Thermodynamic Fluctuations in a Reacting System - Measurement by Fluorescence Correlation Spectroscopy.* Physical Review Letters, 1972. **29** 705.
89. Chiantia, S., J. Ries, and P. Schwille, *Fluorescence correlation spectroscopy in membrane structure elucidation.* Biochim Biophys Acta, 2009. **1788** 225-33.
90. Haustein, E. and P. Schwille, *Fluorescence correlation spectroscopy: novel variations of an established technique.* Annu Rev Biophys Biomol Struct, 2007. **36** 151-69.
91. Dertinger, T., V. Pacheco, I. von der Hocht, R. Hartmann, I. Gregor, and J. Enderlein, *Two-focus fluorescence correlation spectroscopy: a new tool for accurate and absolute diffusion measurements.* Chemphyschem, 2007. **8** 433-43.
92. Petrasek, Z., J. Ries, and P. Schwille, *Scanning FCS for the characterization of protein dynamics in live cells.* Methods Enzymol, 2010. **472** 317-43.
93. Eigen, M. and R. Rigler, *Sorting single molecules: application to diagnostics and evolutionary biotechnology.* Proc Natl Acad Sci U S A, 1994. **91** 5740-7.
94. Schwille, P., F.J. Meyer-Almes, and R. Rigler, *Dual-color fluorescence cross-correlation spectroscopy for multicomponent diffusional analysis in solution.* Biophys J, 1997. **72** 1878-86.
95. Bacia, K., S.A. Kim, and P. Schwille, *Fluorescence cross-correlation spectroscopy in living cells.* Nat Methods, 2006. **3** 83-9.
96. Förster, T., *Zwischenmolekulare Energiewanderung und Fluoreszenz.* Ann. Physik, 1948. **55**.
97. Stryer, L., *Fluorescence energy transfer as a spectroscopic ruler.* Annu Rev Biochem, 1978. **47** 819-46.

98. Gadella, T.W.J., *FRET and FLIM techniques*. 1st ed. Laboratory techniques in biochemistry and molecular biology,. 2009, Amsterdam ; Boston: Elsevier. XXIII, 534.
99. Piston, D.W. and G.J. Kremers, *Fluorescent protein FRET: the good, the bad and the ugly.* Trends Biochem Sci, 2007. **32** 407-14.
100. Yue, P. and J. Turkson, *Targeting STAT3 in cancer: how successful are we?* Expert Opin Investig Drugs, 2009. **18** 45-56.
101. Arcone, R., P. Pucci, F. Zappacosta, V. Fontaine, A. Malorni, G. Marino, and G. Ciliberto, *Single-step purification and structural characterization of human interleukin-6 produced in Escherichia coli from a T7 RNA polymerase expression vector.* Eur J Biochem, 1991. **198** 541-7.
102. Weiergraber, O., U. Hemmann, A. Kuster, G. Muller-Newen, J. Schneider, S. Rose-John, P. Kurschat, J.P. Brakenhoff, M.H. Hart, S. Stabel, and et al., *Soluble human interleukin-6 receptor. Expression in insect cells, purification and characterization.* Eur J Biochem, 1995. **234** 661-9.
103. Schagger, H., W.A. Cramer, and G. von Jagow, *Analysis of molecular masses and oligomeric states of protein complexes by blue native electrophoresis and isolation of membrane protein complexes by two-dimensional native electrophoresis.* Anal Biochem, 1994. **217** 220-30.
104. Pawley, J.B., *Handbook of biological confocal microscopy*. 3rd ed. 2006, New York, NY: Springer. XXVIII, 985.
105. Minsky., M., *Microscopy Apparatus.* US Patent, 1961. **3013467**.
106. G.G., Stokes., Philos. Trans. (Royal Soc.) 142 479, 1852.
107. Shimomura, O., F.H. Johnson, and Y. Saiga, *Extraction, purification and properties of aequorin, a bioluminescent protein from the luminous hydromedusan, Aequorea.* J Cell Comp Physiol, 1962. **59** 223-39.
108. Chalfie, M., Y. Tu, G. Euskirchen, W.W. Ward, and D.C. Prasher, *Green fluorescent protein as a marker for gene expression.* Science, 1994. **263** 802-5.
109. Heim, R., A.B. Cubitt, and R.Y. Tsien, *Improved green fluorescence.* Nature, 1995. **373** 663-4.
110. Tsien, R.Y., *The green fluorescent protein.* Annu Rev Biochem, 1998. **67** 509-44.
111. Sample, V., R.H. Newman, and J. Zhang, *The structure and function of fluorescent proteins.* Chem Soc Rev, 2009. **38** 2852-64.
112. Palm, G.J., A. Zdanov, G.A. Gaitanaris, R. Stauber, G.N. Pavlakis, and A. Wlodawer, *The structural basis for spectral variations in green fluorescent protein.* Nat Struct Biol, 1997. **4** 361-5.
113. Hinner, M.J. and K. Johnsson, *How to obtain labeled proteins and what to do with them.* Current Opinion in Biotechnology, 2010. **21** 766-776.
114. Wibley, J.E., J.H. McKie, K. Embrey, D.S. Marks, K.T. Douglas, M.H. Moore, and P.C. Moody, *A homology model of the three-dimensional structure of human O6-alkylguanine-DNA alkyltransferase based on the crystal structure of the C-terminal domain of the Ada protein from Escherichia coli.* Anticancer Drug Des, 1995. **10** 75-95.
115. Juillerat, A., T. Gronemeyer, A. Keppler, S. Gendreizig, H. Pick, H. Vogel, and K. Johnsson, *Directed evolution of O6-alkylguanine-DNA alkyltransferase for efficient labeling of fusion proteins with small molecules in vivo.* Chem Biol, 2003. **10** 313-7.

116. Keppler, A., S. Gendreizig, T. Gronemeyer, H. Pick, H. Vogel, and K. Johnsson, *A general method for the covalent labeling of fusion proteins with small molecules in vivo.* Nat Biotechnol, 2003. **21** 86-9.
117. Reymond, L., G. Lukinavicius, K. Umezawa, D. Maurel, M.A. Brun, A. Masharina, K. Bojkowska, B. Mollwitz, A. Schena, R. Griss, and K. Johnsson, *Visualizing Biochemical Activities in Living Cells through Chemistry.* Chimia, 2011. **65** 868-871.
118. Muller, C.B., A. Loman, V. Pacheco, F. Koberling, D. Willbold, W. Richtering, and J. Enderlein, *Precise measurement of diffusion by multi-color dual-focus fluorescence correlation spectroscopy.* Epl, 2008. **83**
119. Böhmer, M., Pampaloni, F., Wahl, M., Rahn, H. J., Erdmann, R. and Enderlein, J., *Advanced time-resolved confocal scanning device for ultrasensitive fluorescence detection.* . Rev. Sci. Instrum. , 2001. 4145-4152.
120. Muller, C.B. and W. Richtering, *Sealed and temperature-controlled sample cell for inverted and confocal microscopes and fluorescence correlation spectroscopy.* Colloid and Polymer Science, 2008. **286** 1215-1222.
121. Miyawaki, A., J. Llopis, R. Heim, J.M. McCaffery, J.A. Adams, M. Ikura, and R.Y. Tsien, *Fluorescent indicators for Ca2+ based on green fluorescent proteins and calmodulin.* Nature, 1997. **388** 882-7.
122. Komatsu, N., K. Aoki, M. Yamada, H. Yukinaga, Y. Fujita, Y. Kamioka, and M. Matsuda, *Development of an optimized backbone of FRET biosensors for kinases and GTPases.* Mol Biol Cell, 2011. **22** 4647-56.
123. Wouters, F.S., P.I. Bastiaens, K.W. Wirtz, and T.M. Jovin, *FRET microscopy demonstrates molecular association of non-specific lipid transfer protein (nsL-TP) with fatty acid oxidation enzymes in peroxisomes.* EMBO J, 1998. **17** 7179-89.
124. Huang, Y., J. Qiu, S. Dong, M.S. Redell, V. Poli, M.A. Mancini, and D.J. Tweardy, *Stat3 isoforms, alpha and beta, demonstrate distinct intracellular dynamics with prolonged nuclear retention of Stat3beta mapping to its unique C-terminal end.* J Biol Chem, 2007. **282** 34958-67.
125. Lleres, D., S. Swift, and A.I. Lamond, *Detecting protein-protein interactions in vivo with FRET using multiphoton fluorescence lifetime imaging microscopy (FLIM).* Curr Protoc Cytom, 2007. **12** Unit 12 10.
126. Vamosi, G., N. Baudendistel, C.W. von der Lieth, N. Szaloki, G. Mocsar, G. Muller, P. Brazda, W. Waldeck, S. Damjanovich, J. Langowski, and K. Toth, *Conformation of the c-Fos/c-Jun complex in vivo: a combined FRET, FCCS, and MD-modeling study.* Biophys J, 2008. **94** 2859-68.
127. Maurel, D., L. Comps-Agrar, C. Brock, M.L. Rives, E. Bourrier, M.A. Ayoub, H. Bazin, N. Tinel, T. Durroux, L. Prezeau, E. Trinquet, and J.P. Pin, *Cell-surface protein-protein interaction analysis with time-resolved FRET and snap-tag technologies: application to GPCR oligomerization.* Nat Methods, 2008. **5** 561-7.
128. Padilla-Parra, S., N. Auduge, H. Lalucque, J.C. Mevel, M. Coppey-Moisan, and M. Tramier, *Quantitative comparison of different fluorescent protein couples for fast FRET-FLIM acquisition.* Biophys J, 2009. **97** 2368-76.
129. Timofeeva, O.A., V. Gaponenko, S.J. Lockett, S.G. Tarasov, S. Jiang, C.J. Michejda, A.O. Perantoni, and N.I. Tarasova, *Rationally designed inhibitors identify STAT3 N-domain as a promising anticancer drug target.* ACS Chem Biol, 2007. **2** 799-809.

130. Berney, C. and G. Danuser, *FRET or no FRET: a quantitative comparison.* Biophys J, 2003. **84** 3992-4010.
131. Neculai, D., A.M. Neculai, S. Verrier, K. Straub, K. Klumpp, E. Pfitzner, and S. Becker, *Structure of the unphosphorylated STAT5a dimer.* J Biol Chem, 2005. **280** 40782-7.
132. Husby, J., A.K. Todd, S.M. Haider, G. Zinzalla, D.E. Thurston, and S. Neidle, *Molecular dynamics studies of the STAT3 homodimer:DNA complex: relationships between STAT3 mutations and protein-DNA recognition.* J Chem Inf Model, 2012. **52** 1179-92.
133. Lin, J., R. Buettner, Y.C. Yuan, R. Yip, D. Horne, R. Jove, and N. Vaidehi, *Molecular dynamics simulations of the conformational changes in signal transducers and activators of transcription, Stat1 and Stat3.* J Mol Graph Model, 2009. **28** 347-56.
134. Cimica, V., H.C. Chen, J.K. Iyer, and N.C. Reich, *Dynamics of the STAT3 transcription factor: nuclear import dependent on Ran and importin-beta1.* PLoS One, 2011. **6** 20188.
135. Mao, X., Z. Ren, G.N. Parker, H. Sondermann, M.A. Pastorello, W. Wang, J.S. McMurray, B. Demeler, J.E. Darnell, Jr., and X. Chen, *Structural bases of unphosphorylated STAT1 association and receptor binding.* Mol Cell, 2005. **17** 761-71.
136. Ren, Z., X. Mao, C. Mertens, R. Krishnaraj, J. Qin, P.K. Mandal, M.J. Romanowski, J.S. McMurray, and X. Chen, *Crystal structure of unphosphorylated STAT3 core fragment.* Biochem Biophys Res Commun, 2008. **374** 1-5.
137. Ota, N., T.J. Brett, T.L. Murphy, D.H. Fremont, and K.M. Murphy, *N-domain-dependent nonphosphorylated STAT4 dimers required for cytokine-driven activation.* Nat Immunol, 2004. **5** 208-15.
138. Kim, S.A. and P. Schwille, *Intracellular applications of fluorescence correlation spectroscopy: prospects for neuroscience.* Curr Opin Neurobiol, 2003. **13** 583-90.
139. Vogt, M., T. Domoszlai, D. Kleshchanok, S. Lehmann, A. Schmitt, V. Poli, W. Richtering, and G. Muller-Newen, *The role of the N-terminal domain in dimerization and nucleocytoplasmic shuttling of latent STAT3.* J Cell Sci, 2011. **124** 900-9.
140. Chen, X., R. Bhandari, U. Vinkemeier, F. Van Den Akker, J.E. Darnell, Jr., and J. Kuriyan, *A reinterpretation of the dimerization interface of the N-terminal domains of STATs.* Protein Sci, 2003. **12** 361-5.
141. Xu, X., Y.L. Sun, and T. Hoey, *Cooperative DNA binding and sequence-selective recognition conferred by the STAT amino-terminal domain.* Science, 1996. **273** 794-7.
142. Vinkemeier, U., S.L. Cohen, I. Moarefi, B.T. Chait, J. Kuriyan, and J.E. Darnell, Jr., *DNA binding of in vitro activated Stat1 alpha, Stat1 beta and truncated Stat1: interaction between NH2-terminal domains stabilizes binding of two dimers to tandem DNA sites.* EMBO J, 1996. **15** 5616-26.
143. Zhang, L., D.B. Badgwell, J.J. Bevers, 3rd, K. Schlessinger, P.J. Murray, D.E. Levy, and S.S. Watowich, *IL-6 signaling via the STAT3/SOCS3 pathway: functional analysis of the conserved STAT3 N-domain.* Mol Cell Biochem, 2006. **288** 179-89.

144. Meyer, T., L. Hendry, A. Begitt, S. John, and U. Vinkemeier, *A single residue modulates tyrosine dephosphorylation, oligomerization, and nuclear accumulation of stat transcription factors.* J Biol Chem, 2004. **279** 18998-9007.
145. Vogt, M., *Nukleozytoplasmatisches shuttling des latenten und konstitutiv aktivierten Transkriptionsfaktors STAT3.* Doktorthesis, 2011.
146. Truong, K. and M. Ikura, *The use of FRET imaging microscopy to detect protein-protein interactions and protein conformational changes in vivo.* Curr Opin Struct Biol, 2001. **11** 573-8.
147. Hemmann, U., C. Gerhartz, B. Heesel, J. Sasse, G. Kurapkat, J. Grotzinger, A. Wollmer, Z. Zhong, J.E. Darnell, Jr., L. Graeve, P.C. Heinrich, and F. Horn, *Differential activation of acute phase response factor/Stat3 and Stat1 via the cytoplasmic domain of the interleukin 6 signal transducer gp130. II. Src homology SH2 domains define the specificity of stat factor activation.* J Biol Chem, 1996. **271** 12999-3007.
148. Herrmann, A., M. Vogt, M. Monnigmann, T. Clahsen, U. Sommer, S. Haan, V. Poli, P.C. Heinrich, and G. Muller-Newen, *Nucleocytoplasmic shuttling of persistently activated STAT3.* J Cell Sci, 2007. **120** 3249-61.
149. Mohr, A., *IL-6-Typ-Zytokin-vermittelte Aktivierung und Dynamik von STAT3 in zu Neuronen differenzierten STAT3-YFP knock-in Stammzellen und der Wirkmechanismus von dominant-negativem STAT3.* Doktorthesis, 2012.
150. Yang, J., M. Chatterjee-Kishore, S.M. Staugaitis, H. Nguyen, K. Schlessinger, D.E. Levy, and G.R. Stark, *Novel roles of unphosphorylated STAT3 in oncogenesis and transcriptional regulation.* Cancer Res, 2005. **65** 939-47.
151. Timofeeva, O.A., S. Chasovskikh, I. Lonskaya, N.I. Tarasova, L. Khavrutskii, S.G. Tarasov, X. Zhang, V.R. Korostyshevskiy, A. Cheema, L. Zhang, S. Dakshanamurthy, M.L. Brown, and A. Dritschilo, *Mechanisms of unphosphorylated STAT3 transcription factor binding to DNA.* J Biol Chem, 2012. **287** 14192-200.
152. Haan, S., U. Hemmann, U. Hassiepen, F. Schaper, J. Schneider-Mergener, A. Wollmer, P.C. Heinrich, and J. Grotzinger, *Characterization and binding specificity of the monomeric STAT3-SH2 domain.* J Biol Chem, 1999. **274** 1342-8.

Supporting materials

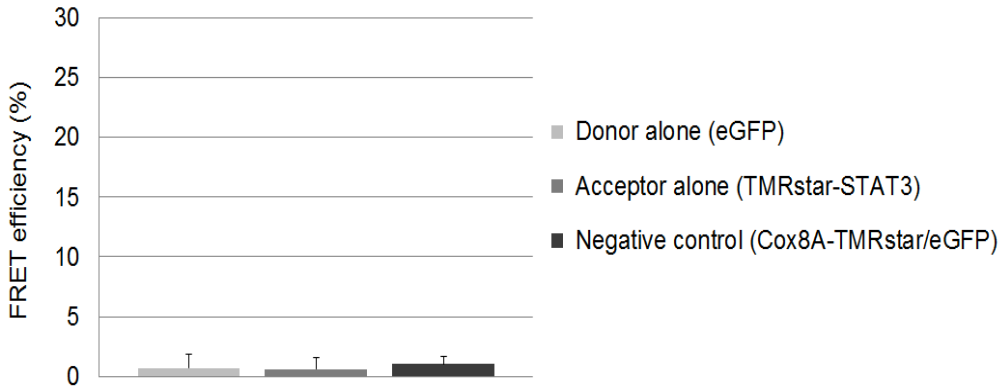


Figure S1. Additional FRET controls. Additional control measurements on donor alone ($FRET_{eff}$: 0.69±1.12%), acceptor alone (0.60±0.98%) and on Cox8A-TMRstar/eGFP cotransfected sample (1.05±0.66%). (N: 20 cells)

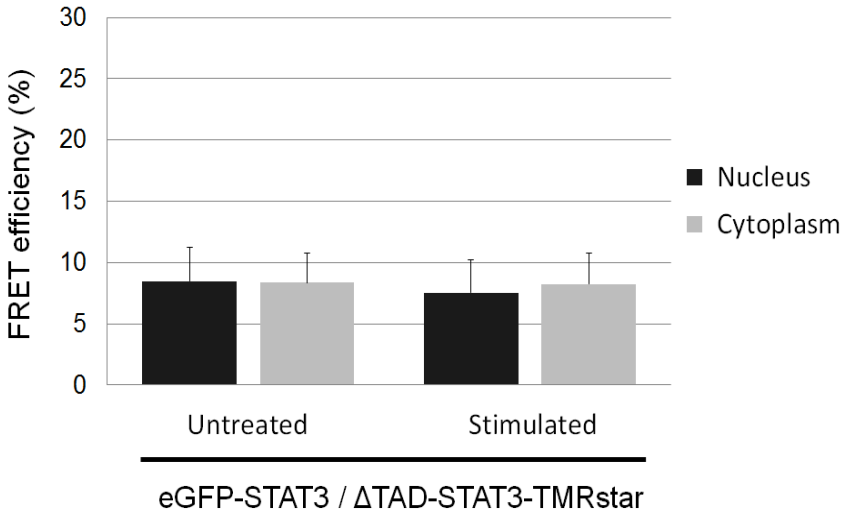


Figure S2. FRET measurements between eGFP-STAT3 and C-terminally deleted STAT3 form (ΔTAD-STAT3-TMRstar). No visible difference detectable in FRET efficiencies between untreated (nucleus: 8.46±2.74%, cytoplasm: 8.37±2.41%) and stimulated (nucleus: 7.52±2.67%, cytoplasm: 8.24±2.52%) samples. (N: 30 cells)

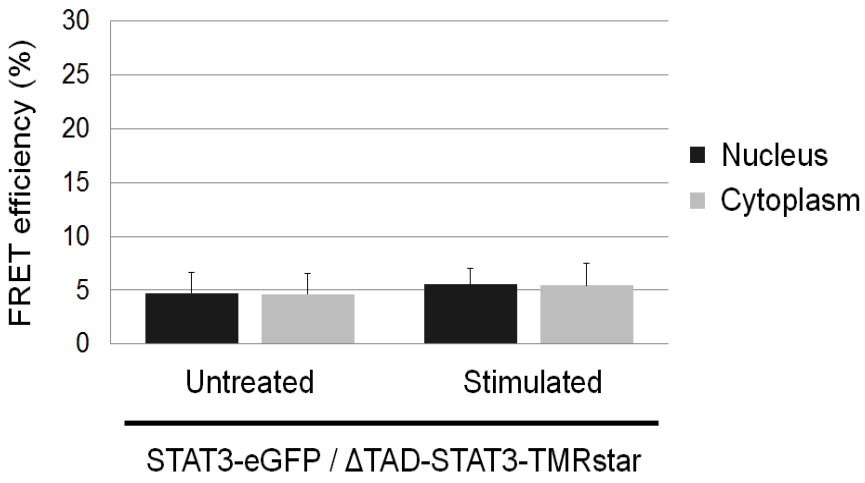


Figure S3. FRET measurements between STAT3-eGFP and C-terminally deleted STAT3 form (ΔTAD-STAT3-TMRstar). Untreated sample (nucleus: 4.75±1.86%, cytoplasm: 4.66±1.89%) represents similar FRET results as the stimulated sample (nucleus: 5.54±1.51%, cytoplasm: 5.45±2.04%). (N: 30 cells)

List of figures and tables

Figure 1: Representative crystal structures of IL-6-type cytokine family members 2
Figure 2: Receptor complexes of the IL-6-type cytokine family 3
Figure 3: Canonical JAK/STAT signalling 4
Figure 4: Non-canonical JAK/STAT signalling 5
Figure 5: STAT family members and their functional domains 8
Figure 6: The identified mutations found in different diseases, targeting structural domains of STAT3 10
Figure 7: Distribution of STAT3 somatic mutations identified in inflammatory hepatocellular adenomas (IHCAs) highlighted in the crystal structure of STAT3 11
Figure 8: Antiparallel and parallel dimer formations of STAT1 12
Figure 9: STAT1 dephosphorylation model 13
Figure 10 A: STAT3 nuclear body formation in response to stimulation in HeLa cells 14
Figure 10 B: STAT3 accumulation in nuclear and axonal region in embryonic stem (ES) cell differentiated neuron-like cells after cytokine addition 14
Figure 11: Basic features of fluorescence correlation spectroscopy (FCS) 16
Figure 12: Fluorescence correlation spectroscopy analyzes the fluctuations of the fluorescence signal 17
Figure 13: Basic principles of Förster resonance energy transfer (FRET) 18
Figure 14: Schematic illustration of the confocal ligth path with respresentative image 34
Figure 15: Structural background of green fluorescent protein (GFP) 35
Figure 16: Structural organization of the SNAP-tag 36
Figure 17: The SNAP-tag labelling mechanism 37
Figure 18: Basic concept of two focus FCS (2f-FCS) and the representative autocorrelation functions (ACFs) 39
Figure 19 A: Acceptor photobleaching (APB) FRET 42
Figure 19 B: Fluorescence intensity traces from the representative images 42
Figure 20: Summary of differently labelled STAT3 constructs used in FRET experiments 44
Figure 21 A: Functional analysis of the STAT3-tag constructs 45
Figure 21 B: Ligand induced nuclear accumulation of the STAT3 fusion proteins 45
Figure 22: Acceptor photobleaching FRET (APB FRET) 46
Figure 23: Representative FRET control experiments 47
Figure 24: FRET efficiencies (%) between N-terminally labelled STAT3 molecules 49

Figure 25: Possible STAT3 dimer formations 49
Figure 26: FRET efficiencies (%) from reciprocally tagged STAT3 constructs 50
Figure 27. Closely oriented reciprocal domains in the acivated STAT3 dimer 51
Figure 28: FRET efficiencies (%) from C-terminally tagged STAT3 constructs 52
Figure 29: STAT3 monomers are associated prior or after stimulation in parallel arrangements 53
Figure 30 A: Representative fluorescence intensity traces from live cell FRET measurement 54
Figure 30 B: Summary of live cell FRET measurements 54
Figure 31: Representative autocorrelation functions (ACFs) from the analyzed samples using 2f-FCS experiments 56
Figure 32: Dimerization study of N-terminally deleted STAT3 with wild type form 57
Figure 33: Deletion of the N-terminal domain prevents the formation of latent STAT3 dimers 58
Figure 34: FRET efficiencies (%) of TMRstar-NTD with the different STAT3-eGFP constructs 59
Figure 35: Inhibition of latent dimer formations visualized by native gel electrophoresis 60
Figure 36: Dissociation of preformed dimers with isolated N-terminal domain 60
Figure 37: L78 mutated N-terminal domain does not interact with STAT3 61
Figure 38. Tetramerization of STAT3 62
Figure 39 A: Inhibition of α2-macroglobulin promoter activity by SNAP-NTD 63
Figure 39 B: L78R mutation in N-terminal domain erases the inhibitory effect of NTD 63
Figure 40: Mutated STAT3 acceptor constructs for FRET imaging 64
Figure 41 A: Functional analysis of the N-terminally mutated STAT3 constructs 65
Figure 41 B: Ligand induced nuclear accumulation of L78 mutated STAT3 fusion proteins 65
Figure 42: Summary of FRET results on L78R mutated STAT3 molecules 66
Figure 43: Live cell FRET measurements on L78R mutated STAT3 molecules 67
Figure 44: FRET on wild type STAT3 versus L78R STAT3 68
Figure 45: Effect of phosphatase inhibition on FRET efficiencis between STAT3-eGFP and STAT3-TMRstar 69
Figure 46: Disruption of the preformed dimers leads to a stronger STAT3 activation 70
Figure 47: Function of preformed dimerization in STAT3 activation 71
Figure 48: Mutation of R609 residue targets the SH2 domain of STAT3 72

Figure 49: STAT3 constructs used for intramolecular FRET measurements 73
Figure 50: Summary of intramolecular FRET measurements on wild type and R609Q mutated STAT3 73
Figure 51: Effect of R609 mutation on STAT3 structure 74
Figure 52: The alternate N-domain dimer of STAT4 76
Figure 53: Summary of FRET results on wild type STAT3 in unstimulated state 77
Figure 54: Summary of FRET results on wild type STAT3 in activated state 81
Figure 55: Tetramerization of STAT3 molecules on DNA 82
Figure 56: Preformed and activated dimers in the JAK/STAT3 pathway 84

Table 1: Functions of the STAT family members 6
Table 2. Summary of plasmid constructs used in this thesis 23
Table 3. Diffusion coefficients and molecular masses derived from 2f-FCS experiments 56